"microRNAs in Myeloma"

Carlo M. Croce, M.D.

The Ohio State University
Comprehensive Cancer Center
The John W. Wolfe Chair in Human Cancer Genetics
Director, Institute of Genetics
Director, Human Cancer Genetics Program

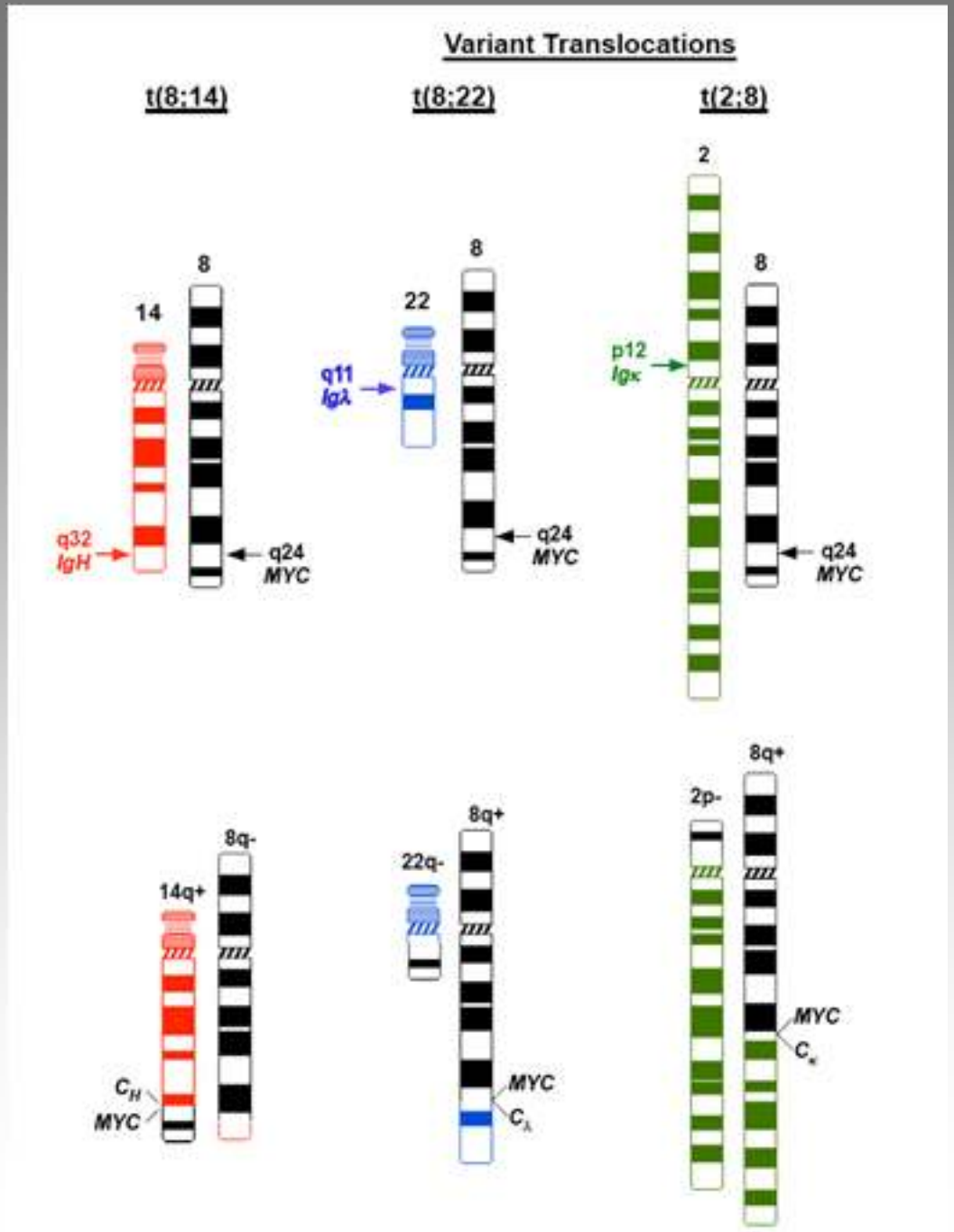
Variant Translocations
t(8;14)
t(8;22)
t(2;8)
14
8
q32
IgH
q24
MYC
22
8
q11
Igλ
q24
MYC
2
8
p12
Igκ
q24
MYC
14q+
8q-
CH
MYC
22q-
8q+
MYC
Cλ
2p-
8q+
MYC
Cκ

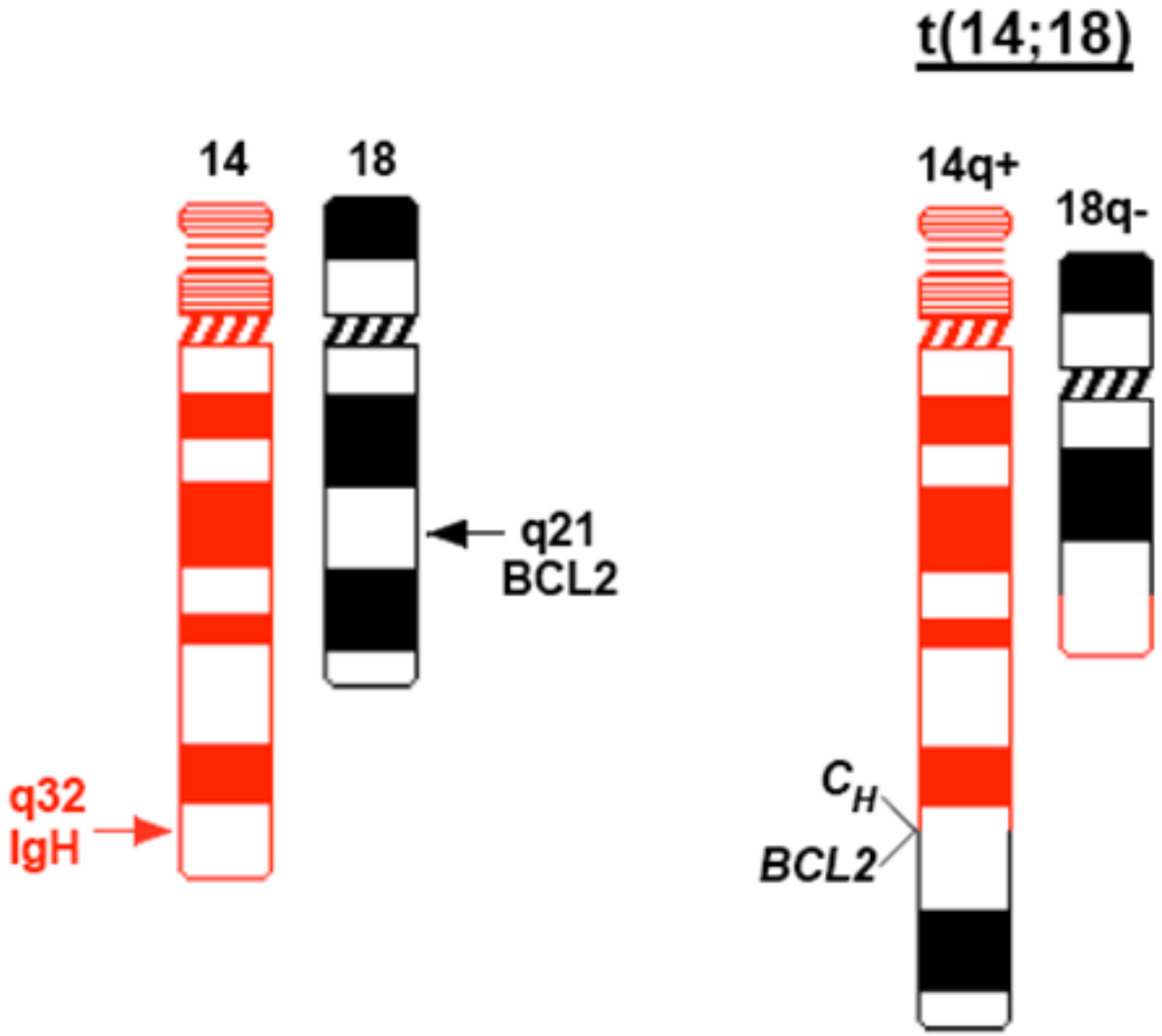
t(14;18)
14
18
q21
BCL2
q32
IgH
14q+
18q-
C_H
BCL2

Occurrence of the most frequent and recurrent chromosomal abnormalities in human CLL

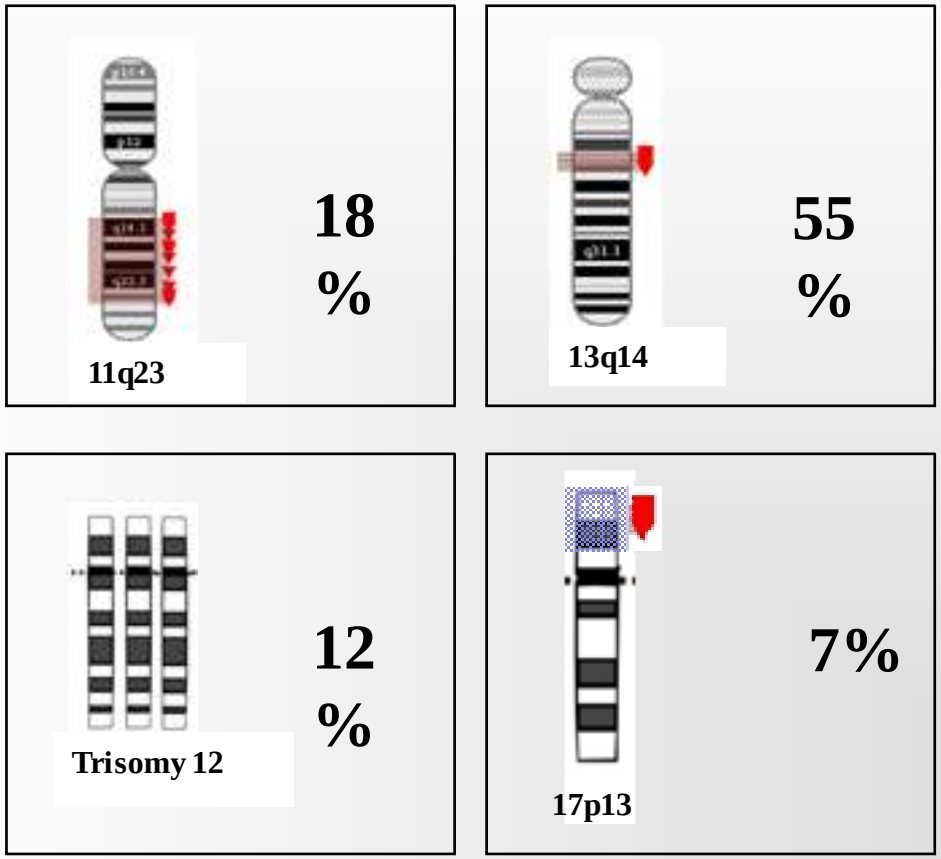

Localization of gene for human p53 tumour antigen to band 17p13

M. Isobe*, B. S. Emanuel†, D. Givol‡, M. Oren‡ & C. M. Croce*

* Wistar Institute, 3601 Spruce Street and † Departments of Pediatrics and Human Genetics, University of Pennsylvania School of Medicine, Philadelphia, Pennsylvania 19104, USA
‡ Department of Chemical Immunology, Rehovot 76100, Israel

Recently the gene for the cellular tumour antigen p53, a phosphoprotein found in increased concentration in a variety of human cells[1], has been mapped to region 17q22 by *in situ* hybridization techniques and has been shown to translocate to the chromosome carrying the translocation [t(15 ; 17)] associated with acute promyelocytic leukaemia (APL)[2]. Based on this finding it has been postulated that this gene has a role in the pathogenesis of APL[2]. Here we present evidence that the gene for p53 is not located on the long arm of chromosome 17, but maps to band 17p13. We therefore suggest that this gene is not directly involved in the chromosome translocation observed in APL.

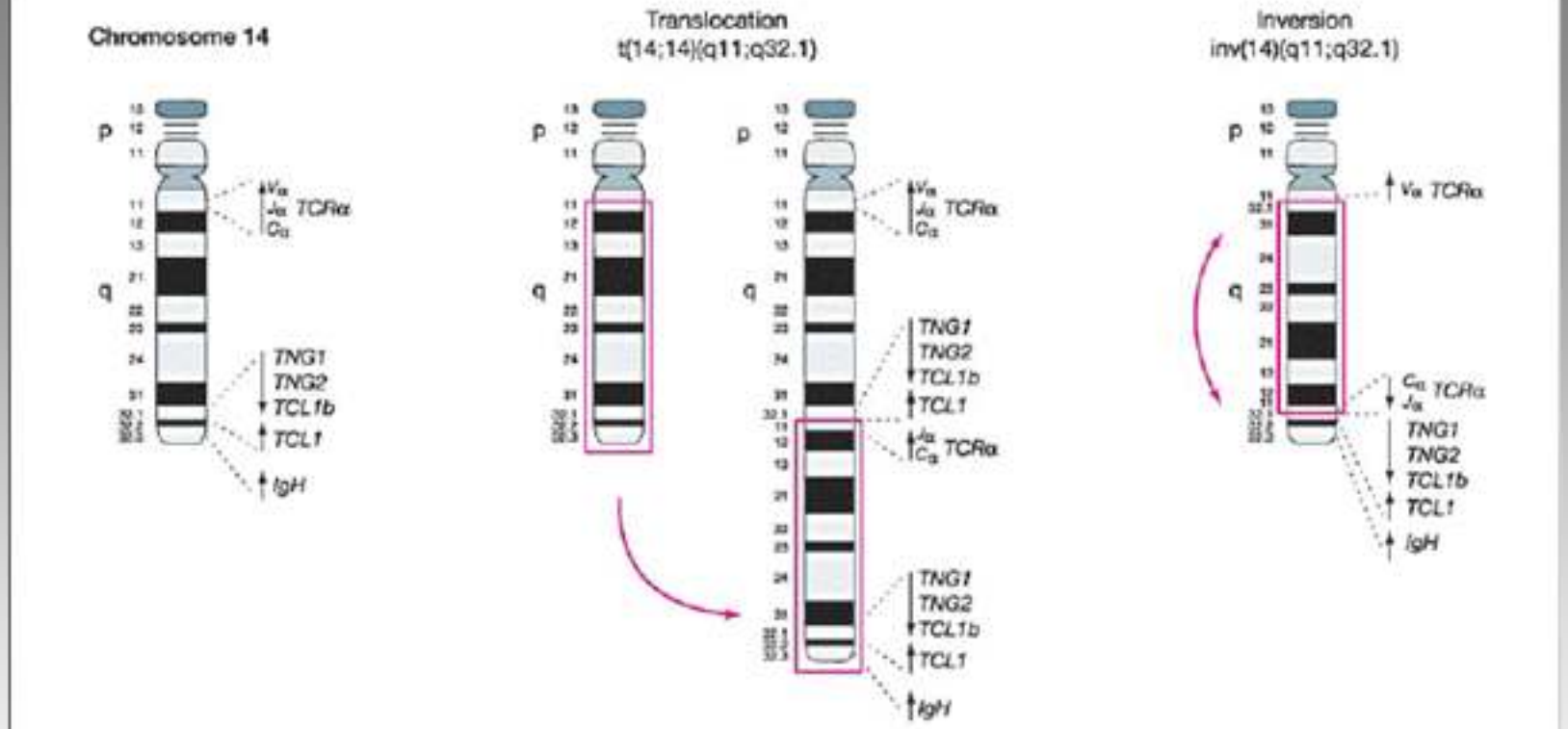
Chromosome 14
Translocation
t(14;14)(q11;q32.1)
Inversion
inv(14)(q11;q32.1)
p
q
Vα
Jα
Cα
TCRα
TNG1
TNG2
TCL1b
TCL1
IgH

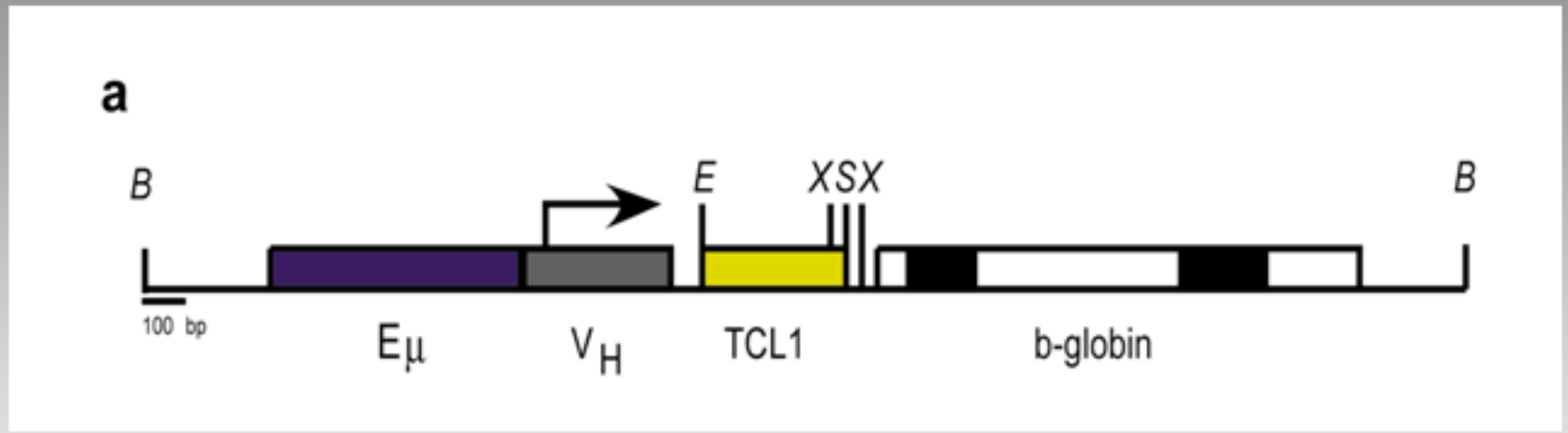
a
B
E
XSX
B
100 bp
Eμ
VH
TCL1
b-globin

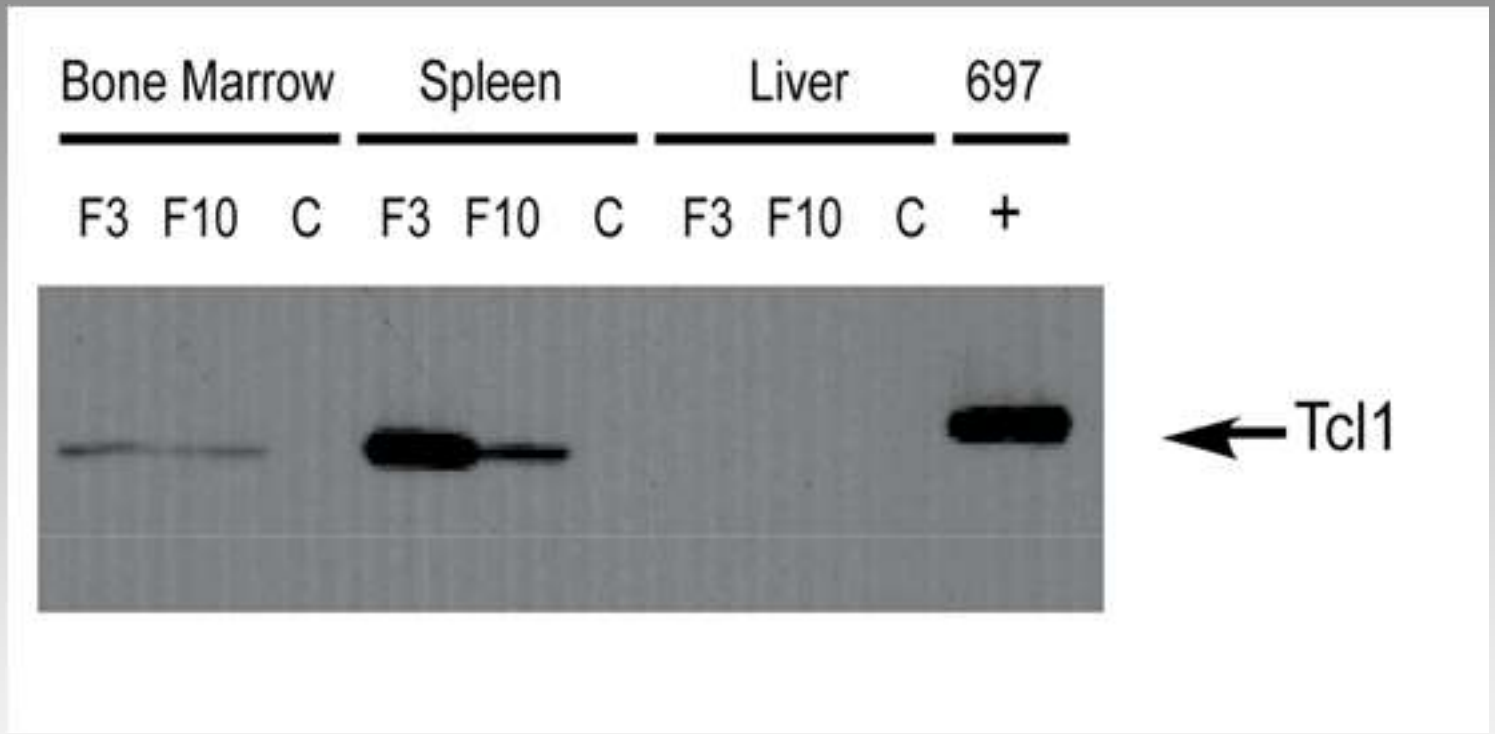
Bone Marrow
Spleen
Liver
697
F3 F10 C F3 F10 C F3 F10 C +
Tcl1

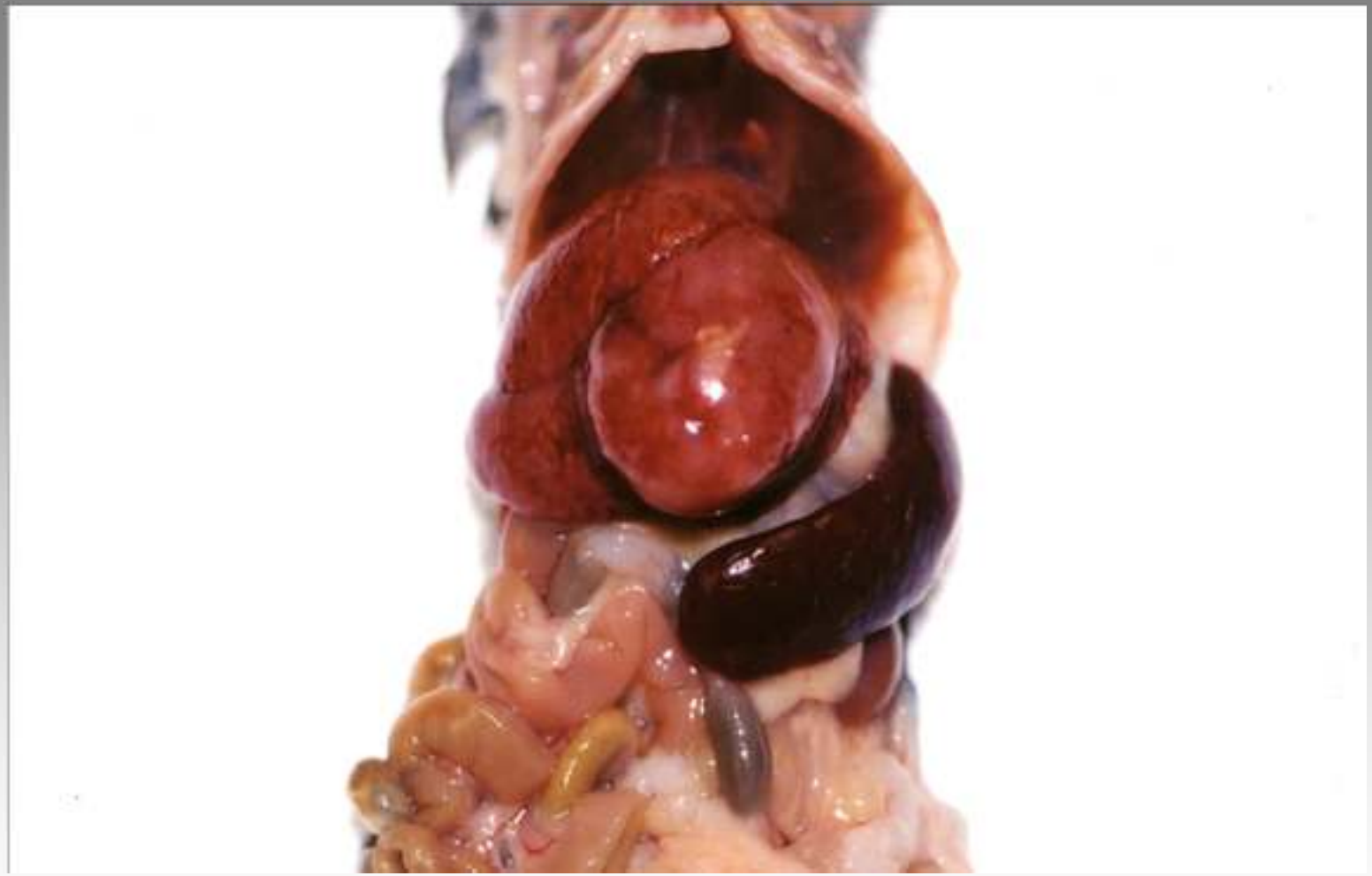

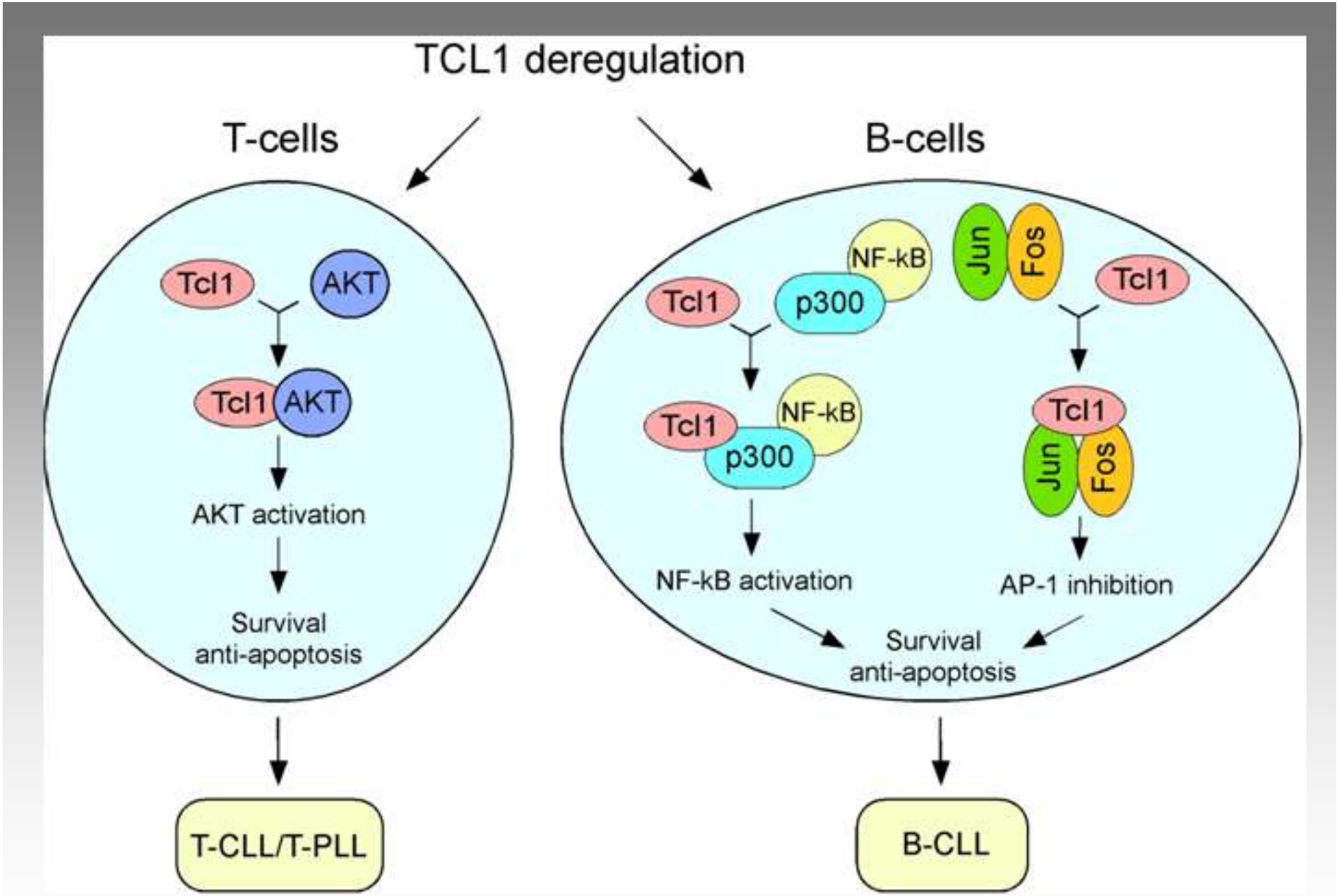
TCL1 deregulation
T-cells
B-cells
Tcl1
AKT
Tcl1
AKT
AKT activation
Survival
anti-apoptosis
T-CLL/T-PLL
NF-kB
p300
Tcl1
Jun
Fos
Tcl1
Tcl1
NF-kB
p300
Tcl1
Jun
Fos
NF-kB activation
AP-1 inhibition
Survival
anti-apoptosis
B-CLL

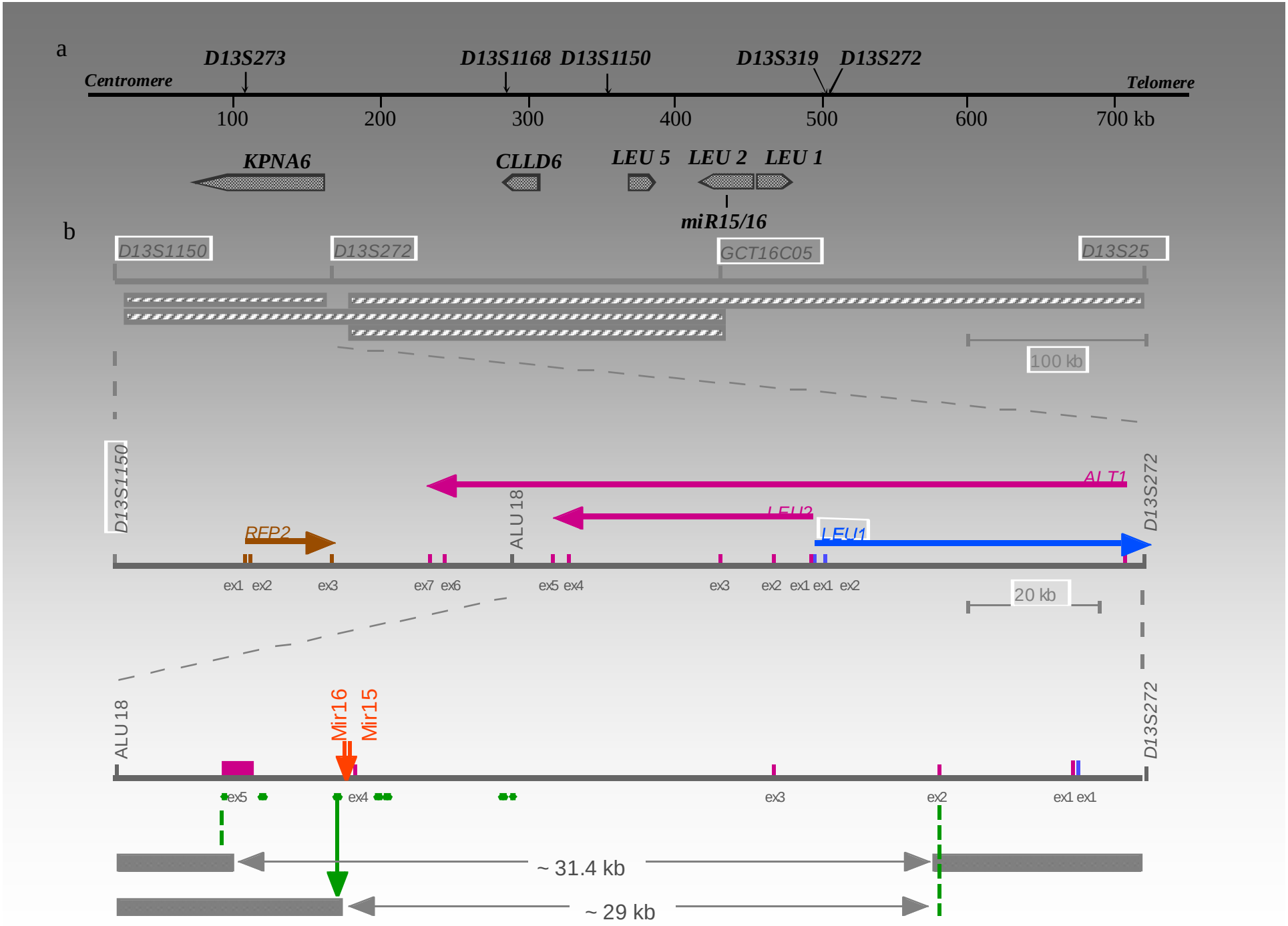
a
D13S273
D13S1168
D13S1150
D13S319
D13S272
Centromere
Telomere
100
200
300
400
500
600
700 kb
KPNA6
CLLD6
LEU 5
LEU 2
LEU 1
miR15/16
b
D13S1150
D13S272
GCT16C05
D13S25
100 kb
D13S1150
ALT1
LEU2
LEU1
RFP2
ALU 18
D13S272
ex1 ex2 ex3 ex7 ex6 ex5 ex4 ex3 ex2 ex1 ex1 ex2
20 kb
ALU18
Mir16
Mir15
D13S272
ex5 ex4 ex3 ex2 ex1 ex1
~ 31.4 kb
~ 29 kb

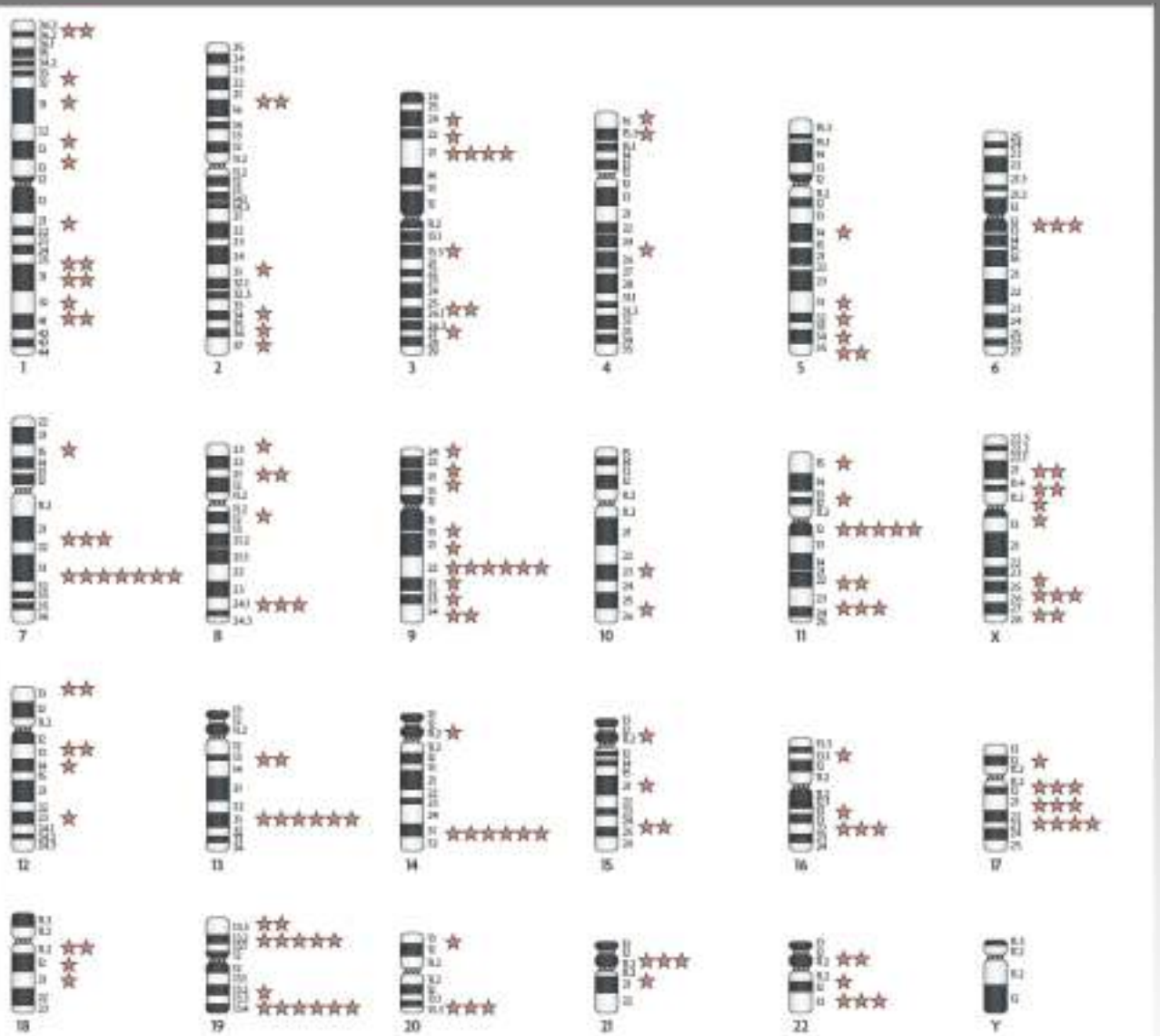

Figure 1 | **MicroRNA genes map to chromosomal regions that are involved in alterations in human cancer.** The 24 human chromosomes are shown, with stars indicating the locations of microRNA-gene-containing regions that are implicated in cancer (one star = one microRNA gene). Many microRNAs map to chromosome regions that are involved in rearrangements in human cancer. For example, *miR-15-a* and *miR-16-1* map to 13q14, a region that is frequently deleted in chronic lymphocytic leukaemia. *miR-29a* and *miR-29b* map to 7q32, a region that is deleted in myelodysplastic syndrome and acute myeloid leukaemia. The *let-7g–let-7a1* cluster maps to 3p2, the *let-7f-1–let-7d* cluster maps to 9q22.3, *let-7a-2* maps to 11q23-q24 and *let-7c* maps to 21q21 — all of these regions are involved in deletions in a range of solid malignancies, including lung, urothelial, breast, ovarian and cervical cancers.

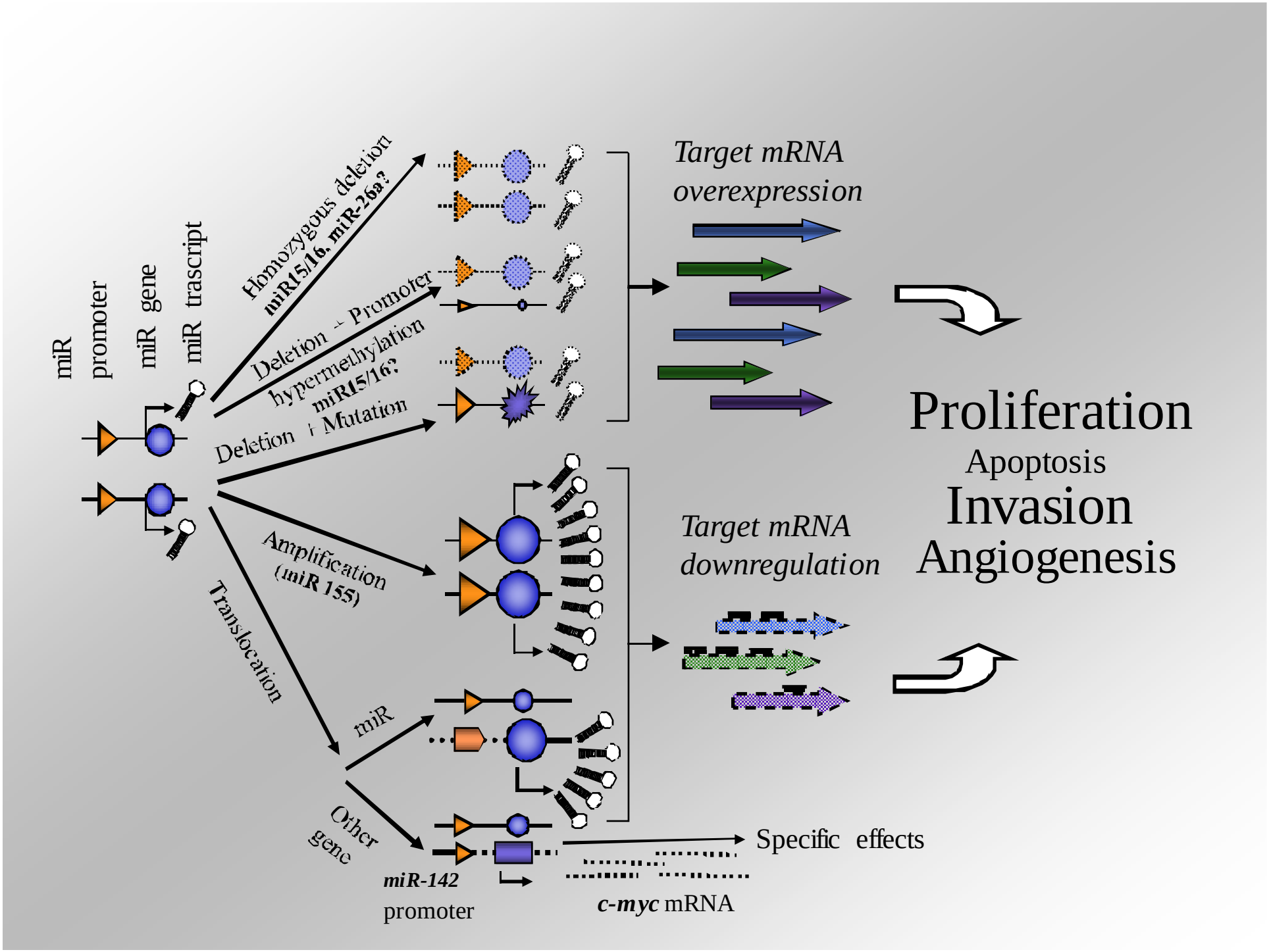
miR promoter
miR gene
miR trascript
Homozygous deletion miR15/16, miR-26a?
Deletion + Promoter hypermethylation miR15/16?
Deletion + Mutation
Target mRNA overexpression
Proliferation
Apoptosis
Invasion
Angiogenesis
Amplification (miR 155)
Translocation
Target mRNA downregulation
miR
Other gene
Specific effects
miR-142 promoter
c-myc mRNA

Proc. Natl. Acad. Sci. USA
Vol. 86, pp. 8867–8871, November 1989
Genetics

Activation of *MYC* in a masked t(8;17) translocation results in an aggressive B-cell leukemia

(*BCL3* gene/oncogene activation/tumor progression)

C. E. GAUWERKY*, K. HUEBNER*, M. ISOBE*, P. C. NOWELL†, AND C. M. CROCE*

*The Fels Institute for Cancer Research and Molecular Biology, Temple University School of Medicine, 3420 North Broad Street, Philadelphia, PA 19140; and †Department of Pathology and Laboratory Medicine, University of Pennsylvania School of Medicine, Philadelphia, PA 19104

Contributed by P. C. Nowell, July 24, 1989

ABSTRACT We have analyzed the oncogene rearrangements involving *BCL2* and *MYC* in the leukemia cells of a patient with an aggressive prolymphocytic leukemia that had an abnormal karyotype including a t(14;18) translocation and a chromosome 17q+. Molecular analysis showed that *BCL2* was rearranged in the major breakpoint cluster region and had joined into the immunoglobulin heavy chain gene as in follicular lymphoma. Cloning and sequence analysis of the rearranged *MYC* gene revealed that *MYC* was truncated at the *Pvu* II site at the end of the first exon of *MYC* and had joined into the regulatory elements of a gene that we called *BCL3* (B-cell leukemia/lymphoma 3). The *BCL3* locus was mapped to chromosome 17 band q22. We found *BCL3* transcribed as a message of 1.7 kilobases in many hematopoietic cell lines representing all hematopoietic lineages. In the patient's leukemia cells, the truncated *MYC* gene was highly expressed under the influence of *BCL3* regulatory elements, leading to an aggressive B-cell leukemia that presumably had been derived from an indolent lymphoma carrying a rearranged *BCL2* gene.

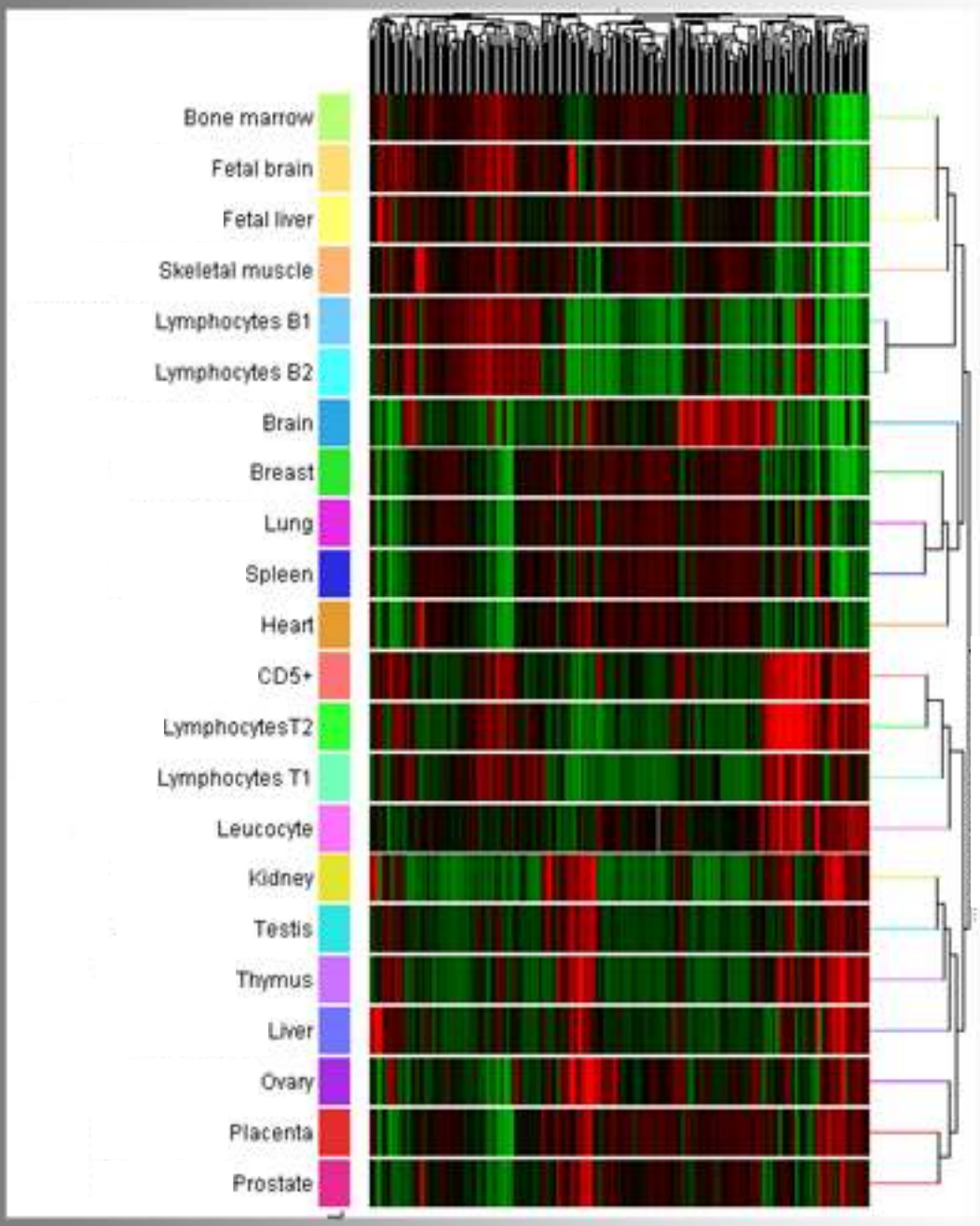
Bone marrow
Fetal brain
Fetal liver
Skeletal muscle
Lymphocytes B1
Lymphocytes B2
Brain
Breast
Lung
Spleen
Heart
CD5+
LymphocytesT2
Lymphocytes T1
Leucocyte
Kidney
Testis
Thymus
Liver
Ovary
Placenta
Prostate

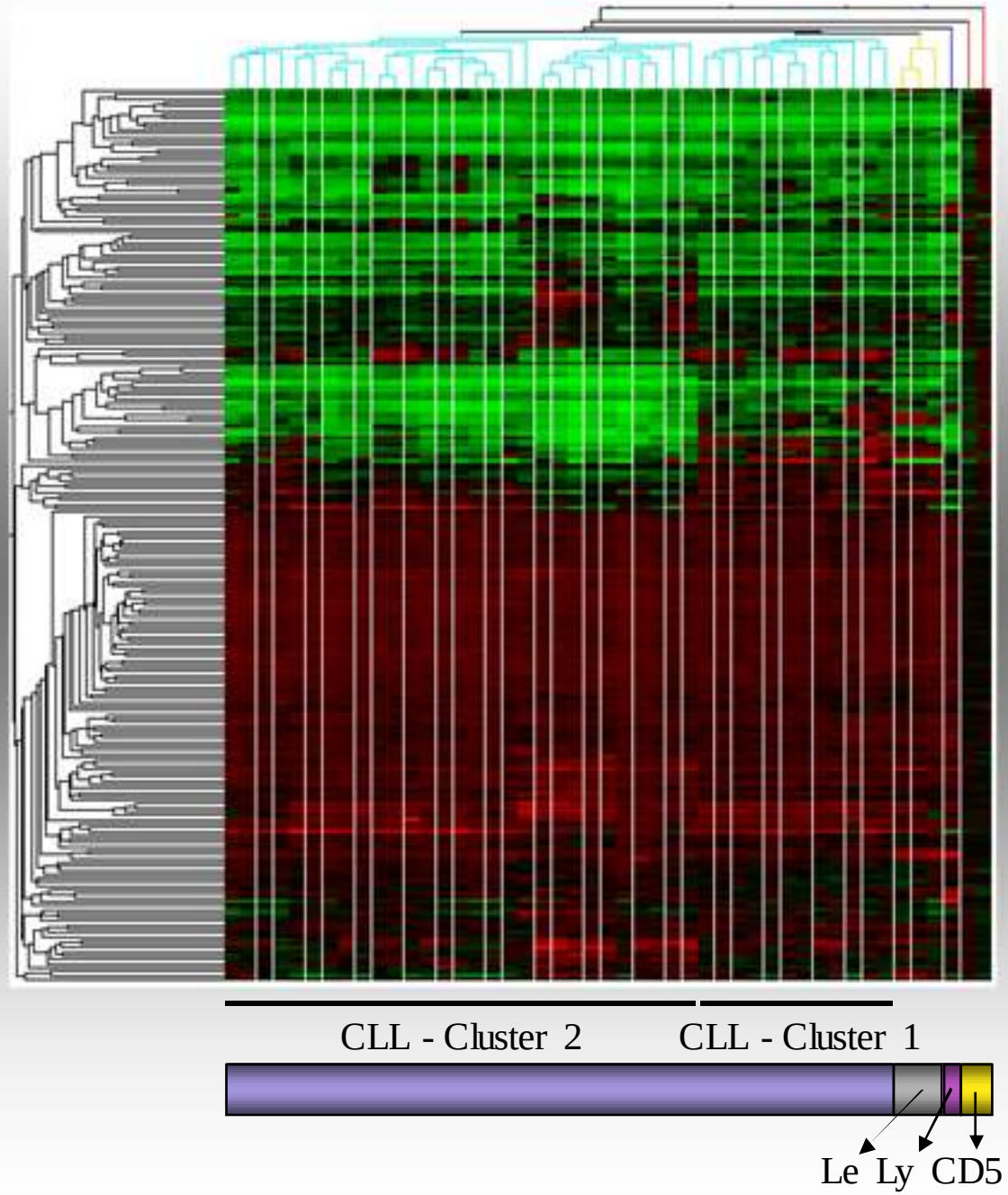
CLL - Cluster 2
CLL - Cluster 1
Le
Ly
CD5

Characteristics of patients analyzed with the miRNACHIP.

Characteristic	Value
Male sex – no. of patients (%)	58 (61.7)
Age at diagnosis – yrs.	
median	57.3
range	38-78
Therapy begun	
No	
No. of patients	53
Time since diagnosis – mo.	87
Yes	
No. of patients	41
Time between diagnosis and therapy – mo.	40
ZAP-70 level	
≤ 20%	48
>20%	46
IgV_H	
Unmutated (≥98% homology)	57
Mutated (<98% homology)	37

miRNA signature associated with prognostic factors (ZAP70 and IgVH mutations) and disease progression in CLL patients*.

Nr. Crt.	Component	Map	P value	Group 4 expression**	Putative targets ***	Observation****
1	***miR-15a***	13q14.3	0,018	high	NA	cluster 15a/16-1 del CLL & Prostate ca. (ref (10)
2	***miR-195***	17p13	0,017	high	NA	del HCC
3	***miR-221***	Xp11.3	0,010	high	HECTD2, CDKN1B, NOVA1, ZFPM2, PHF2	cluster 221/222
4	***miR-23b***	9q22.1	0,009	high	FNBP1L, WTAP, PDE4B, SATB1, SEMA6D	cluster 24-1/23b FRA 9D; del Urothelial ca. (ref (13)
5	***miR-155***	21q21	0,009	high	ZNF537, PICALM, RREB1, BDNF, QKI	amp child Burkitt's lymphoma (ref (16)
6	***miR-223***	Xq12-13.3	0,007	low	PTBP2, SYNCRIP, WTAP, FBXW7, QKI	normally expression restricted to myeloid lineage (ref (27)
7	***miR-29a-2***	7q32	0,004	low	NA	cluster 29a-2/29b-1 FRA7H; del Prostate ca. (ref (13)
8	***miR-24-1***	9q22.1	0,003	high	TOP1, FLJ45187, RSBN1L, RAP2C, PRPF4B	cluster 24-1/23b FRA 9D; del Urothelial ca. (ref (13)
9	***miR-29b-2 (miR-102)***	1q32.2-32.3	0,0007	low	NA	
10	***miR-146***	5q34	0,0007	high	NOVA1, NFE2L1, C1orf16, ABL2, ZFYVE1	
11	***miR-16-1***	13q14.3	0,0004	high	BCL2, CNOT6L, USP15, PAFAH1B1, ESRRG	cluster 15a/16-1 del CLL, prostate ca. (ref (10)
12	***miR-16-2***	3q26.1	0,0003	high	see miR-16-1	identical miR-16-1
13	***miR-29c***	1q32.2-32.3	0,0002	low	NA	

Note: * - All the members of the signature are mature miRNAs;

*** - top five predictions using TargetScan at http://genes.mit.edu/targetscan (32) were included. NA – not available; for specific gene names – see the NCBI site at http://www.ncbi.nlm.nih.gov/entrez.

**** - FRA = fragile site; del = deletion; HCC = hepatocellular carcinoma; ca. = carcinoma.

Genetic variations in the genomic sequences of miRNAs in CLL patients *.

miRNA	Location **	CLL	Normals	miRNACHIP expression	Observation
miR-16-1	Germline pri-miRNA (CtoT)+7bp in 3'	2/75	0/160	Reduced to 15% and 40% of normal, respectively	Normal allele deleted in CLL cells in both patients (FISH, LOH); For one patient: Previous breast cancer; Mother died with CLL; sister died with breast ca;
miR-27b	Germline pri-miRNA (GtoA)+50bp in 3'	1/75	0/160	Normal	Mother throat and lung cancer at 58. Father lung cancer at 57.
miR-29b-2	pri-miRNA (GtoT)+212 in 3'	1/75	0/160	Reduced to 75%	Sister breast cancer at 88 (still living). Brother "some type of blood cancer" at 70.
miR-29b-2	pri-miRNAs ins (+A)+107 in 3'	3/75	0/160	Reduced to 80%	For two patients: Fam history of unspecified cancer
miR-187	pri-miRNA (TtoC)+73 in 3'	1/75	0/160	NA	Unknown
miR-206	pre-miRNA 49(GtoT)	2/75	0/160	Reduced to 25%	Prostate cancer; mother esophogeal cancer. Brother prostate cancer sister breast cancer
miR-206	Somatic pri-miRNA (AtoT)-116 in 5'	1/75	0/160	Reduced to 25% (data only for one pt)	Aunt some type of leukemia (dead)
miR-29c	pri-miRNA (GtoA)31 in 5'	2/75	1/160	NA	Paternal grandmother CLL; sister breast ca. (one pt).
miR-122a	pre-miRNA 53(CtoT)	1/75	2/160	Reduced to 33%	Paternal uncle colon cancer.
miR-187	pre-miRNA 34(GtoA)	1/75	1/160	NA	Grandfather polycythemia vera. Father a history of cancer but not lymphoma.

Note: * - For each patient/normal control more than 12kb of genomic DNAs was sequenced and, in total, we screened by direct sequencing ~627kb of tumor DNA and about 700kb of normal DNA. The position of the mutations are reported in respect with the precursor miRNA molecule. The list of 42 microRNAs analyzed includes 15 members of the specific signature or members of the same clusters, *miR-15a, miR-16-1, miR-23a, miR-23b, miR-24-1, miR-24-2, miR-27a, miR-27b, miR-29b-2, miR-29c, miR-146, miR-155, miR-221, miR-222, miR-223* and 27 other microRNAs (randomly selected): *let-7a2, let-7b, miR-17-3p, miR-17-5p, miR-18, miR-19a, miR-19b-1, miR-20, miR-21, miR-30b, miR-30c-1, miR-30d, miR-30e, miR-32, miR-100, miR-105-1, miR-108, miR-122, miR-125b-1, miR-142-5p, miR-142-3p, miR-193, miR-181a, miR-187, miR-206, miR-224, miR-346.*

** - When normal correspondent DNA from bucal mucosa was available, the alteration was identified as germline when present or somatic when absent, respectively. FISH = fluorescence *in situ* hybridization; LOH = loss of heterozygosity; NA = not available

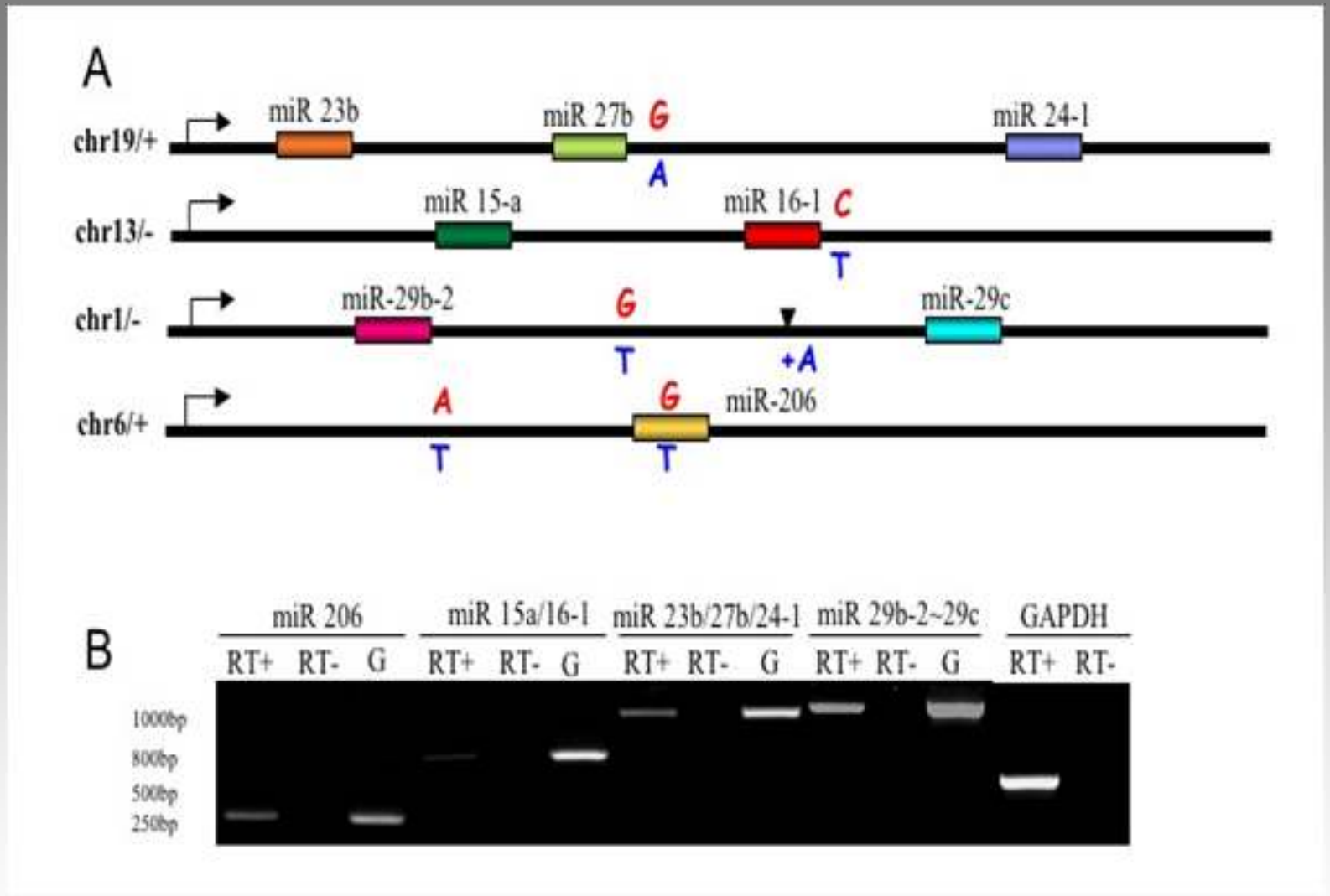
A
chr19/+
miR 23b
miR 27b
G
A
miR 24-1
chr13/-
miR 15-a
miR 16-1
C
T
chr1/-
miR-29b-2
G
T
+A
miR-29c
chr6/+
A
T
G
T
miR-206
B
miR 206
miR 15a/16-1
miR 23b/27b/24-1
miR 29b-2~29c
GAPDH
RT+ RT- G RT+ RT- G RT+ RT- G RT+ RT- G RT+ RT-
1000bp
800bp
500bp
250bp

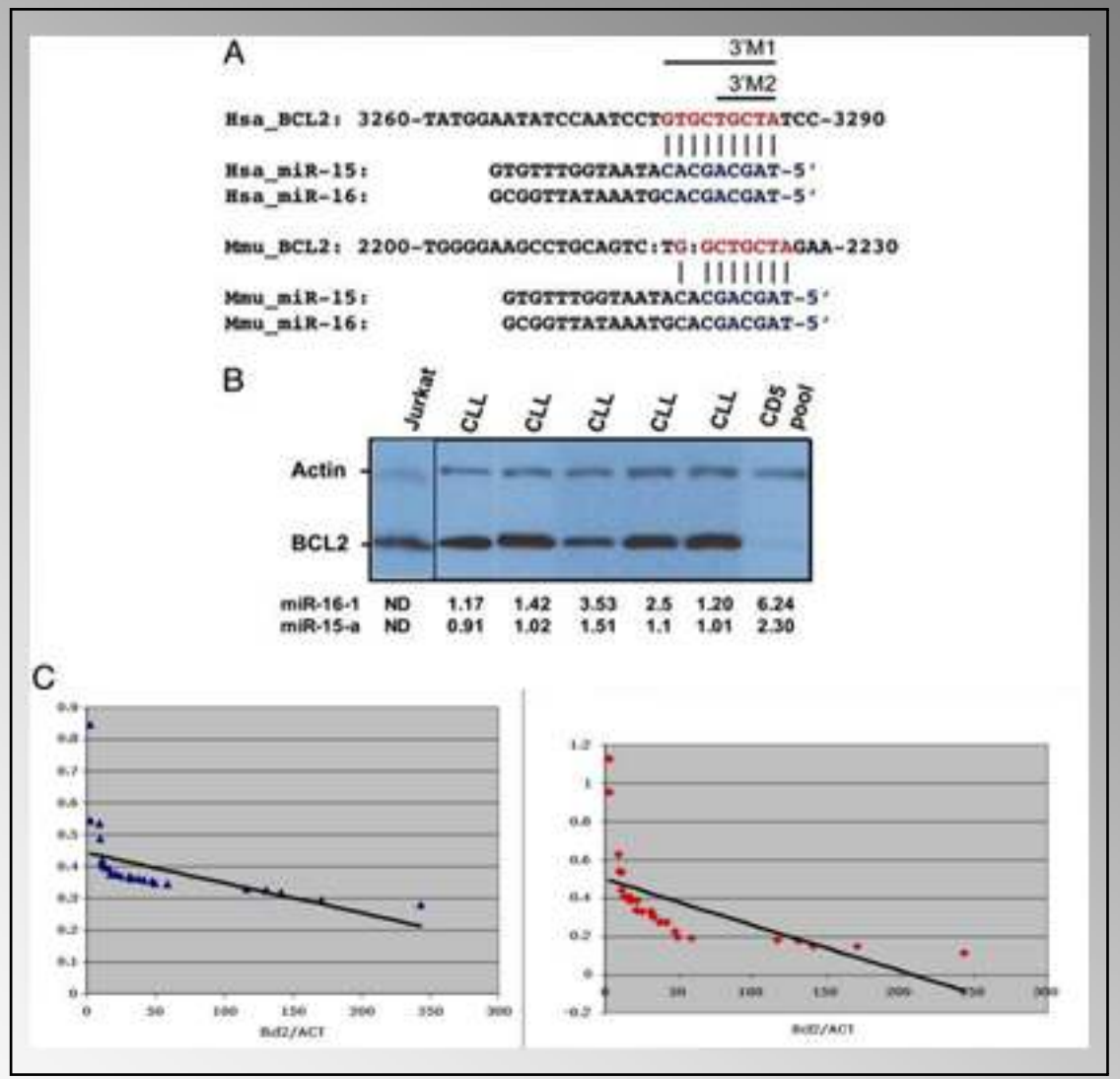

Bcl2 protein expression is inversely correlated with *miR-15a* and *miR-16-1* miRNAs expression in CLL patients. (*A*) The unique site of complementarity miR::mRNA is conserved in human and mouse and is the same for all four human m protein are inversely correlated with *miR-15a* and *miR-16-1* expression. Five different CLL cases are presented, and the normal cells were pools of $CD5^+$ B lymphocytes. The T cell leukemia Jurkat was used as control for Bcl2 protein expression. For normalization we used β-actin. The numbers represent normalized expression on miRNACHIP. ND, not determined. (*C*) The inverse correlation in the full set of 26 samples of CLL between miR-15a / miR-16-1 and Bcl2 protein expressions. The normalized Bcl2 expression is on abscissa vs. *miR-15a* (*Left*) and *miR-16-1* (*Right*) levels by miRNA chip on ordinates. ACT, β-actin.

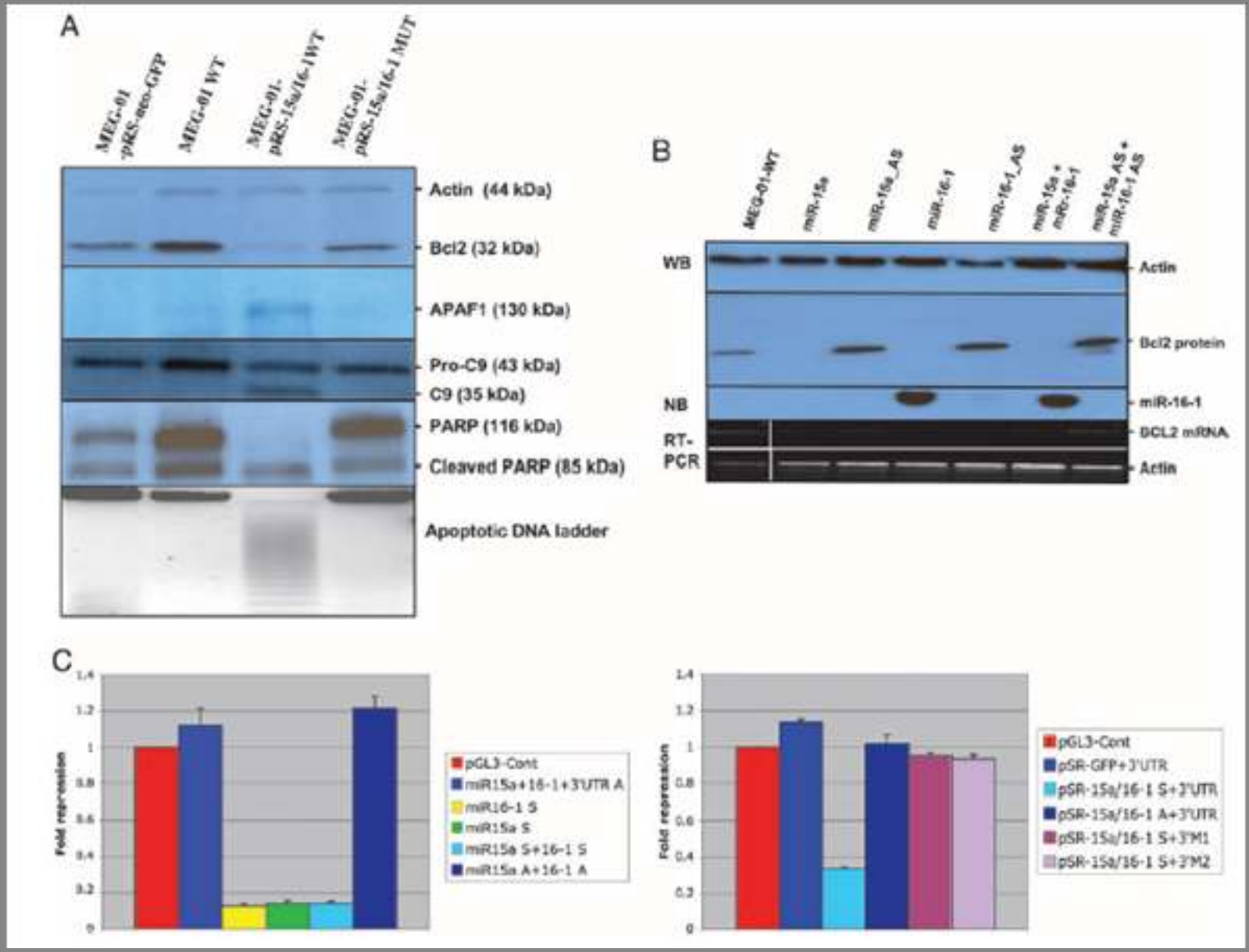
A
MEG-01 pRS-ato-GFP
MEG-01 WT
MEG-01-pRS-15a/16-1WT
MEG-01-pRS-15a/16-1 MUT
Actin (44 kDa)
Bcl2 (32 kDa)
APAF1 (130 kDa)
Pro-C9 (43 kDa)
C9 (35 kDa)
PARP (116 kDa)
Cleaved PARP (85 kDa)
Apoptotic DNA ladder
B
MEG-01-WT
miR-15a
miR-15a_AS
miR-16-1
miR-16-1_AS
miR-15a + miR-16-1
miR-15a AS + miR-16-1 AS
WB
NB
RT-PCR
Actin
Bcl2 protein
miR-16-1
BCL2 mRNA
Actin
C
Fold repression
pGL3-Cont
miR15a+16-1+3'UTR A
miR16-1 S
miR15a S
miR15a S+16-1 S
miR15a A+16-1 A
Fold repression
pGL3-Cont
pSR-GFP+3'UTR
pSR-15a/16-1 S+3'UTR
pSR-15a/16-1 A+3'UTR
pSR-15a/16-1 S+3'M1
pSR-15a/16-1 S+3'M2

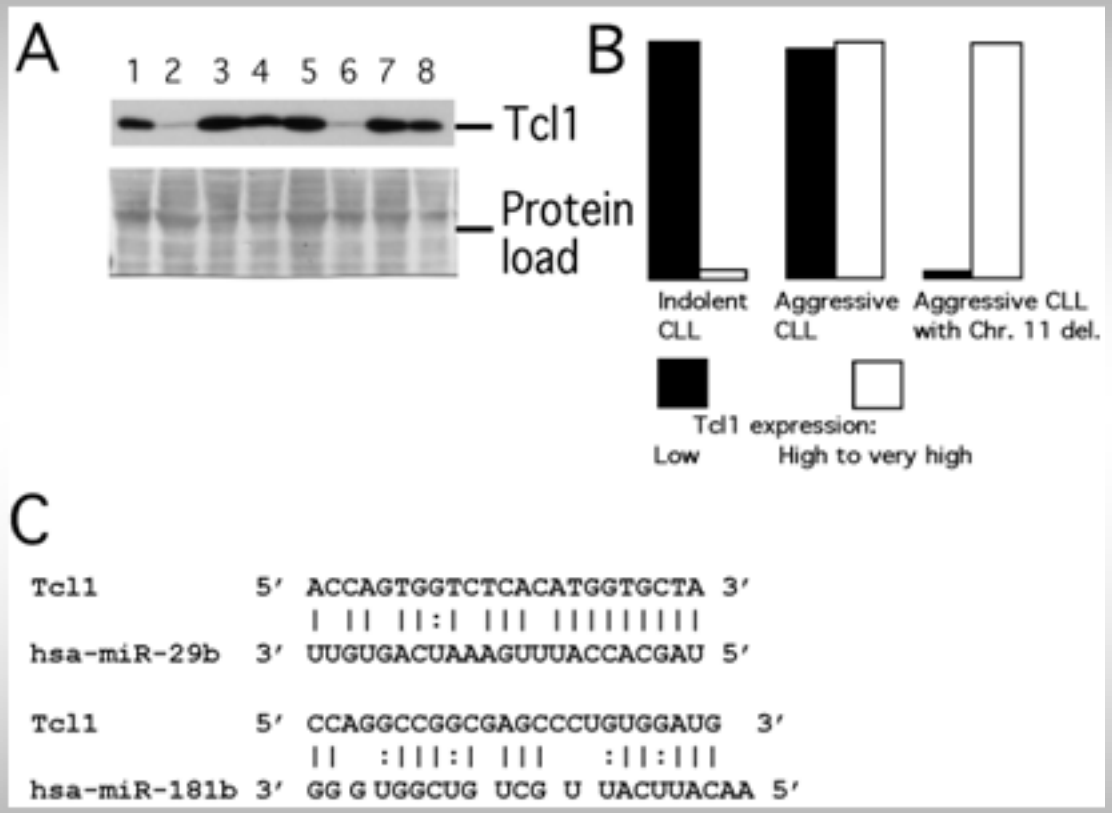
A
1 2 3 4 5 6 7 8
Tcl1
Protein load
B
Indolent CLL
Aggressive CLL
Aggressive CLL with Chr. 11 del.
Tcl1 expression:
Low
High to very high
C
Tcl1 5′ ACCAGTGGTCTCACATGGTGCTA 3′
hsa-miR-29b 3′ UUGUGACUAAAGUUUACCACGAU 5′
Tcl1 5′ CCAGGCCGGCGAGCCCUGUGGAUG 3′
hsa-miR-181b 3′ GG G UGGCUG UCG U UACUUACAA 5′

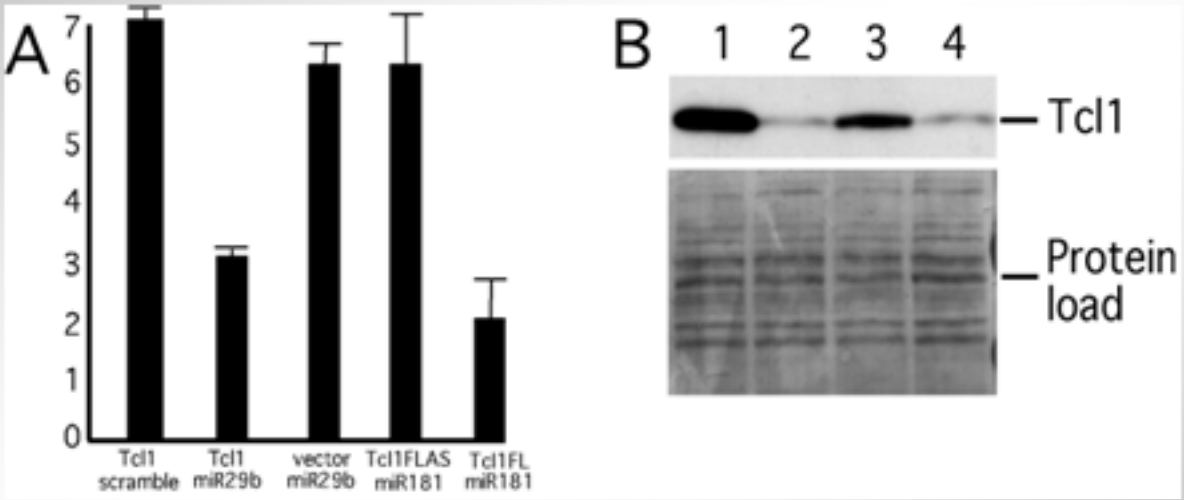
A
7
6
5
4
3
2
1
0
Tcl1 scramble
Tcl1 miR29b
vector miR29b
Tcl1FLAS miR181
Tcl1FL miR181
B
1
2
3
4
Tcl1
Protein load

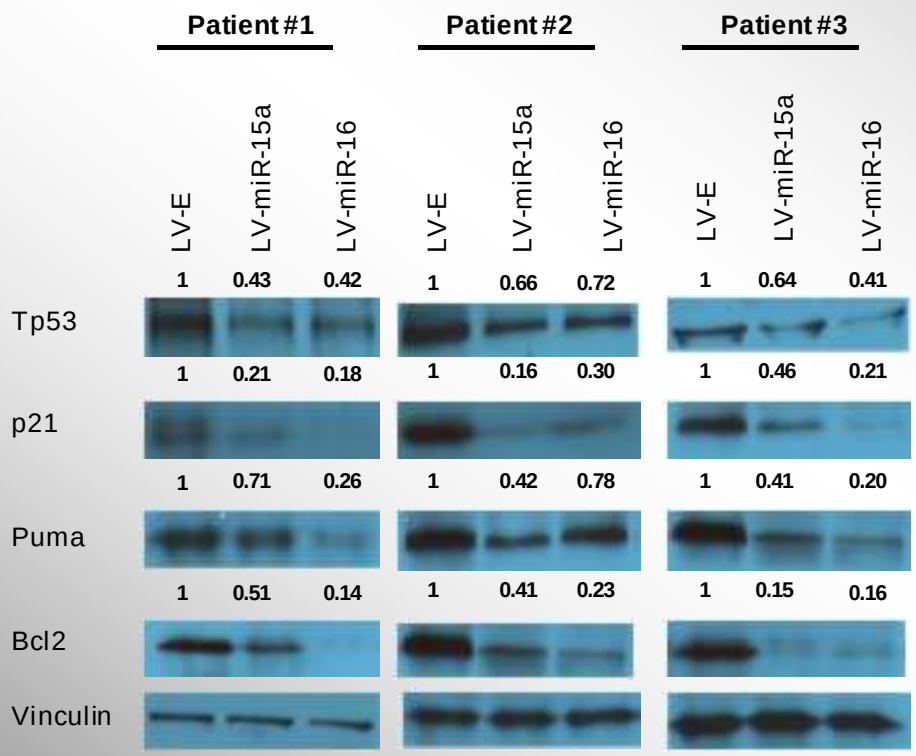

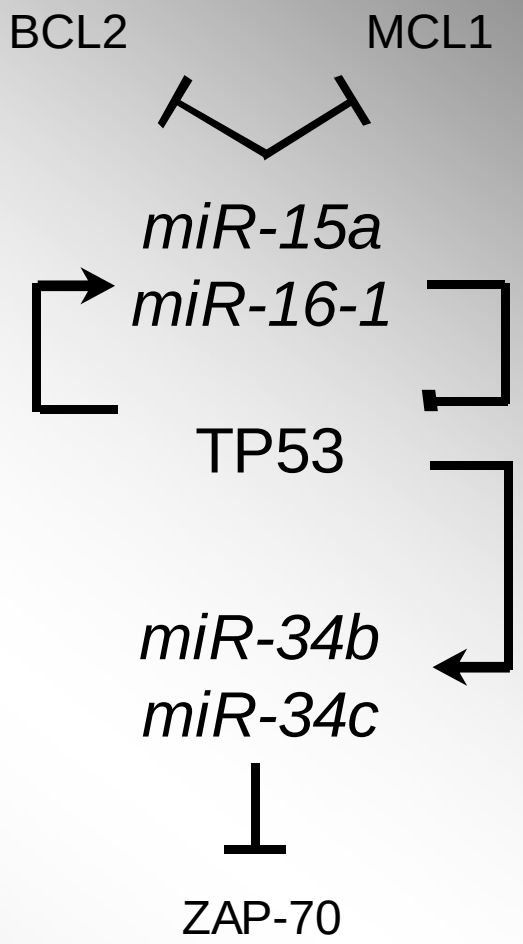

(Fabbri and Botoni et al, JAMA,)

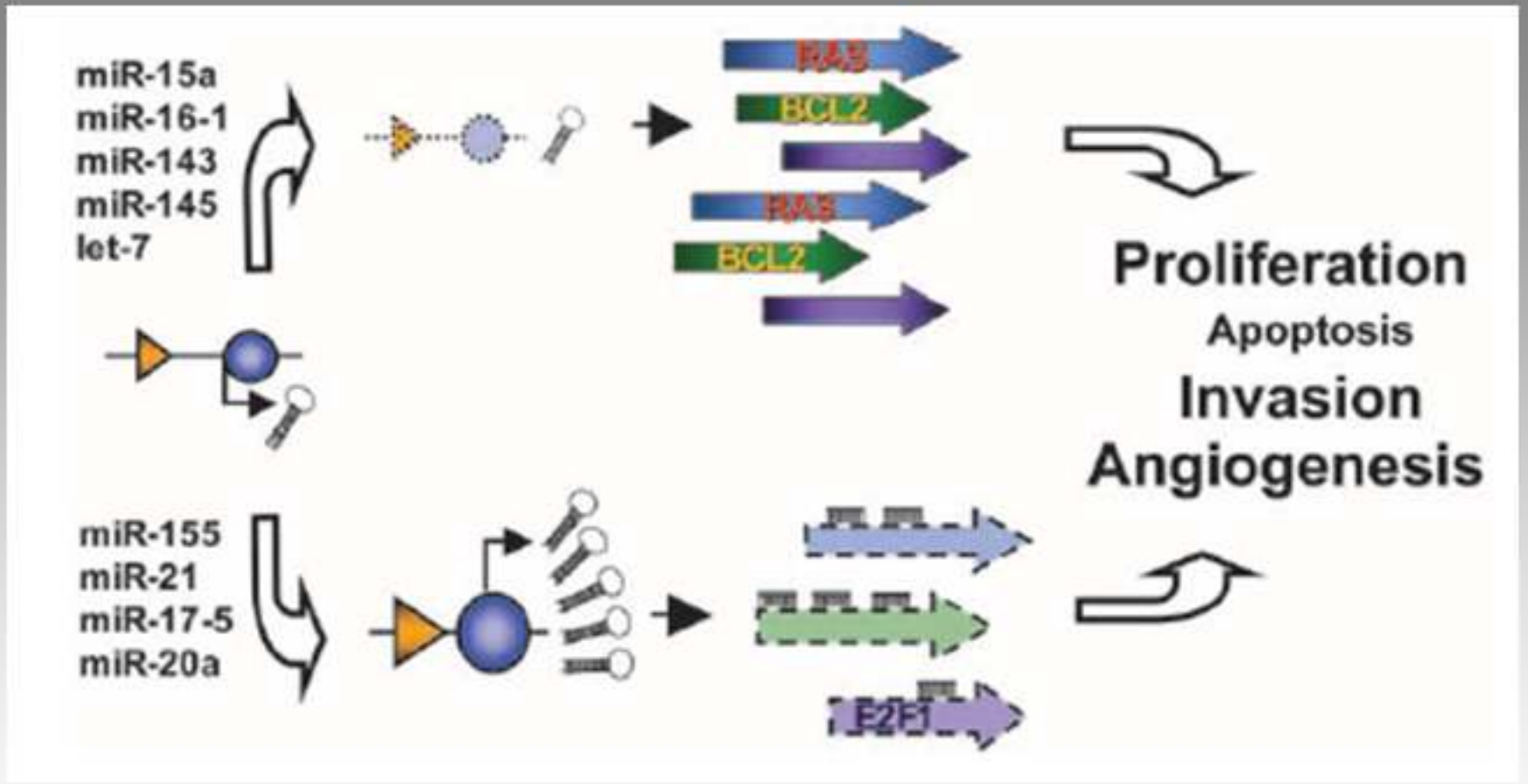
miR-15a
miR-16-1
miR-143
miR-145
let-7
RAS
BCL2
RAS
BCL2
Proliferation
Apoptosis
Invasion
Angiogenesis
miR-155
miR-21
miR-17-5
miR-20a
E2F1

Table 1 | **MicroRNAs that function as oncogenes or tumour suppressor genes in human cancers**

MicroRNA	Dysregulation	Function	Validated targets	Oncogene (ONC) or tumour suppressor (TS)	Refs
miR-15a and *miR-16-1*	Loss in CLL, prostate cancer and multiple myeloma	Induces apoptosis and inhibits tumorigenesis	BCL2, WT1 RAB9B and MAGE83	TS	15,20,23, 30,52,69
let-7 (*a*, *b*, *c*, *d*, *e*, *f*, *g* and *i*)	Loss in lung and breast cancer and in various solid and haematopoietic malignancies	Induces apoptosis and inhibits tumorigenesis	RAS, MYC and HMGA2	TS	22,26, 42,70
miR-29 (*a*, *b* and *c*)	Loss in aggressive CLL, AML (11q23), MDS lung and breast cancers and cholangiocarcinoma	Induces apoptosis and inhibits tumorigenicity. Reactivates silenced tumour suppressor genes	TCL1, MCL1 and DNMTs	TS	30,64, 71,72
miR-34	Loss in pancreatic, colon, breast and liver cancers	Induces apoptosis	CDK4, CDK6, cyclin E2, EZF3 and MET	TS	56–58
miR-145	Loss in breast cancer	Inhibits proliferation and induces apoptosis of breast cancer cells	ERG	TS	31
miR-221 and *miR-222*	Loss in erythroblastic leukaemia	Inhibits proliferation in erythroblasts	KIT	TS	30
miR-221 and *miR-222*	Overexpression in aggressive CLL, thyroid carcinoma and hepatocellular carcinoma	Promotes cell proliferation and inhibits apoptosis in various solid malignancies	p27, p57, PTEN and TIMP3	ONC	43,51,73
miR-155	Upregulated in aggressive CLL, Burkitt's lymphoma and lung, breast and colon cancers	Induces cell proliferation and leukaemia or lymphoma in mice	MAF and SHIP1	ONC	32–34, 36,37
miR-17–92 cluster	Upregulated in lymphomas and in breast, lung, colon, stomach and pancreatic cancers	Induces proliferation	E2F1, BIM and PTEN	ONC	19,34,35, 40,41
miR-21	Upregulated in glioblastomas, AML (11q23), aggressive CLL and breast, colon, pancreatic, lung, prostate, liver and stomach cancers	Inhibits apoptosis and increases tumorigenicity	PTEN, PDCD4, TPM1 and TIMP3	ONC	31,37–39, 44–50
miR-372 and *miR-373*	Upregulated in testicular tumours	Promotes tumorigenicity in cooperation with RAS	LATS2	ONC	74

AML, acute myeloid leukaemia; BCL2, B cell leukaemia/lymphoma 2; BIM, Bcl2-interacting mediator of cell death; CLL, chronic lymphocytic leukaemia; DNMT, DNA methyltransferase; HMGA2, high mobility group AT-hook 2; LATS2, large tumour suppressor homologue 2; MCL1, myeloid cell leukaemia sequence 1; MDS, myelodysplastic syndrome; PDCD4, programmed cell death 4; PTEN, phosphatase and tensin homologue; SHIP1, SH2 domain-containing inositol-5'-phosphatase 1; TCL1, T cell lymphoma breakpoint 1; TIMP3, tissue inhibitor of metalloproteinases 3; TPM1, tropomyosin 1; WT1, Wilms tumour 1.

MiR155 transgene

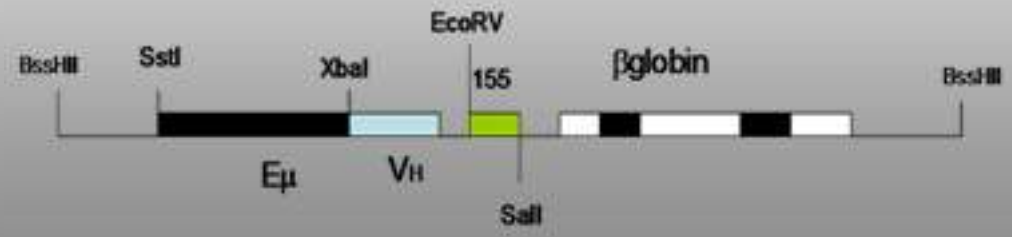

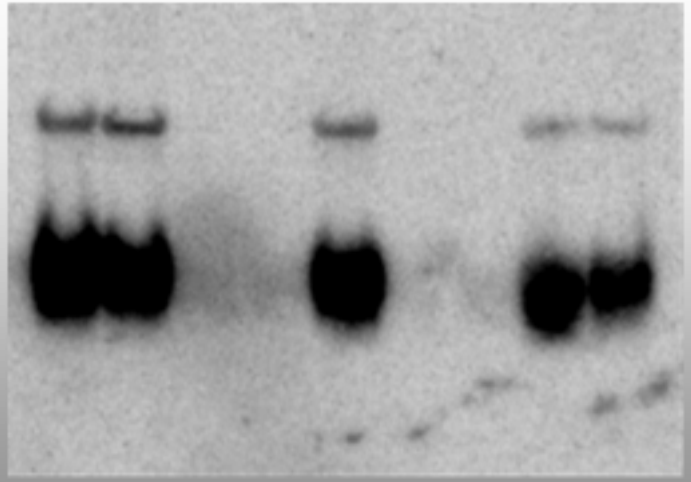

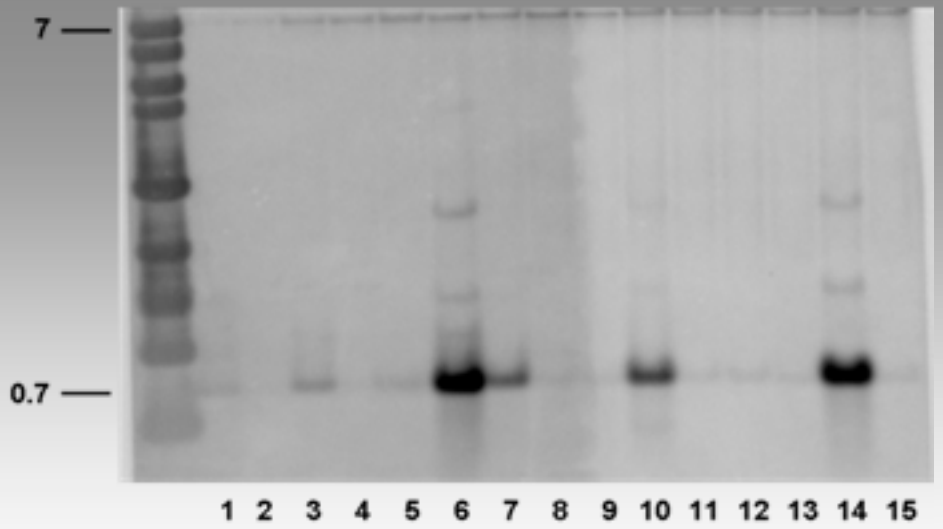

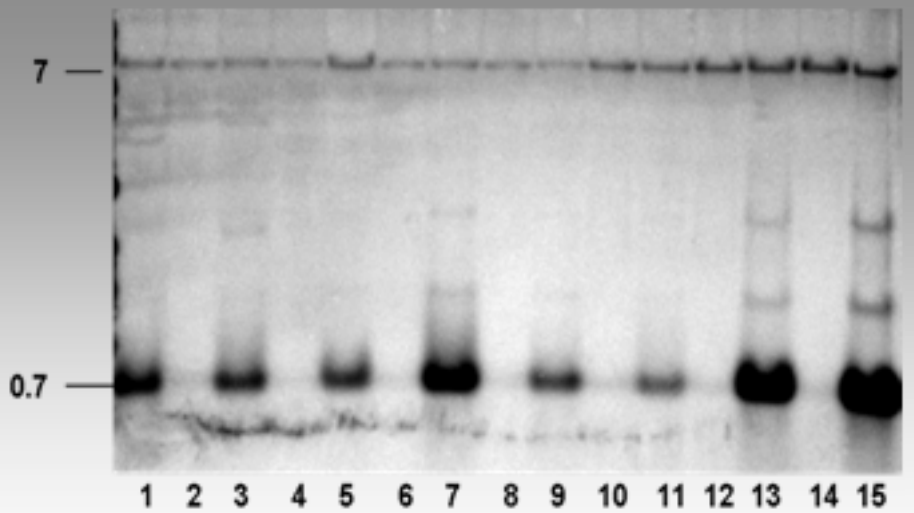

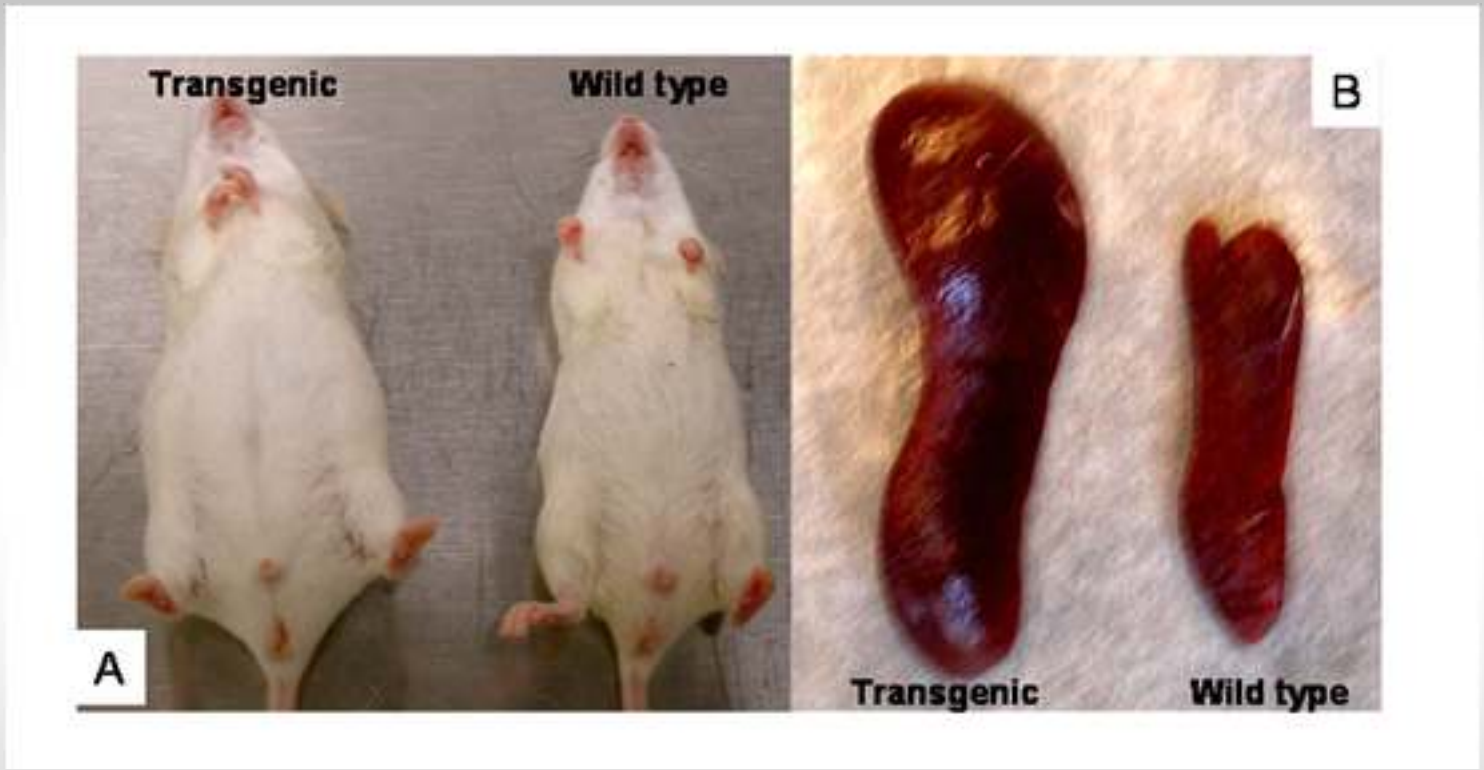
Transgenic
Wild type
A
B
Transgenic
Wild type

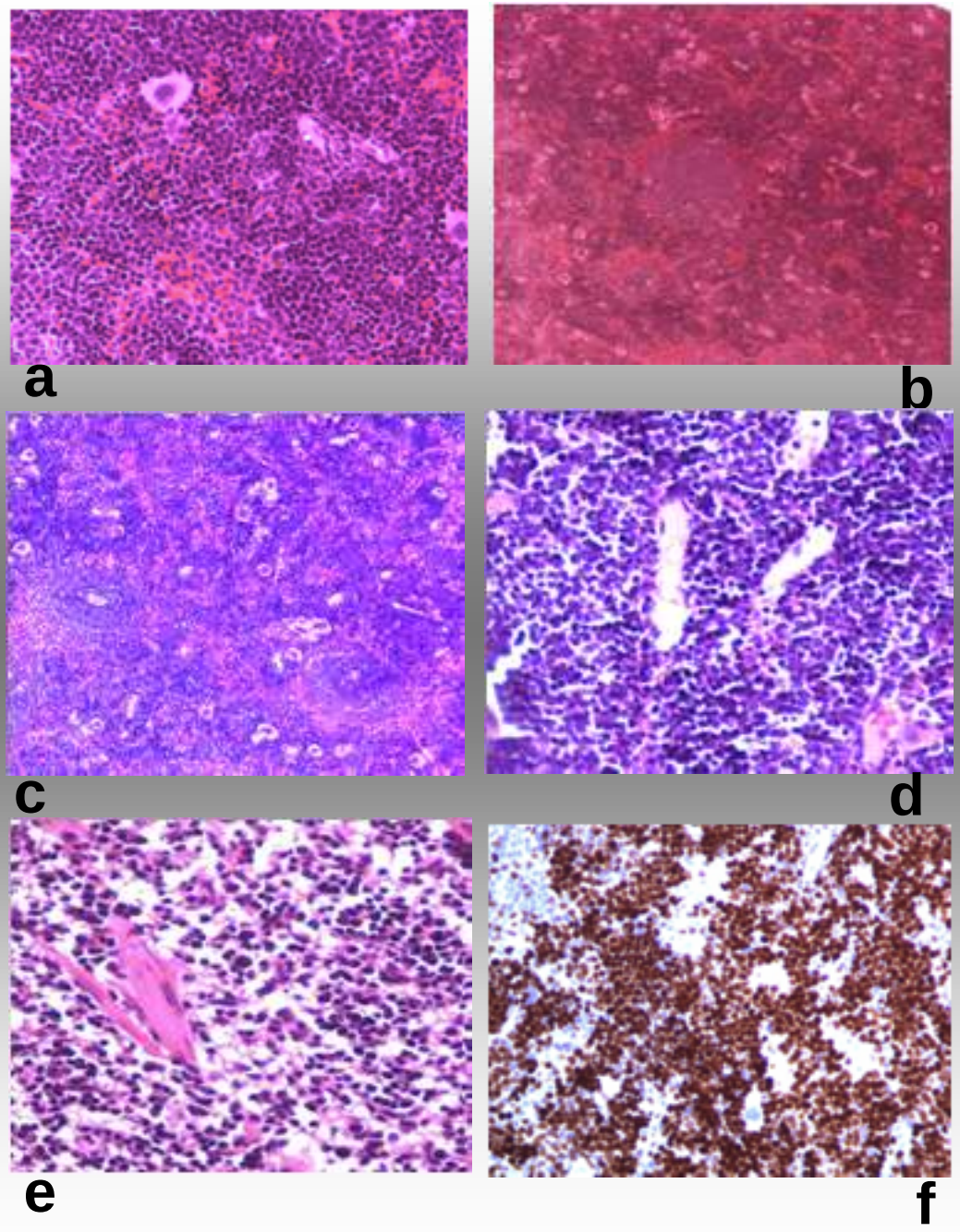
a
b
c
d
e
f

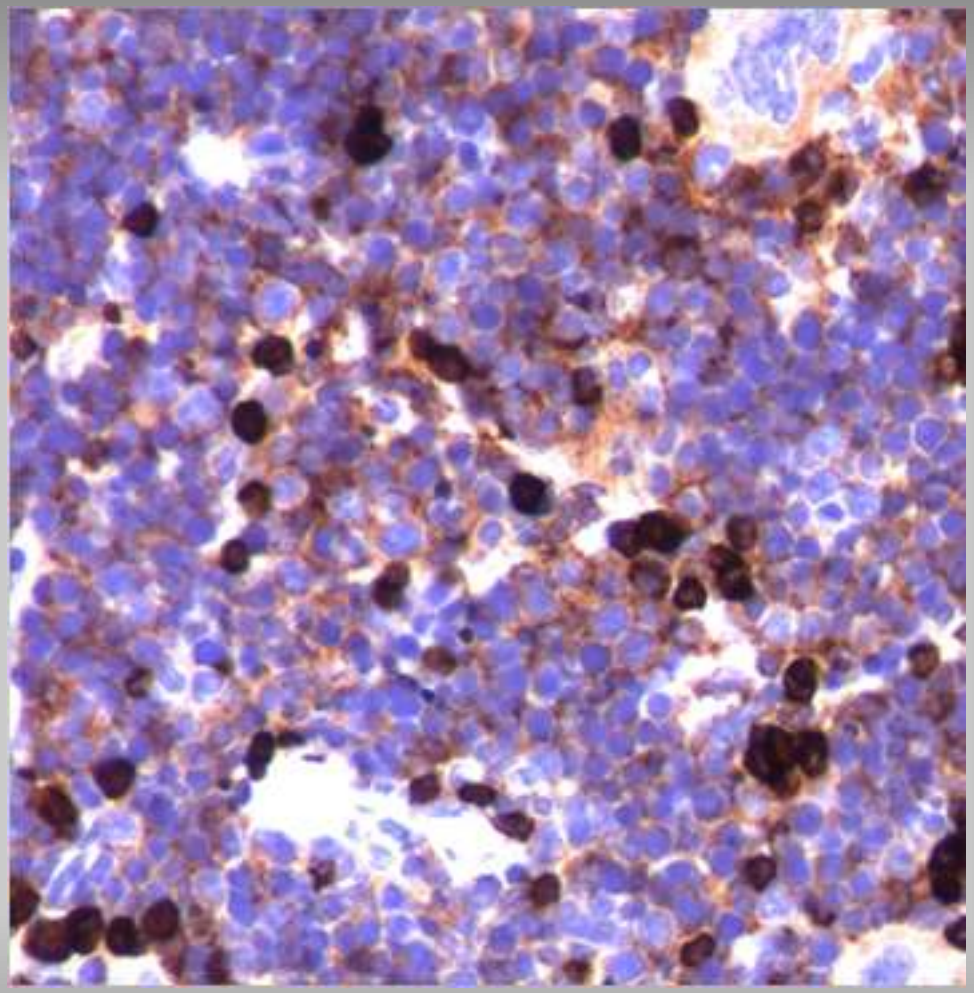

Examples of proteins down-regulated by the *miR-15a/16-1* cluster identified by proteomics in MEG-01 cells

Group	Protein	Gene description	Z-Score	Comments
Cell growth & cell cycle	Ruvbl1	RuvB-like 1; TATA binding protein interacting protein 49 KDa	2.01	—
	Sugt1	Suppressor of G2 allele of SKP1	2.43	—
	Cdc2	Cell division cycle 2, G_1 to S and G_2 to M	2.43	—
	Psf1	GINS complex subunit 1 (Psf1 homolog)	2.43	—
Antiapoptotic	Grp78	Heat shock 70-kDa protein 5 (glucose-related protein, 78 kDa)	2.43	—
	Bcl2	B-cell CLL/lymphoma 2	2.43	Predicted and validated target of miR-15a/16 (22)
	Pdia2	Protein disulfide isomerase family A, member 2	2.43	—
Oncogenesis	Wt1	Wilms tumor 1	2.43	Predicted target of miR-15a/16; Validated qRT-PCR in MEG-01
	MageB3	Melanoma antigen family B, 3	2.43	—
	Rab9B	RAB9B member RAS oncogene family	2.16	Predicted target of miR-15a/16
Others	Cdh26	Cadherin-like 26	2.43	—
	Crhbp	Corticotropin releasing hormone-binding protein	2.43	Predicted target of miR-16
	Actr1A	ARP1 actin-related protein 1 homolog A, centractin alpha	2.43	Predicted target of miR-15a/16
	Cshl1	Chorionic somatomammotropin hormone-like 1 precursor	2.43	Predicted target of miR-16
	Hla-B	Major histocompatibility complex, class I, B	2.43	—
	Tpi1	Triosephosphate isomerase 1	2.43	Predicted target of miR-15a/16
	Hsp90AB1	Heat shock protein 90-kD protein 1, β	2.43	—
	Cfl2	Cofilin 2	1.72	Predicted target of miR-16
	AldoA	Aldolase A, fructose-bisphosphate	2.43	—

Examples of the CLL signature of *miR-15a/16-1* down-regulated genes by microarray

Gene symbol	Map	Gene name	P	
			CLL	MEG-01
HSDL2	9q32	Hydroxysteroid dehydrogenase like 2	0.00178	0.00254
SLC35A1	6q15	Solute carrier family 35 (CMP-sialic acid transporter), member A1	0.00178	0.00341
ECHDC1	6q22.33	Enoyl coenzyme A hydratase domain containing 1	0.00323	0.00582
CARD8	19q13.32	Caspase recruitment domain family, member 8	0.00446	0.00078
OMA1	1p32.2-p32.1	OMA1 homolog, zinc metallopeptidase (S. cerevisiae)	0.00446	0.0158
UGP2	2p14-p13	UDP-glucose pyrophosphorylase 2	0.00446	0.000629
CREBL2	12p13	cAMP responsive element binding protein-like 2	0.00457	0.0199
Cep63	3q22.1	Centrosome protein Cep63	0.0049	0.0137
PNN	14q21.1	Pinin, desmosome-associated protein	0.0049	0.00359
TRA1	12q24.2-q24.3	Tumor rejection antigen (gp96) 1	0.00496	0.0211
SLC35B3	6p24.3	Solute carrier family 35, member B3	0.00601	0.0208
RHOT1	17q11.2	Ras homolog gene family, member T1	0.00695	0.0197
LARS	5q32	Leucyl-tRNA synthetase	0.00696	0.00239
RAD51C	17q22-q23	RAD51 homolog C (S. cerevisiae)	0.0075	0.00334
WASPIP	2q31.1	Wiskott–Aldrich syndrome protein interacting protein	0.00783	0.0108
MCL1	1q21	Myeloid cell leukemia sequence 1 (BCL2-related)	0.00863	0.011
ASXL2	2p24.1	Additional sex combs like 2 (Drosophila)	0.00875	0.000503
ARFIP1	4q31.3	ADP-ribosylation factor interacting protein 1 (arfaptin 1)	0.0114	0.0108
HERC6	4q22.1	Hect domain and RLD 6	0.0116	0.00107
TIA1	2p13	TIA1 cytotoxic granule-associated RNA-binding protein	0.0116	0.0116
VPS45A	1q21-q22	Vacuolar protein sorting 45a (yeast)	0.0117	0.000788
HLC-8	17q25.1	Lung cancer-related protein 8	0.0124	0.0164
HACE1	6q21	HECT domain and ankyrin repeat containing, E3 ubiquitin protein ligase 1	0.0125	0.0115
ARV1	1q42.2	ARV1 homolog (yeast)	0.0156	0.000825
NT5C2L1	6q22.1	5′ nucleotidase, cytosolic II-like 1	0.0172	0.0139
PDCD6IP	3p23	Programmed cell death 6 interacting protein	0.0214	0.00276
GTF2H1	11p15.1-p14	General transcription factor IIH, polypeptide 1, 62 kda	0.0217	0.00125
MSH2	2p22-p21	mutS homolog 2, colon cancer, nonpolyposis type 1 (E. coli)	0.0242	0.00192
JUN	1p32-p31	v-jun sarcoma virus 17 oncogene homolog (avian)	0.0281	0.00059
ALDH6A1	14q24.3	Aldehyde dehydrogenase 6 family, member A1	0.0297	0.00798
SCAP2	7p21-p15	Src family-associated phosphoprotein 2	0.0298	0.0108

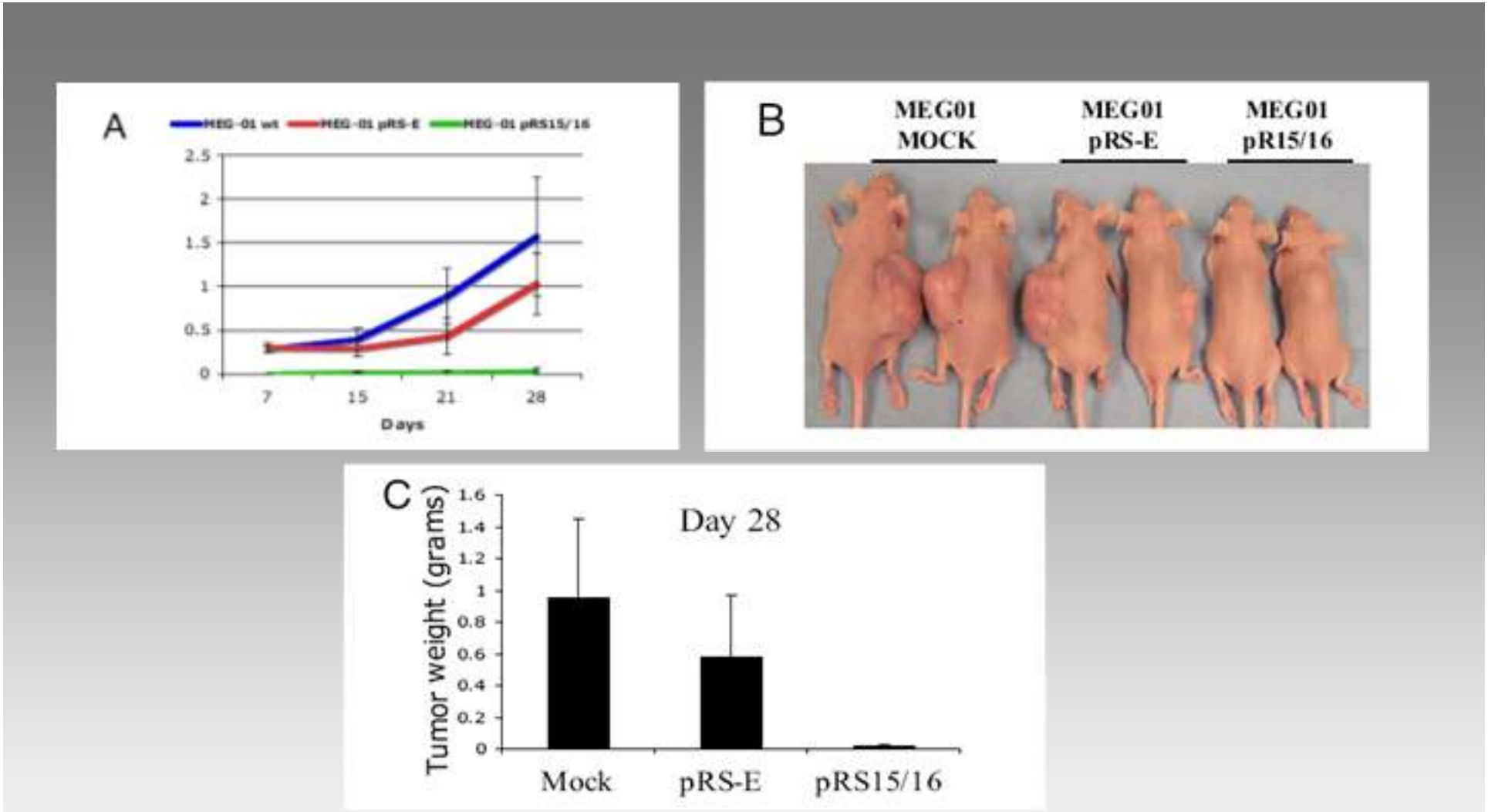

MiR15a/16-1 cluster inhibits the growth of MEG-01 tumor engraftments in nude mice. (*A*) Growth curve of engrafted tumors in nude mice injected with MEG-01 cells pretransfected with pRS-E or pRS15/16 or mock transfected. (*B*) Comparison of tumor engraftment sizes of mock-, pRS-E-, and pRS15/16-transfected MEG-01 cells 28 days after injection in nude mice. (*C*) Tumor weights SD in nude mice.

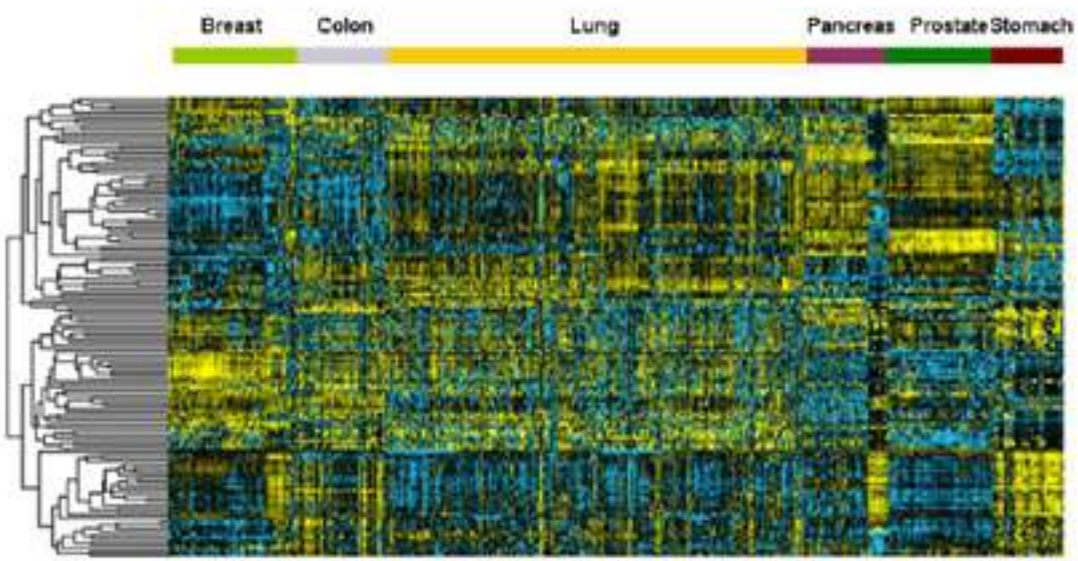

Clustering analysis of 540 samples representing 6 solid cancers and the respective normal tissues. MiRNAs were included in the tree when their expression level (background-subtracted intensity) was higher than the threshold value (256) in at least 50% of the samples. One hundred thirty seven microRNAs were retained for clustering. Arrays were median-centered and normalized by using Gene Cluster 2.0. Average linkage clustering was performed by using uncentered correlation metric.

Table 7. miRNAs used to classify human cancers and normal tissues

Cancer	Up-regulated miRs	Down-regulated miRs	Misclassification error after 10-fold cross validation
Breast	15	12	0.08
Colon	21	1	0.09
Lung	35	3	0.31
Pancreas	55	2	0.02
Prostate	39	6	0.11
Stomach	22	6	0.19

Median normalization was performed, and the method of the nearest shrunken centroids was used to select predictive miRNAs (28).

Table 8 The miRNAs shared by the signatures of the six solid cancers

miR	*N*	Tumor type
miR-21	6	Breast, colon, lung, pancreas, prostate, stomach
miR-17-5p	5	Breast, colon, lung, pancreas, prostate
miR-191	5	Colon, lung, pancreas, prostate, stomach
miR-29b-2	4	Breast, colon, pancreas, prostate
miR-223	4	Colon, pancreas, prostate, stomach
miR-128b	3	Colon, lung, pancreas
miR-199a-1	3	Lung, pancreas, prostate
miR-24-1	3	Colon, pancreas, stomach
miR-24-2	3	Colon, pancreas, stomach
miR-146	3	Breast, pancreas, prostate
miR-155	3	Breast, colon, lung
miR-181b-1	3	Breast, pancreas, prostate
miR-20a	3	Colon, pancreas, prostate
miR-107	3	Colon, pancreas, stomach
miR-32	3	Colon, pancreas, prostate
miR-92-2	3	Pancreas, prostate, stomach
miR-214	3	Pancreas, prostate, stomach
miR-30c	3	Colon, pancreas, prostate
miR-25	3	Pancreas, prostate, stomach
miR-221	3	Colon, pancreas, stomach
miR-106a	3	Colon, pancreas, prostate

The list includes 21 commonly up-regulated microRNAs in 3 or more (*N*) types of solid cancers (*P* value = 2.5×10^{-3}).

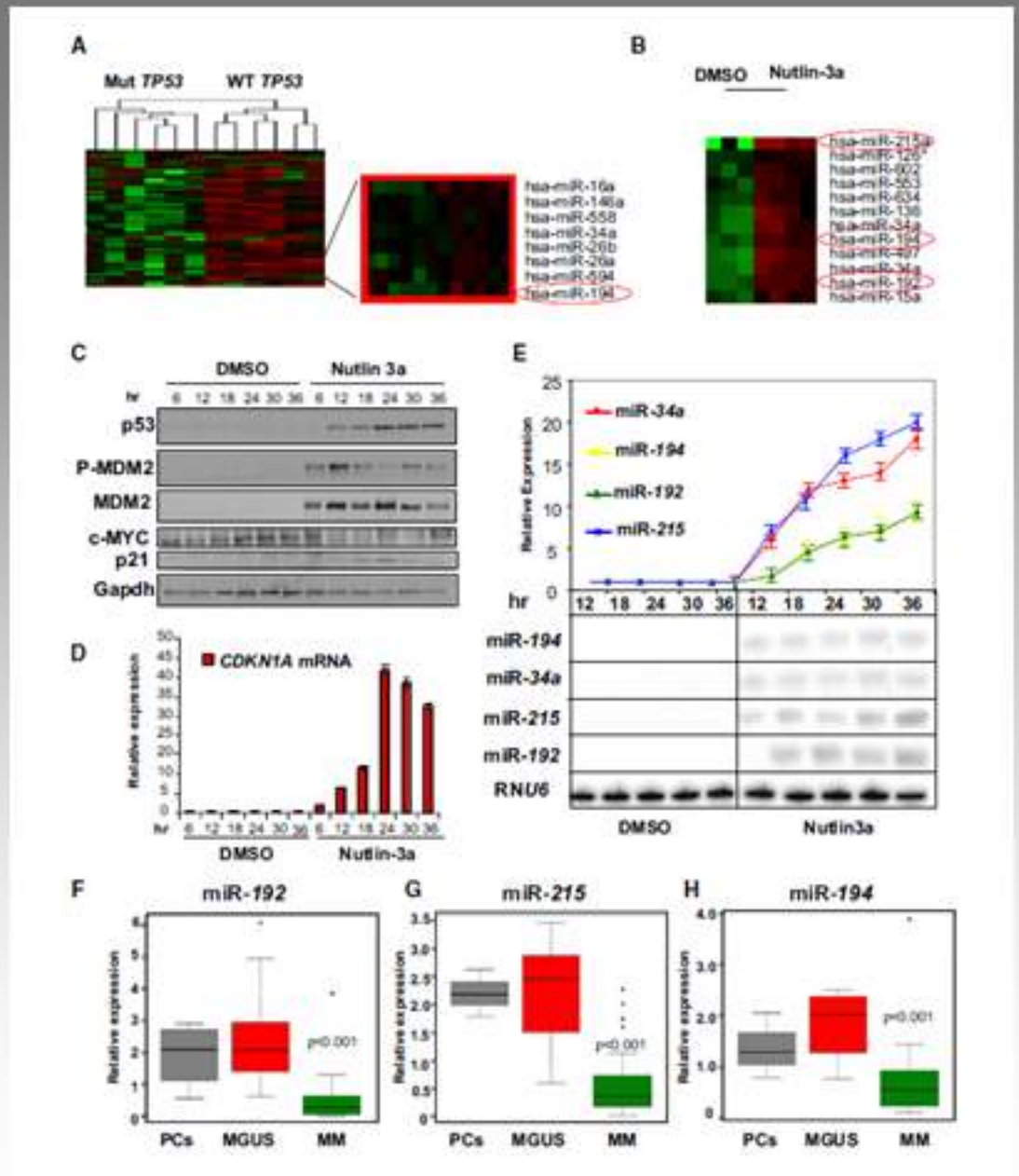
A
Mut TP53
WT TP53
hsa-miR-16a
hsa-miR-146a
hsa-miR-558
hsa-miR-34a
hsa-miR-26b
hsa-miR-26a
hsa-miR-594
hsa-miR-194
B
DMSO
Nutlin-3a
hsa-miR-215
hsa-miR-192
hsa-miR-194
hsa-miR-34a
C
DMSO
Nutlin 3a
hr
6 12 18 24 30 36 6 12 18 24 30 36
p53
P-MDM2
MDM2
c-MYC
p21
Gapdh
D
CDKN1A mRNA
Relative expression
DMSO
Nutlin-3a
E
miR-34a
miR-194
miR-192
miR-215
Relative Expression
hr
12 18 24 30 36 12 18 24 30 36
miR-194
miR-34a
miR-215
miR-192
RNU6
DMSO
Nutlin3a
F
miR-192
G
miR-215
H
miR-194
Relative expression
p<0.001
PCs
MGUS
MM

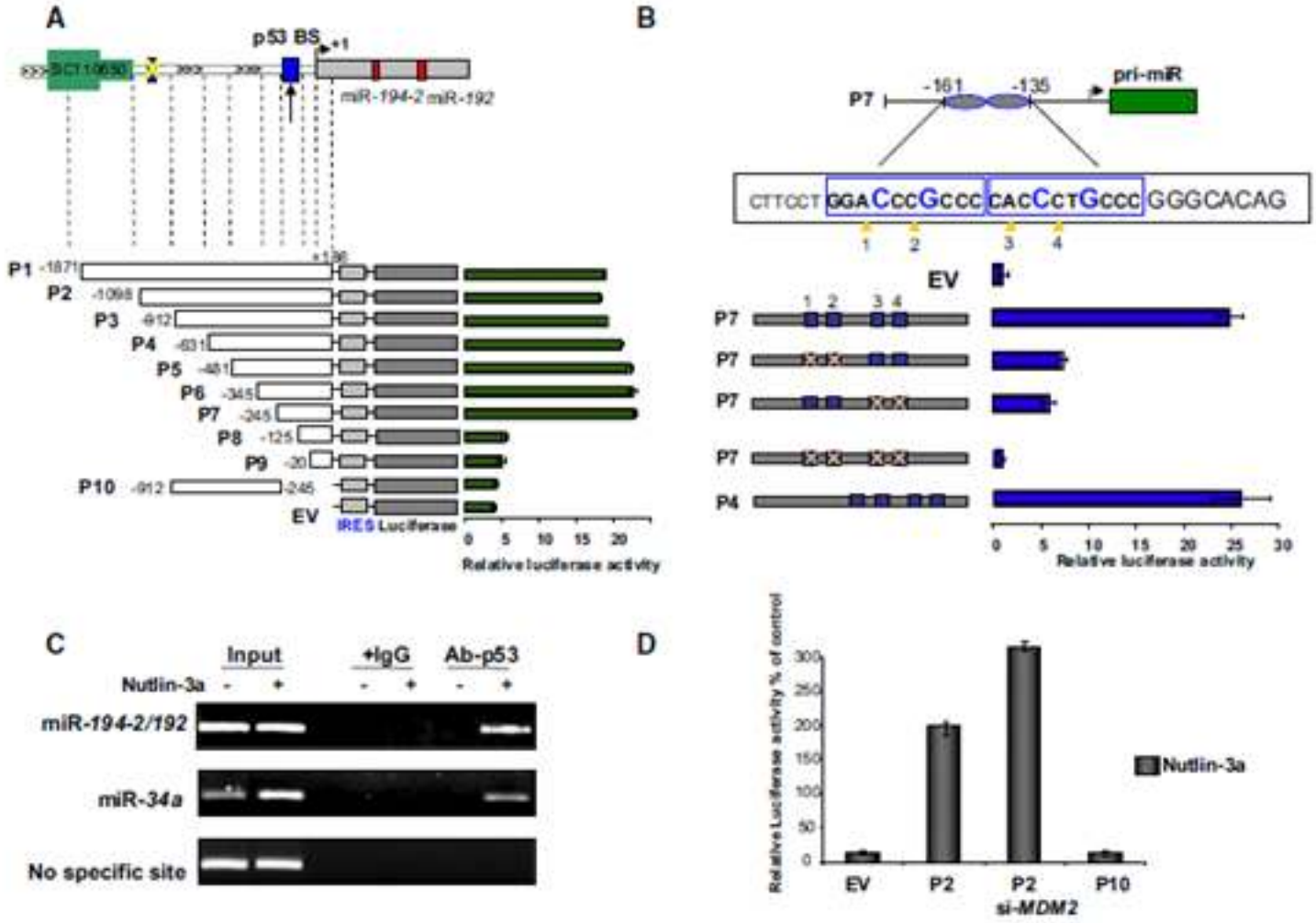

Figure 2. miR-194-2-192 Cluster Is Induced Following p53 Activation

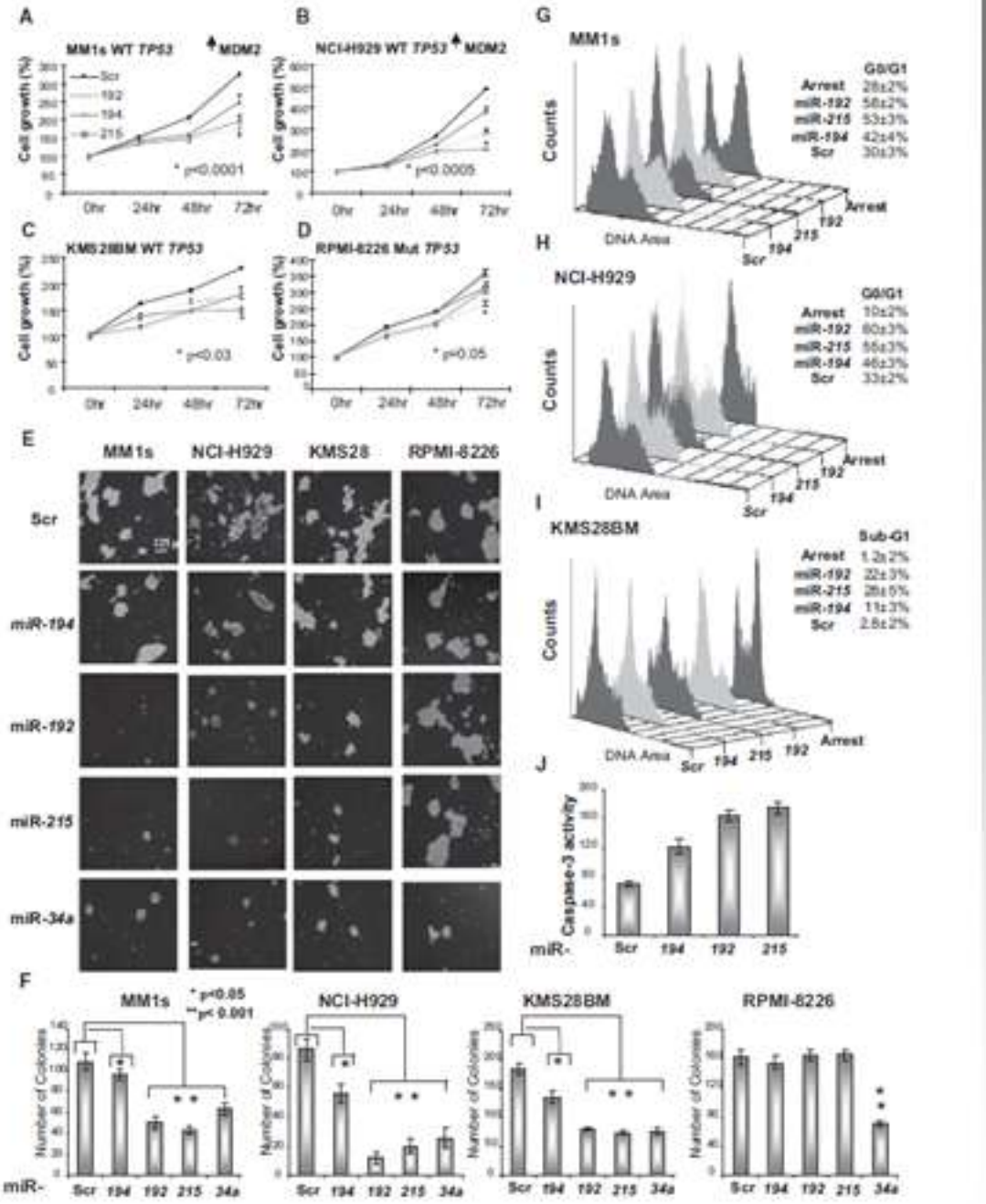

Figure 3. miR-192-194-215 Induce Decrease of Proliferation and Cell-Cycle Arrest in WT TP53 MM Cells

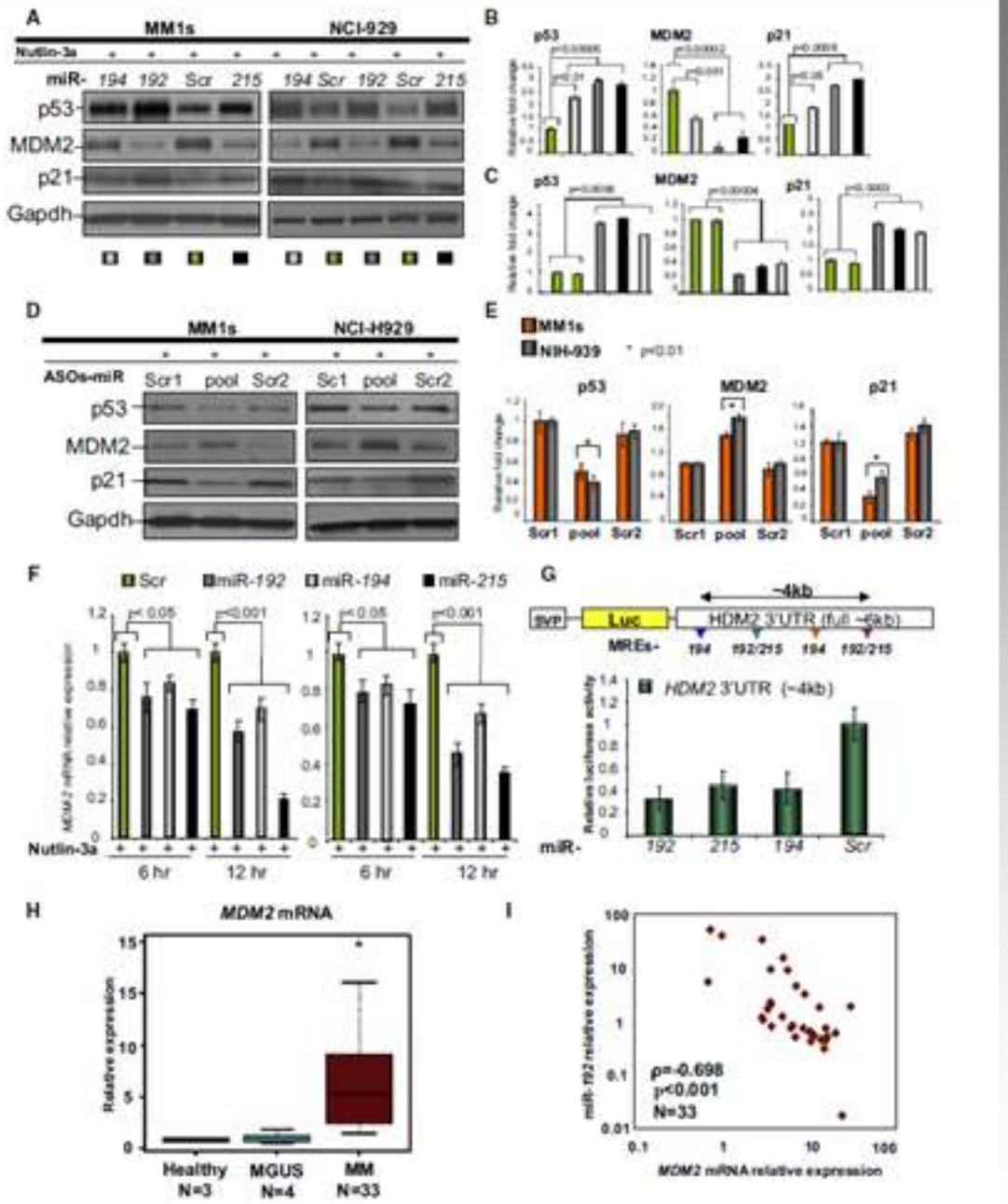

Figure 4. miRNA-192-194 and 215 Target MDM2 at the mRNA and Protein Levels in MM Cells

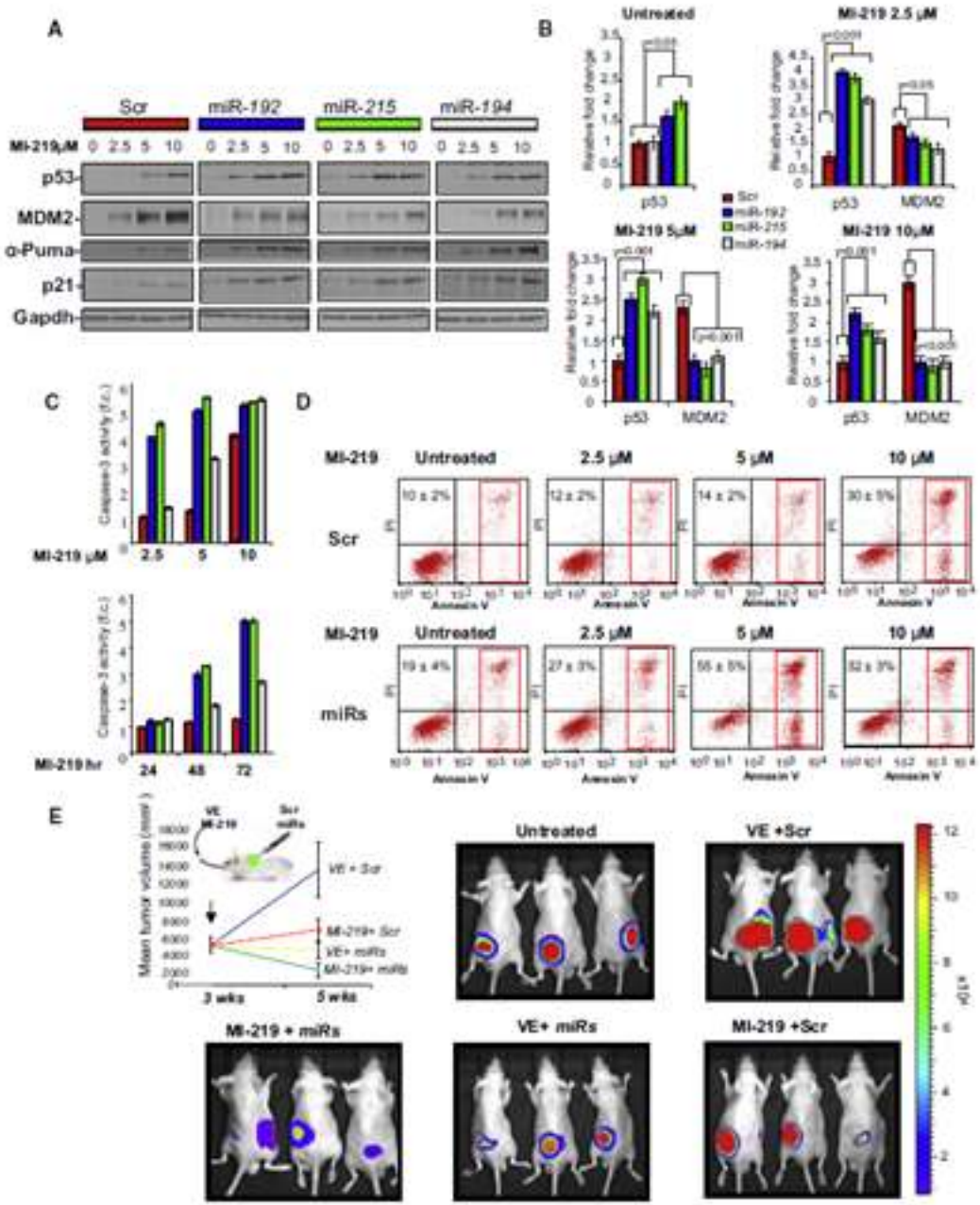

Figure 5. miR-192, 194, and 215 Increase Sensitivity to MI-219 In Vitro and In Vivo by Targeting *MDM2*

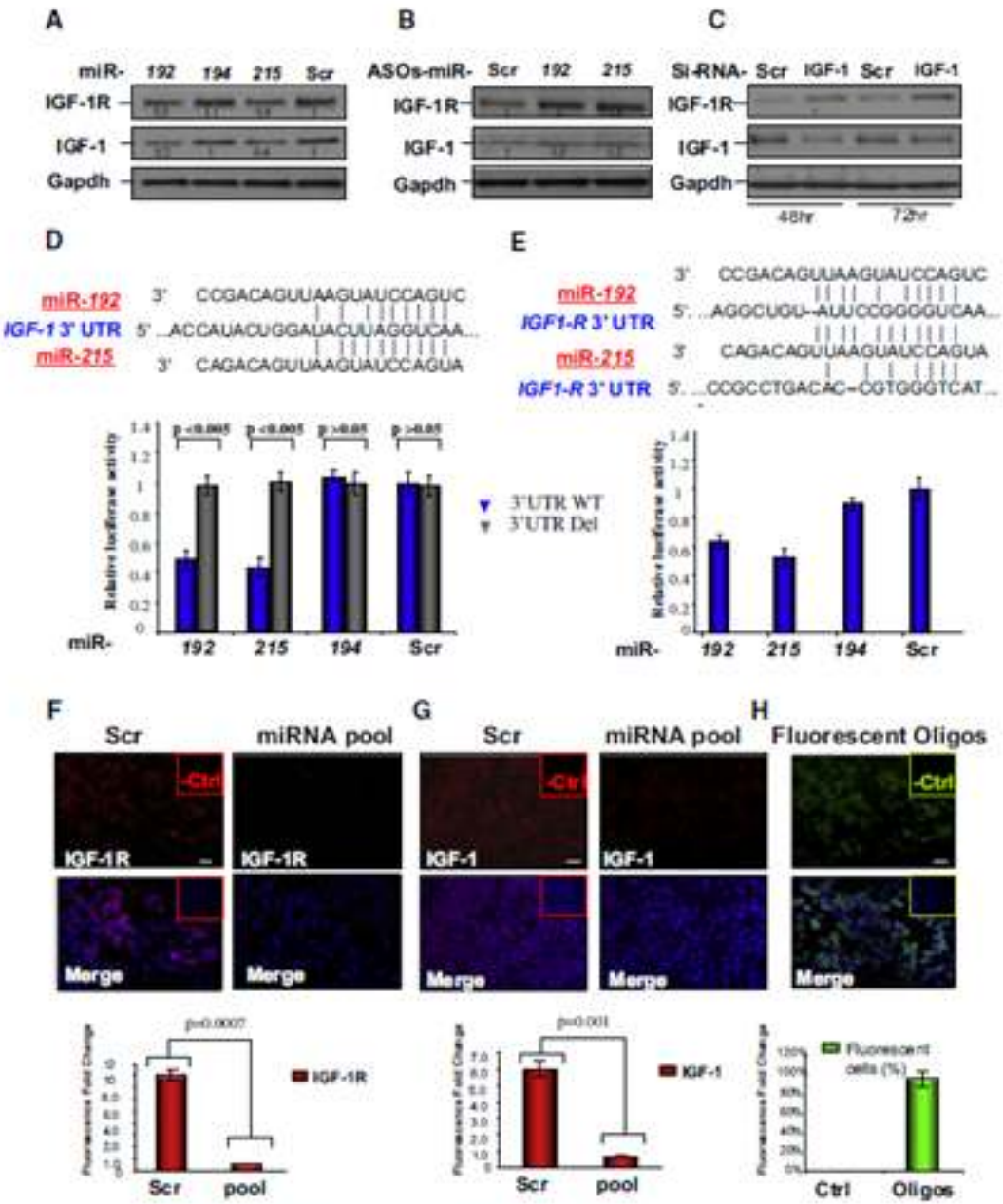

Figure 6. miR-192-215 Regulate IGF-1 and IGF1-R Expression in MM Cells

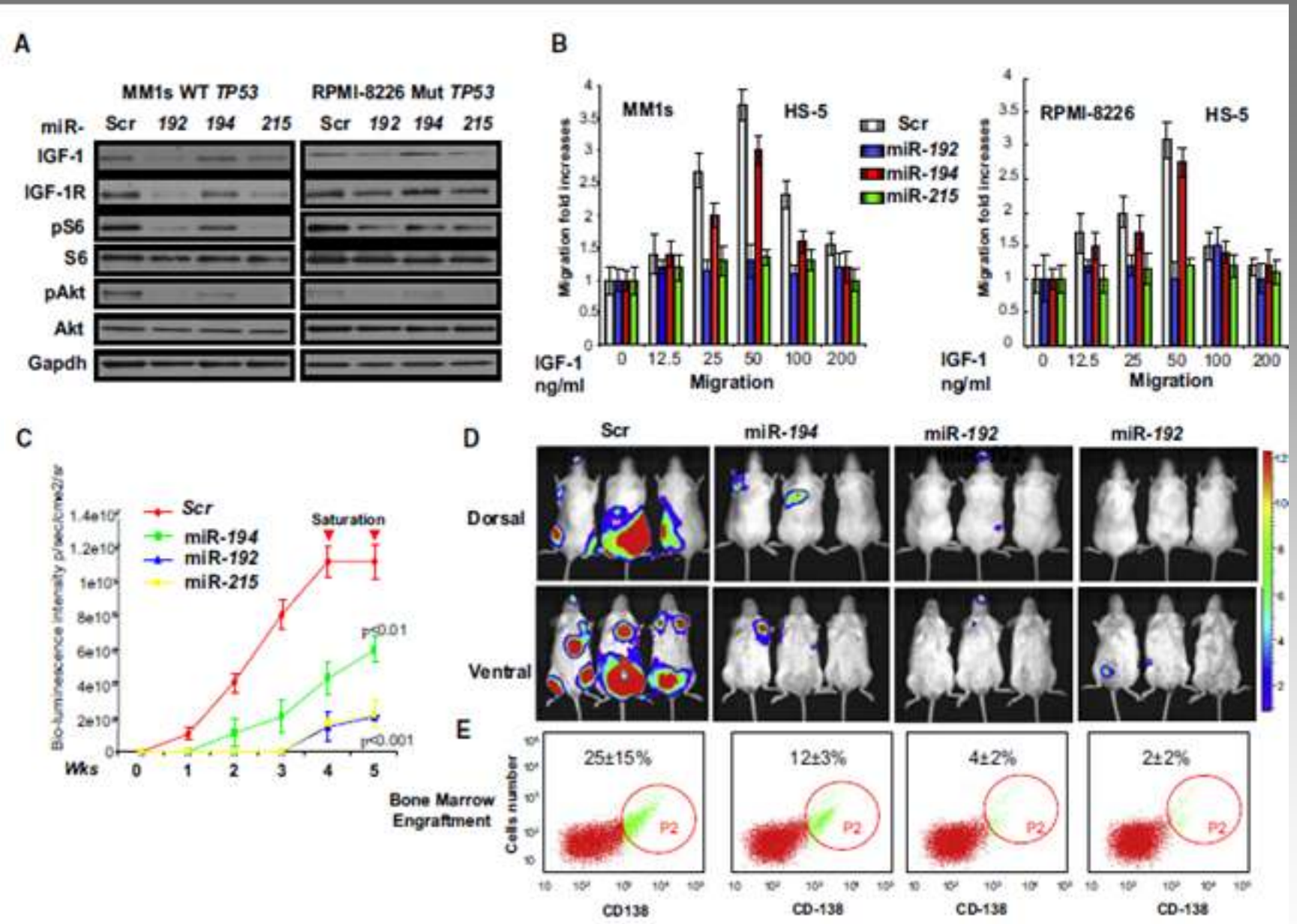

Figure 7. miR-*194*, *215*, and *194* Block Invasion Ability of MM Cells

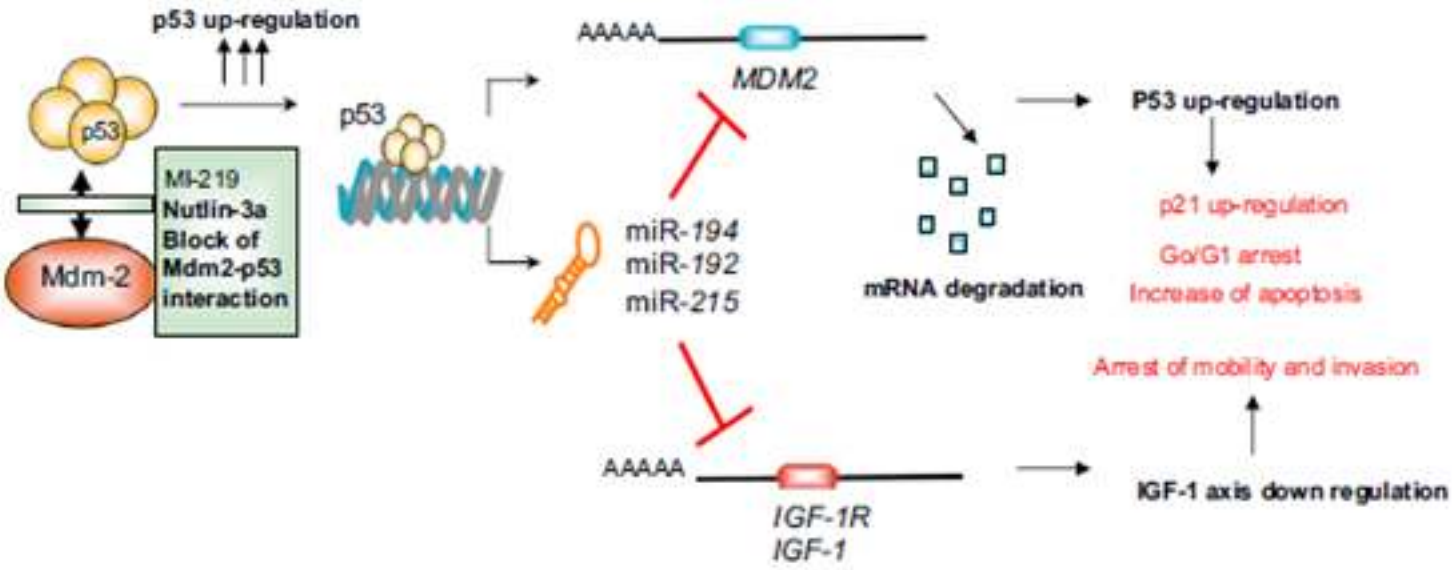

Figure 8. miR-*192*, *215*, and *194* Impair the p53/MDM2 Autoregulatory Loop

Modulation of mismatch repair and genomic stability by miR-155

Nicola Valeri[a,b,1], Pierluigi Gasparini[a,1], Muller Fabbri[a,c,1], Chiara Braconi[d], Angelo Veronese[a], Francesca Lovat[a], Brett Adair[a], Ivan Vannini[e], Francesca Fanini[e], Arianna Bottoni[a], Stefan Costinean[a], Sukhinder K. Sandhu[a], Gerard J Nuovo[a], Hansjuerg Alder[a], Roberta Gafà[f], Federica Calore[a], Manuela Ferracin[f], Giovanni Lanza[f], Stefano Volinia[a,b], Massimo Negrini[f], Michael A. McIlhatton[a], Dino Amadori[c], Richard Fishel[a,g,2], and Carlo M. Croce[a,2,3]

[a]Department of Molecular Virology, Immunology and Medical Genetics, Ohio State University Medical Center and Comprehensive Cancer Center, Columbus, OH 43210; [b]Department of Embryology and Morphology, University of Ferrara, Ferrara 44121, Italy; [c]Istituto Scientifico Romagnolo per lo Studio e la Cura dei Tumori, Meldola (FORI, Italy; [d]Department of Internal Medicine, Ohio State University Medical Center and Comprehensive Cancer Center, Columbus, OH 43210; [e]Department of Pathology, Ohio State University Medical Center, Columbus, OH 43210; [f]Department of Experimental and Diagnostic Medicine, University of Ferrara, Ferrara 44121, Italy; and [g]Department of Physics, Ohio State University, Columbus, OH 43210

Contributed by Carlo M. Croce, February 25, 2010 (sent for review February 5, 2010)

Inactivation of mismatch repair (MMR) is the cause of the common cancer predisposition disorder Lynch syndrome (LS), also known as hereditary nonpolyposis colorectal cancer (HNPCC), as well as 10–40% of sporadic colorectal, endometrial, ovarian, gastric, and urothelial cancers. Elevated mutation rates (mutator phenotype), including simple repeat instability (microsatellite instability (MSI)) are a signature of MMR defects. MicroRNAs (miRs) have been implicated in the control of critical cellular pathways involved in development and cancer. Here we show that overexpression of miR-155 significantly down-regulates the core MMR proteins, hMSH2, hMSH6, and hMLH1, inducing a mutator phenotype and MSI. An inverse correlation between the expression of miR-155 and the expression of MLH1 or MSH2 proteins was found in human colorectal cancer. Finally, a number of MSI tumors with unknown cause of MMR inactivation displayed miR-155 overexpression. These data provide support for miR-155 modulation of MMR as a mechanism of cancer pathogenesis.

colorectal cancer | DNA repair | microRNA

Mismatched nucleotides may arise from polymerase misincorporation errors, recombination between heteroallelic parental chromosomes, or chemical and physical damage to the DNA (1). MutS homologs (MSH) and MutL homologs (MLH/PMS) are highly conserved proteins that are essential for the mismatch repair (MMR) excision reaction (2). In human cells, hMSH2 and hMLH1 are the fundamental components of MMR. The hMSH2 protein forms a heterodimer with hMSH3 or hMSH6 and is required for mismatch/lesion recognition, whereas the hMLH1 protein forms a heterodimer with hMLH3 or hPMS2 and forms a ternary complex with MSH heterodimers to complete the excision repair reaction (2, 3). Human cells contain at least 10-fold more of the hMSH2-hMSH6/hMLH1-hPMS2 complex, which repairs single nucleotide and small insertion-deletion loop (IDL) mismatches, compared with the hMSH2-hMSH3/hMLH1-hMLH3 complex, which primarily repairs large IDL mismatches (4–6). In addition to MMR, the hMSH2-hMSH6/hMLH1-hPMS2 components have been uniquely shown to recognize lesions in DNA and to signal cell cycle arrest and apoptosis (7, 8).

Mutations in the hMSH2, hMSH6, hMLH1, and *hPMS2* core MMR genes have been linked to Lynch syndrome (LS), also known as hereditary nonpolyposis colorectal cancer (HNPCC) (9). These observations have provided considerable support for the mutator hypothesis, because defects in the *MSH* and *MLH/PMS* genes significantly increase cellular mutation rates, which then may drive the evolution of numerous oncogenic and tumor-suppressor gene mutations found in cancers (10). The most obvious signature of a mutator phenotype is instability of simple repeat sequences or microsatellite DNA [ie., microsatellite instability (MSI)] (11, 12). Virtually all LS/HNPCC tumors display MSI resulting from mutation or inherited epigenetic inactivation of the core MMR genes (13–15). Most of the 10–40% of sporadic CRC, endometrial, ovarian, gastric, and urothelial tumors that display MSI are a result of acquired *hMLH1* promoter methylation (16). Approximately 95% of MSI tumors can be accounted for, at least partially, by mutation and/or epigenetic inactivation of the core MMR components (14). The remaining 5%, as well as a significant proportion of the biallelic MMR inactivation mechanism, remain poorly understood.

MicroRNAs (miRs) are noncoding RNAs that play a role in the posttranscriptional regulation of >30% of the human genes controlling critical biological processes, including development, cell differentiation, apoptosis, and proliferation (17, 18). Overexpression of miR-155 has been observed in CRC (19–21), and appears to be more frequent in MSI than MSS CRCs (22). These data are consistent with the hypothesis that miR-155 might regulate components of the MMR machinery and, consequently, rates of mutation and MSI.

Results

hMLH1, hMSH2, and hMSH6 Are Targets of miR-155. We used in silico prediction models to identify potential binding sites for miR-155 in the mRNA of the core MMR genes (23, 24). Two putative sites were found in *hMLH1* using RNAhybrid (BiBiServ; NCBI NM_000249.2), one in the 3′-UTR and the other in the coding sequence (CDS) (NCBI NM_000249.2). One site was found in the 3′-UTR of *hMSH2* using TargetScan (Whitehead Institute, MIT; NCBI NM_000251.1), and one site was found in the CDS of *hMSH6* using RNAhybrid (BiBiServ; NCBI NM_000179.2) (Fig. 1*A* and Fig. S1). As a functional screen, we subcloned the coding and 3′-regions including the predicted miR-155 seed regions of *MLH1*, *MSH2*, or *MSH6* downstream of the luciferase gene and recorded luciferase protein activity (25). We used MMR-proficient Colo-320 DM CRC cells for these studies, because they contain a low basal level of miR-155 (26). The Colo-320 DM cells were transfected with the luciferase reporter constructs and with a miR-155 precursor (premiR-155) or con-

Author contributions: N.V., P.G., M. Fabbri, R.F., and C.M.C. designed research; N.V., P.G., M. Fabbri, A.V., F.L., B.A., I.V., F.F., A.B., S.C., S.S., G.J.N., H.A., F.C., M. Ferracin, G.L., S.V., M.M., M.A.M., and D.A. performed research; R.A. contributed new reagents/analytic tools; N.V., P.G., M. Fabbri, C.B., A.V., G.J.N., M.M., R.F., and C.M.C. analyzed data; and N.V., P.G., M. Fabbri, C.B., R.F., and C.M.C. wrote the paper.

The authors declare no conflict of interest.

Freely available online through the PNAS open access option.

N.V., P.G., and M. Fabbri contributed equally to this work.

[2]To whom correspondence may be addressed. E-mail: carlo.croce@osumc.edu or rfishel@osu.edu.

This article contains supporting information online at www.pnas.org/cgi/content/full/1002472107/DCSupplemental.

MicroRNA-21 induces resistance to 5-fluorouracil by down-regulating human DNA MutS homolog 2 (hMSH2)

Nicola Valeri[a,b,c,1], Pierluigi Gasparini[a,b,1], Chiara Braconi[b,d], Alessio Paone[a,b], Francesca Lovat[a,b], Muller Fabbri[a,b,e], Khlea M. Sumani[a,b], Hansjuerg Alder[a,b], Dino Amadori[e], Tushar Patel[b,f], Gerard J. Nuovo[f], Richard Fishel[a,b,g,2], and Carlo M. Croce[a,b,h,2]

Departments of [a]Molecular Virology, Immunology, and Medical Genetics, [b]Internal Medicine, [c]Pathology, and [g]Physics, and [h]Ohio State University Comprehensive Cancer Center, Ohio State University, Columbus, OH 43210; Departments of [d]Embryology and Morphology and [e]Experimental and Diagnostic Medicine, University of Ferrara, 44011 Ferrara, Italy; and [f]Istituto Scientifico Romagnolo per lo Studio e la Cura dei Tumori, 47014 Meldola, Italy

Contributed by Carlo M. Croce, October 19, 2010 (sent for review September 22, 2010)

The overexpression of microRNA-21 (miR-21) is linked to a number of human tumors including colorectal cancer, where it appears to regulate the expression of tumor suppressor genes including p21, phosphatase and tensin homolog, TGFβ receptor II, and B-cell leukemia/lymphoma 2 –associated X protein. Here we demonstrate that miR-21 targets and down-regulates the core mismatch repair (MMR) recognition protein complex, human mutS homolog 2 (hMSH2) and 6 (hMSH6). Colorectal tumors that express a high level of miR-21 display reduced hMSH2 protein expression. Cells that overproduce miR-21 exhibit significantly reduced 5-fluorouracil (5-FU)–induced G2/M damage arrest and apoptosis that is characteristic of defects in the core MMR component. Moreover, xenograft studies demonstrate that miR-21 overexpression dramatically reduces the therapeutic efficacy of 5-FU. These studies suggest that the down-regulation of the MMR mutator gene associated with miR-21 overexpression may be an important clinical indicator of therapeutic efficacy in colorectal cancer.

colon cancer | non coding RNA | DNA repair

Colorectal cancer (CRC) is one of the most frequently occurring cancers in United States with more than 140,000 new cases and about 50,000 deaths expected to occur in 2010 (1). 5-fluorouracil (5-FU)–based chemotherapy represents the gold standard for CRC treatment both in the adjuvant and metastatic setting (2). However, primary or acquired resistance to pyrimidine analog treatments is a common problem in the management of CRC patients (2). These observations highlight the need for a better understanding of resistance mechanisms and more effective therapies.

MicroRNAs are a class of small, noncoding RNAs that act as posttranscriptional regulators of gene expression and cell homeostasis (3). Overexpression of miR-21 is a common trait of many solid and hematological malignancies (4). miR-21 overexpression has been found in blood and stool samples from patients affected by CRC (5, 6). Moreover, miR-21 overexpression is associated with poor benefit from 5-FU adjuvant chemotherapy in stage-II and -III CRC (7).

The mismatch repair (MMR) system is involved in DNA damage recognition and repair. Human mutS homolog 2 (hMSH2) and human mutL homolog 1 (hMLH1) function as core MMR proteins and form heterodimers with protein homologs hMSH3 or hMSH6 and hMLH3 or hPMS2, respectively (8). Heterodimer formation is fundamental for the DNA damage recognition and represents a crucial step for the stability of the MMR protein homologs (9). Defects in MMR proteins have been associated with reduced or absent benefit from 5-FU adjuvant chemotherapy in clinical trials (10). MMR impairment appears to cause reduced incorporation of 5-FU metabolites into DNA, leading to reduced G2/M arrest and apoptosis after 5-FU treatment (11, 12).

Results

miR-21 Directly Targets hMSH2 and hMSH6 Protein Expression. *In silico* analysis suggested that miR-21 might target *hMSH2* [National Center for Biotechnology Information (NCBI) NM_000249.2] and *hMSH6* (NCBI NM_000179.2) mRNA (TargetScan, Whitehead Institute, MIT; Fig. S1) (13). We identified putative binding sites for miR-21 in both the *hMSH2* and the *hMSH6* 3′ UTR. We examined the effect of miR-21 expression on endogenous *hMSH2* and *hMSH6* mRNA expression in CRC Colo-320DM and SW620 cells. Both cell lines display low basal miR-21 expression. We transfected these cell lines with miR-21 precursor or a scrambled miR precursor control (Fig. S2). Overexpression of an siRNA specific to *hMSH2* (anti-MSH2) or *hMSH6* (anti-MSH6) did not affect the levels of miR-21 (Fig. S3*A*). The mRNA levels of *hMSH2* and *hMSH6* were unaffected by overexpression of miR-21 (Fig. 1*B*). In contrast, anti-MSH2 and anti-MSH6 siRNA specifically reduced the expression of *hMSH2* and *hMSH6* mRNA, respectively (Fig. 1*B*). We note a consistent reduction in the expression of *hMSH6* mRNA with the anti-MSH2 siRNA. This reduction could be a result of degenerate hybridization of the anti-MSH2 siRNA with the *hMSH6* mRNA or of reduced *hMSH6* mRNA stability resulting from the diminished heteroduplex protein partner hMSH2. These results suggest that miR-21 overexpression does not affect the mRNA levels of *hMSH2* or *hMSH6*.

We examined the protein levels of hMSH2 and hMSH6 following transfection of miR-21 in Colo-320DM and SW620 cells by Western blot analysis (Fig. 1*C* and Fig. S3*B*). hMSH2 and hMSH6 protein were significantly reduced in cells overexpressing miR-21 compared with cells overexpressing the scrambled miR. The anti-MSH2 and anti-MSH6 siRNA were transfected in these cell lines in parallel. We observed that cells transfected with miR-21 displayed a down-regulation of hMSH2 and hMSH6 that appeared comparable to levels in cells transfected with siRNAs. Conversely, we transfected CRC SW480, HCT-116, and RKO cells that contain high levels of endogenous miR-21 with a locked nucleic acid (LNA) against miR-21 (anti-miR-21) or a scrambled LNA (anti-miR control). We found that cells transfected with anti-miR-21 showed an increase in both hMSH2 and hMSH6 protein expres-

Author contributions: N.V., R.F., and C.M.C. designed research; N.V., P.G., A.P., F.L., K.M.S., and G.J.N. performed research; N.V., M.F., H.A., D.A., T.P., R.F., and C.M.C. contributed new reagents/analytic tools; N.V. and G.J.N. analyzed data; and N.V., P.G., C.B., R.F., and C.M.C. wrote the paper.

The authors declare no conflict of interest.

Freely available online through the PNAS open access option.

[1]N.V. and P.G. contributed equally to this work.

[2]To whom correspondence may be addressed. E-mail: rfishel@osu.edu or carlo.croce@osumc.edu.

This article contains supporting information online at www.pnas.org/lookup/suppl/doi:10.1073/pnas.1015541107/-/DCSupplemental.

Mutator activity induced by microRNA-155 (*miR-155*) links inflammation and cancer

Esmerina Tili[a], Jean-Jacques Michaille[a,b], Dorothee Wernicke[a], Hansjuerg Alder[a], Stefan Costinean[a], Stefano Volinia[a], and Carlo M. Croce[a,1]

[a]Department of Molecular Virology, Immunology and Medical Genetics, The Ohio State University Medical Center and Comprehensive Cancer Center, Columbus, OH 43210; and [b]Laboratoire de Biochimie Métabolique et Nutritionnelle-Institut National de la Santé et de la Recherche Médicale U866, Faculté Gabriel, Université de Bourgogne, 21000 Dijon, France

Contributed by Carlo M. Croce, February 3, 2011 (sent for review January 26, 2011)

Infection-driven inflammation has been implicated in the pathogenesis of ~15–20% of human tumors. Expression of microRNA-155 (miR-155) is elevated during innate immune response and autoimmune disorders as well as in various malignancies. However, the molecular mechanisms providing *miR-155* with its oncogenic properties remain unclear. We examined the effects of *miR-155* overexpression and proinflammatory environment on the frequency of spontaneous hypoxanthine phosphoribosyltransferase (HPRT) mutations that can be detected based on the resistance to 6-thioguanine. Both *miR-155* overexpression and inflammatory environment increased the frequency of *HPRT* mutations and down-regulated WEE1 (WEE1 homolog-S. pombe), a kinase that blocks cell-cycle progression. The increased frequency of *HPRT* mutation was only modestly attributable to defects in mismatch repair machinery. This result suggests that *miR-155* enhances the mutation rate by simultaneously targeting different genes that suppress mutations and decreasing the efficiency of DNA safeguard mechanisms by targeting of cell-cycle regulators such as WEE1. By simultaneously targeting tumor suppressor genes and inducing a mutator phenotype, *miR-155* may allow the selection of gene alterations required for tumor development and progression. Hence, we anticipate that the development of drugs reducing endogenous *miR-155* levels might be key in the treatment of inflammation-related cancers.

genome stability | LPS | TNF | proliferation | transgenic mice

It now is well established that chronic and persistent inflammation contributes to cancer development (1–3). Infection-driven inflammation is involved in the pathogenesis of ~15–20% of human tumors, and tumor-infiltrating leukocytes, such as monocytes/macrophages, T lymphocytes, and neutrophils, are prime regulators of cancer inflammation (1–3). Furthermore, even tumors that are not epidemiologically linked to pathogens are characterized by the presence of an inflammatory component in their microenvironment.

MicroRNAs (miR) are a class of short, noncoding RNAs that are implicated in many aspects of cell biology. *MiR-155* is implicated in hematopoiesis, the innate and acquired immune response, and autoimmune disorders (4–9). A direct link between elevated levels of *miR-155* and the formation and development of tumors such as leukemias and breast, lung, or gastric cancers has been established recently (4, 5, 9–12). Thus, transgenic mice overexpressing *miR-155* in B cells or hematopoietic stem cells show enhanced proliferative disorder that results in high-grade lymphoma (13, 14). Being oncogenic and implicated in inflammation, *miR-155* is the prototype of microRNAs that stand between inflammation and carcinogenesis. However, the molecular mechanisms behind this link remain unclear. Because *miR-155* targets transcripts implicated in DNA repair (15), we evaluated the mutator activity of *miR-155* and that of the *miR-155*–linked inflammatory environment as a potential mechanism connecting inflammation and cancer. In this study we report that *miR-155* and inflammatory stimuli increase the spontaneous mutation rate.

Results

Overexpression of *MiR-155* Results in Enhanced Mutation Rate. *MiR-155* targets core components of the DNA mismatch repair (MMR) machinery, among other mutator pathways (15), suggesting that elevated levels of *miR-155* might enhance the rate of spontaneous mutations. To measure the mutation rate, we took advantage of the hypoxanthine phosphoribosyltransferase (HPRT) locus, which is a well-established method for estimating mutation rate. The HPRT enzyme catalyzes the conversion of purine into purine monophosphate and hypoxanthine into inosine monophosphate in the purine salvage pathway (16, 17). The loss of HPRT function confers resistance to 6-thioguanine (6-TG), because 6-TG becomes cytotoxic only after phosphoribosylation by HPRT. This resistance can be used to identify cells that have acquired mutations at the HPRT locus (16, 17). Because the acquired mutations are thought to occur randomly, the HPRT gene can be used as a reporter gene, and the frequency of mutation at the HPRT locus can be used as an estimate of global genomic instability. To measure the effects of *miR-155* on mutation rate, we first developed stable clones of SW620 colorectal adenocarcinoma cells and MDA-MB-231 breast adenocarcinoma cells expressing mature *miR-155* under the control of the *Tet-On* inducible system. Incubation of SW620 clones 8A, 22C, and 23A with doxycycline increased *miR-155* expression by 2.94 ± 0.23-, 5.58 ± 0.43-, and 8.10 ± 0.65-fold, respectively (mean ± SD) (Fig. S1 and Table S1). Similarly, doxycycline treatment increased *miR-155* expression by 12.01 ± 2.34-, 26.42 ± 1.11-, and 32.07 ± 3.27-fold in MDA-MB-231 clones 9C, 2B, and 19B, respectively.

The cell growth-adjusted *HPRT* mutation rate, estimated based on a modified version of fluctuation analysis (16), increased with *miR-155* levels in both SW620 and MDA-MB-231 cell clones (Fig. 1 *A* and *B*). Constant elevated expression of *miR-155* the enhanced mutation rate by up to 3.39-fold in SW620 clones and up to 3.47-fold in MDA-MB-231 clones (Table S1). Moreover, HCT116 colorectal carcinoma cells transiently overexpressing *miR-155* by 19.57 ± 0.62-fold under the control of *Tet-On* inducible system (Fig. S2) showed a 2.81-fold higher mutation rate (Table S1). These results establish a direct link between mutation rate and *miR-155* levels.

As expected, the basal spontaneous cell growth-adjusted mutation rates of SW620 and MDA-MB-231 cells was comparable ($0.75 \pm 0.27 \times 10^{-7}$ and 1.28×10^{-7} mutations per cell, respectively) and were ~4.46-fold lower than the spontaneous mutation

Author contributions: CMC designed research; ET, J.-J.M., DW, H.A., SC, and SV performed research; ET, J.-J.M., and CM.C analyzed data; and ET, J.-J.M., and C.M.C wrote the paper.

The authors declare no conflict of interest.

Freely available online through the PNAS open access option.

Data deposition: Microarray data have been submitted to the MIAMExpress database (http://www.ebi.ac.uk/microarray-as/aer/entry) with accession no. E-TABM-1118.

[1]To whom correspondence should be addressed. E-mail: carlo.croce@osumc.edu.

This article contains supporting information online at www.pnas.org/lookup/suppl/doi:10.1073/pnas.1101968108/-/DCSupplemental.

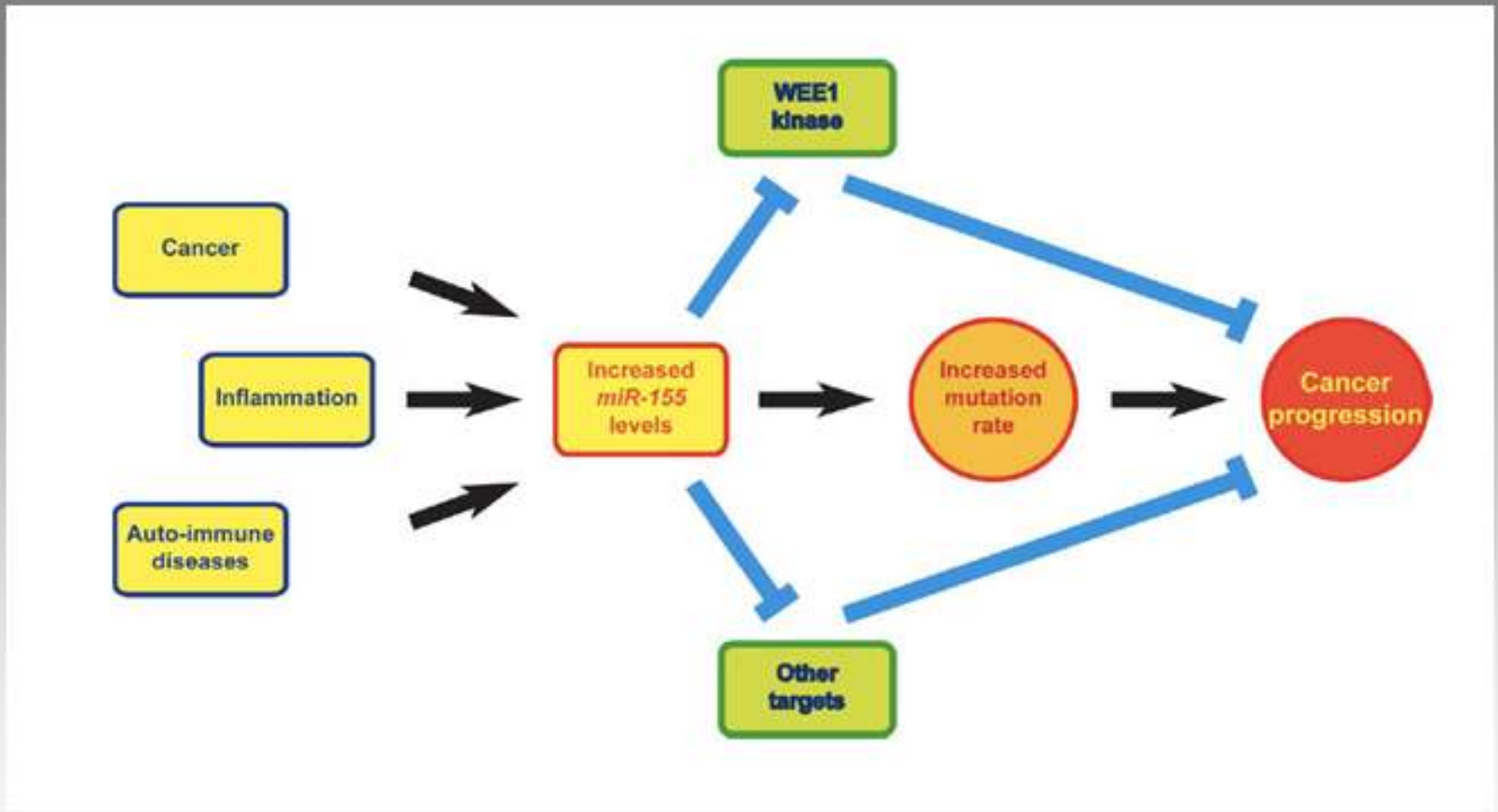
WEE1 kinase
Cancer
Inflammation
Auto-immune diseases
Increased miR-155 levels
Increased mutation rate
Cancer progression
Other targets

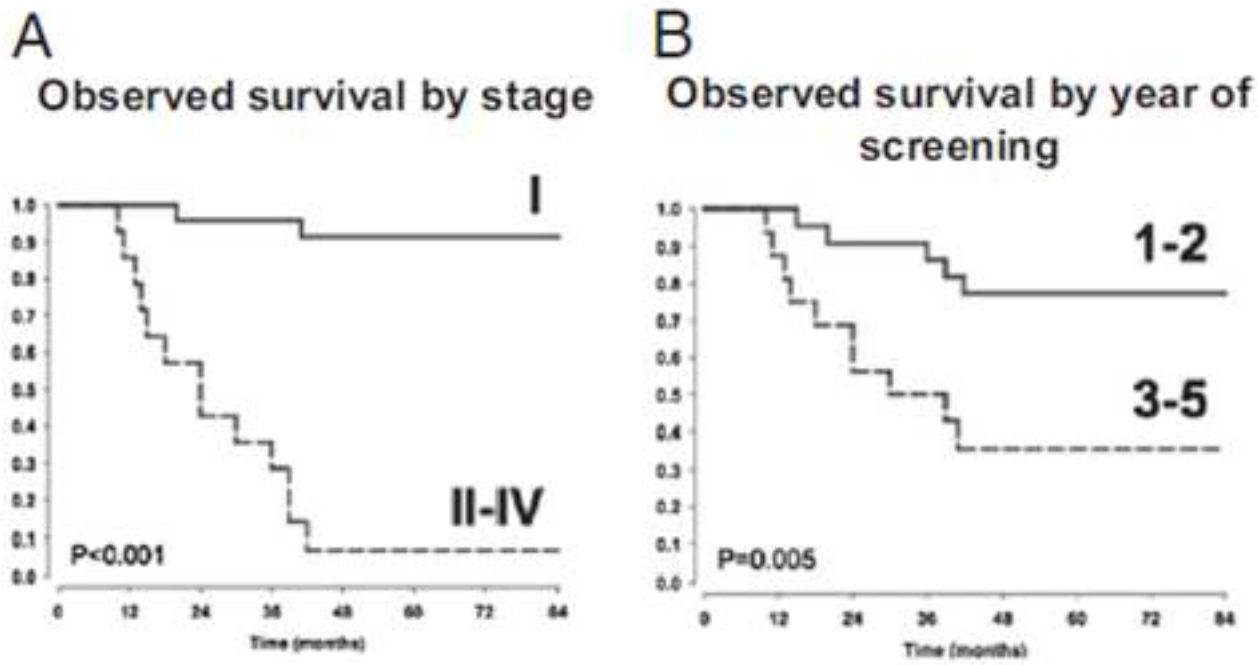

Fig. 1. Kaplan–Meier estimates of observed 5-y survival in CT-screening INT-IEO trial. (*A*) Data arranged according to the extent of disease: 92% for stage I (95% CI: 70.0–97.8) and 7% for stage II–IV (95% CI: 0.5–27.5, $P < 0.001$). (*B*) Data arranged according to the year of CT-detection: 77% for lung cancers detected in the first 2 y of the study (95% CI: 53.7–89.8) and 36% for lung cancers diagnosed from third to fifth years (95% CI: 13.7–58.7, $P = 0.005$)

Table 1. Top 10 miRNAs deregulated between tumor and normal lung tissue (class comparison analysis)

	Tumor vs. normal tissues	
miRNAs deregulated ($P < 0.001$)	Direction	Fold change
mir-7-2-prec	Up	1.3
mir-126	Down	0.4
mir-200b	Up	1.3
mir-210	Up	3
mir-219-1	Up	1.6
mir-21	Up	2.9
mir-324-5p	Up	1.3
mir-451	Down	0.5
mir-486-5p	Down	0.5
mir-30a	Down	0.6

Table 2. Associations between miRNA expression in tumor and normal tissues and clinical–pathological characteristics of patients

	Tumor tissue			Normal tissue		
Clinical–pathological characteristics	miRNA	Direction	*P* value	miRNA	Direction	*P* value
Histotype (ADC vs. SCC or others)	mir-205	Down	<0.001			
	mir-21-pre	Up	<0.001			
Growth rate diameter (≤50% vs. >50%)	mir-518e	Up	<0.001	mir-30d*	Up	<0.001
	mir-144-pre	Up	<0.001			
Disease-free survival (alive vs. dead or relapse)	mir-429	Down	0.003	mir-34b	Up	0.001

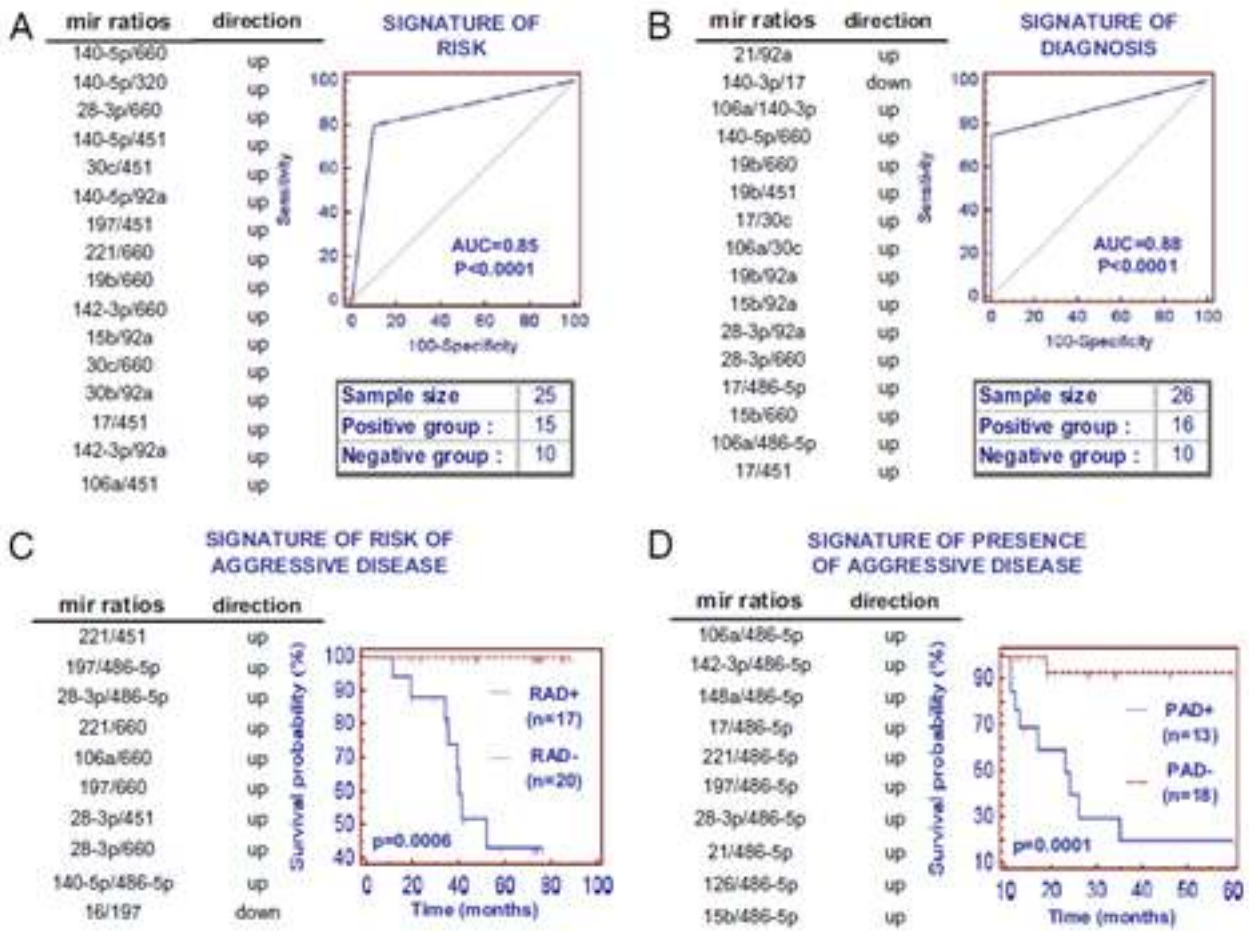

Fig. 4. miRNA expression analyses in plasma samples collected before the onset and at the time of disease. The signatures of miRNA ratios and their direction in the analyses are listed in the tables. (*A*) miRNA signature of risk to develop lung cancer and (*B*) miRNA signature of lung cancer diagnosis. The ROC curves of samples belonging to the validation set are shown. (*C*) Kaplan–Meier survival curves of patients with miRNA signatures of risk of aggressive disease (RAD) in plasma samples collected 1–2 y before CT-detection of lung cancer. (*D*) Kaplan–Meier survival curves of patients with miRNA signatures of presence of aggressive disease (PAD) in plasma samples collected at the time of CT-detected lung cancer. The RAD- or PAD-positive patients show a significantly worse survival rate than RAD- or PAD-negative patients ($P = 0.0006$ and $P = 0.0001$, respectively).

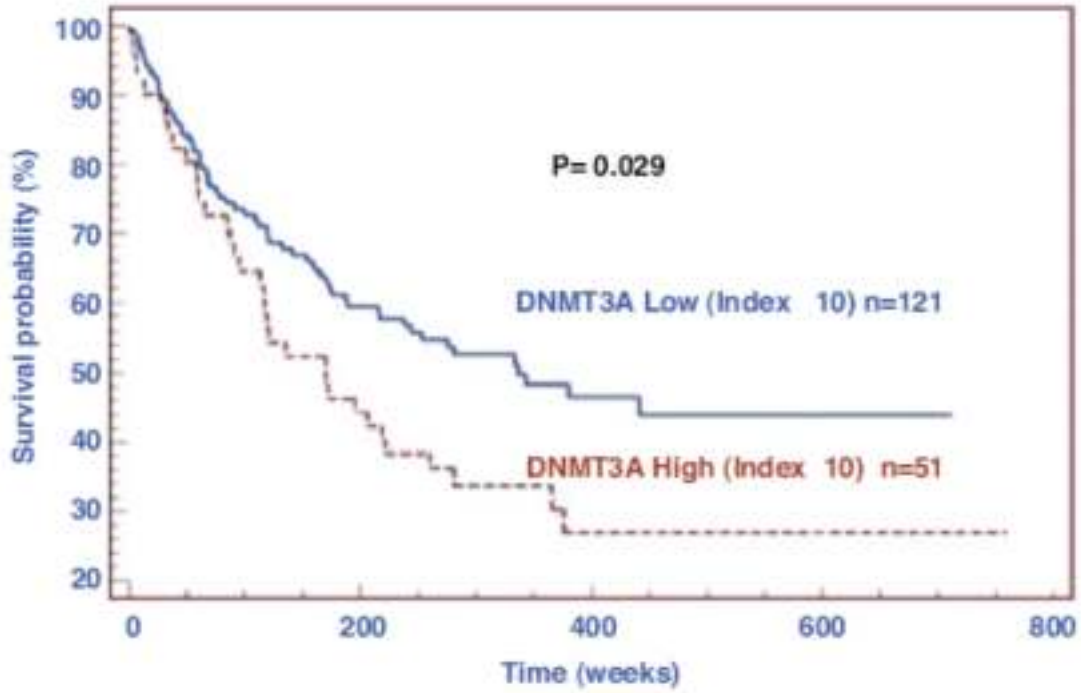

Fig. 1. Dnmt3A protein expression level in NSCLCs is inversely associated with overall survival. Kaplan–Meier curve showing survival of 172 NSCLC patients with different levels of Dnmt3A expression in tumors relative to adjacent normal lung. Patients with higher expression of Dnmt3A had shorter overall survival ($P = 0.029$).

Fig. 2. Complementarity sites for miR-29s in the 3′-UTR region of *DNMT3A* and *-3B*. The capital and bold letters identify perfect base matches, according to the TARGETSCAN 3.1 software. The PicTar software identifies two additional match regions between miR-29a and *DNMT3B*, indicated with an asterisk.

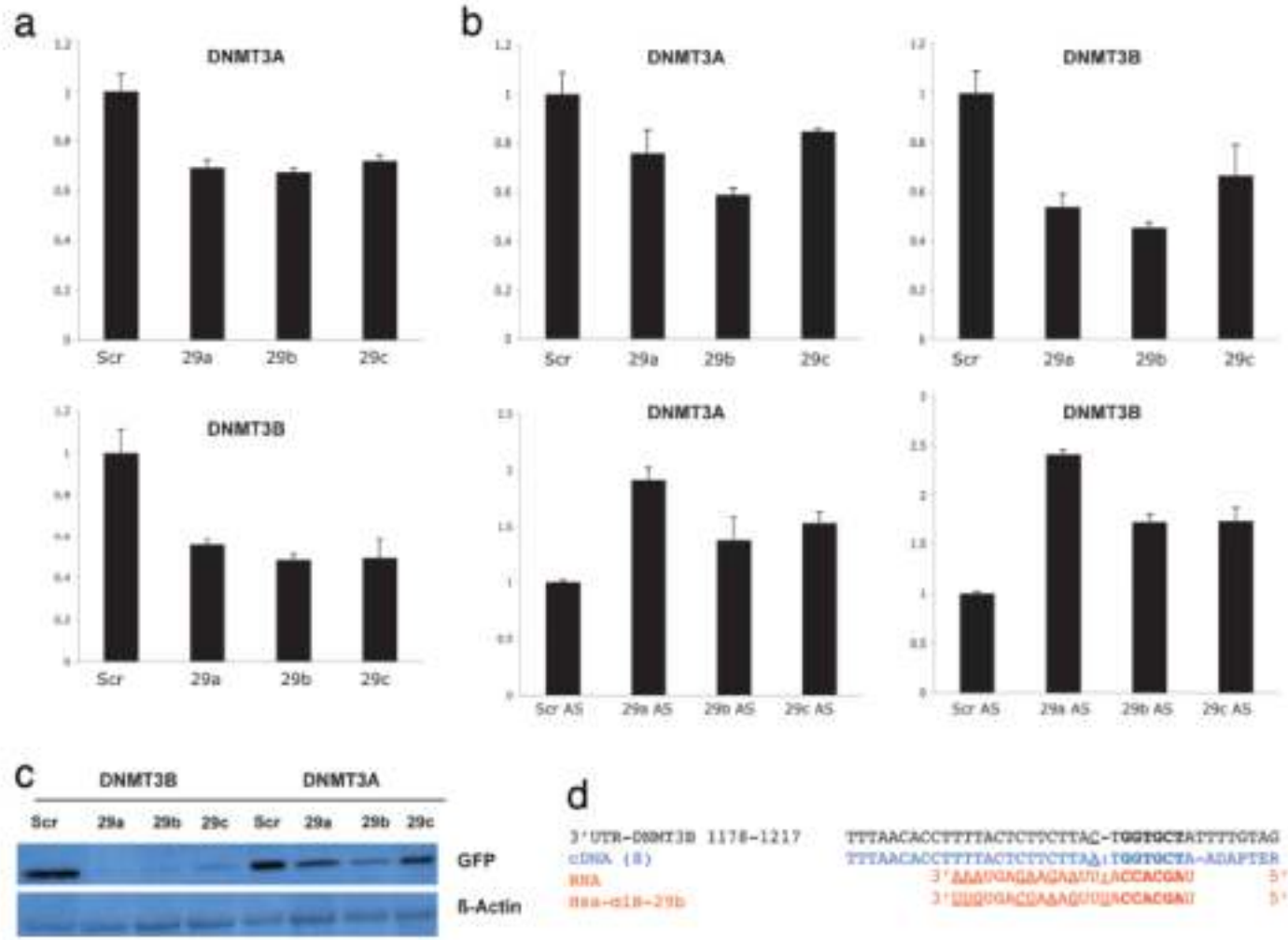

Fig. 3. MIR-29s directly target *DNMT3A* and *-B*. (*a*) Results of the luciferase assay for DNMT3s expression after transfection with miR-29s in A549 cells. (*b*) (*Upper*) Assessment of expression of *DNMT3A* and *DNMT3B* mRNAs by qRT-PCR, after transfection of A549 cells with miR-29s or a negative control. (*Lower*) Silencing of miR-29s with antisense molecules (AS) induces increased expression of *DNMT3A* and *DNMT3B* mRNA. (*c*) Western blot of proteins extracted from A549 cells that were cotransfected with the GFP repression vectors for the *DNMT3A* and *-B*—3′-UTR plus miR-29s or scrambled (Scr) oligonucleotides. (*d*) miR-29b acts as an endogenous primer to retrotranscribe its predicted *DNMT3B* mRNA target. Black, *DNMT3B* cDNA (GenBank accession no. NM_175848); blue, cloned and sequenced cDNAs experimentally obtained (eight clones analyzed); red, deduced RNA sequences and corresponding miR-29b. The upper underlined black and blue nucleotides have no homology between target and experimental cDNAs. The lower underlined red nucleotides represent RNA sequence complementary to cDNAs that lack homology to the miR-29b sequence. Nucleotides in bold represent the PicTar-predicted match site.

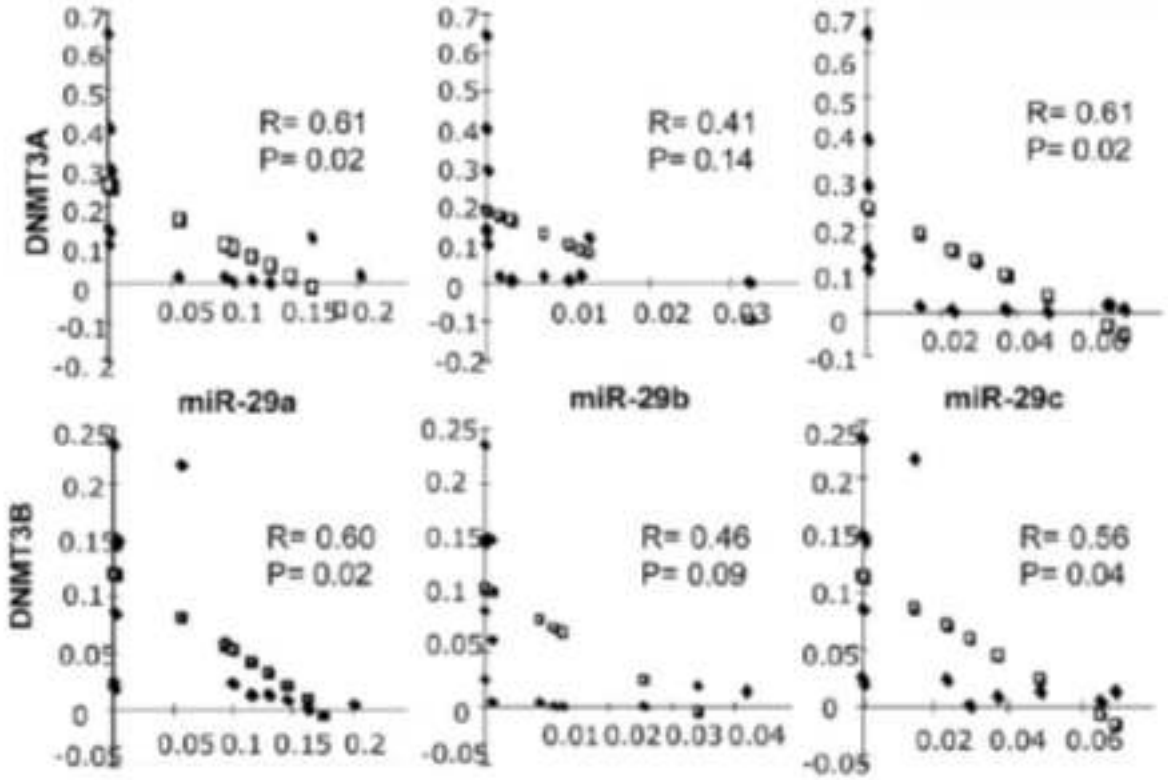

Fig. 4. Correlation of endogenous miR-29 levels with *DNMT3A/B* mRNA levels. Inverse correlation between endogenous mRNA levels of DNMT3A and DNMT3B and endogenous levels of miR-29s determined by qRT-PCR in 14 NSCLCs. R, regression coefficient; □, regression line; ◆, actual sample correlations.

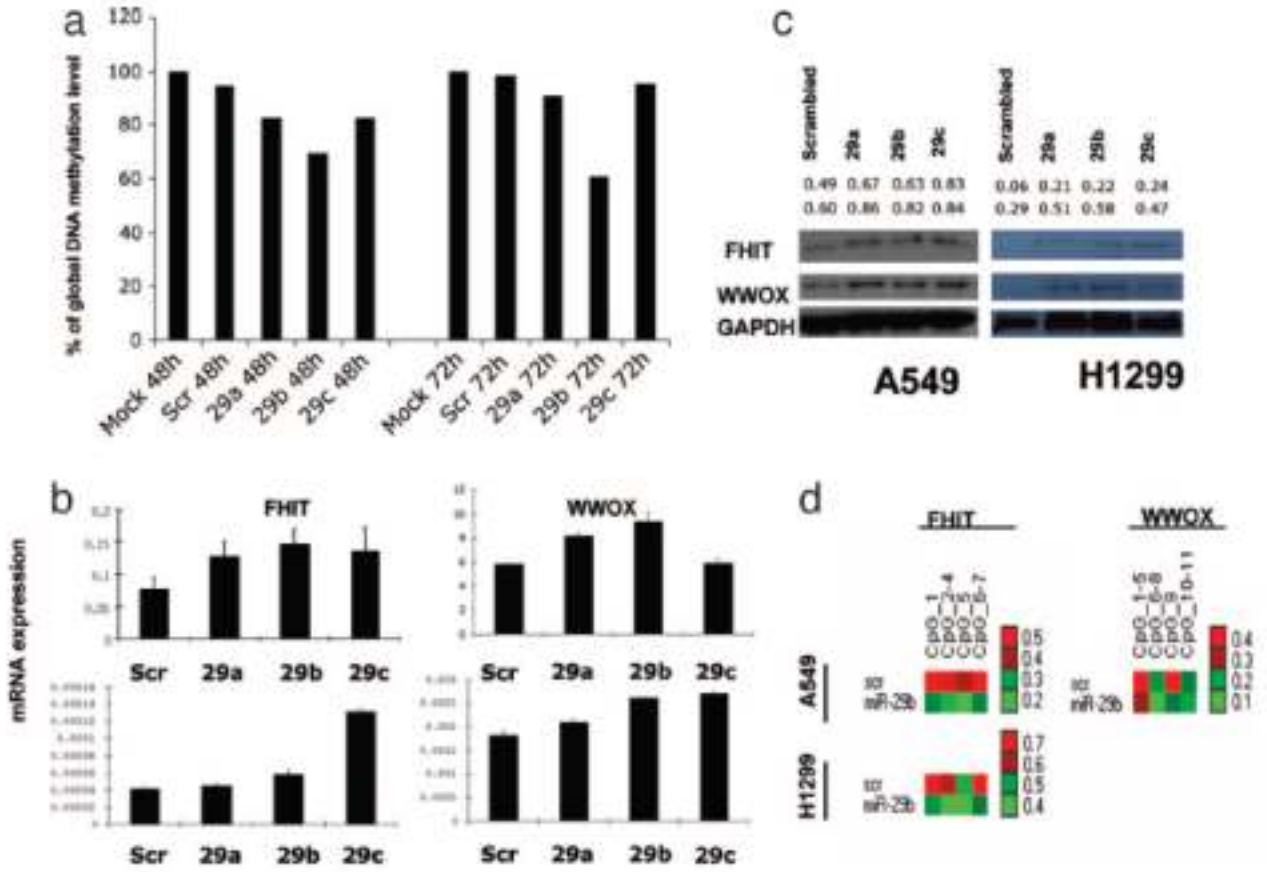

Fig. 5. Effect of restoration of miR-29s on the cancer cell epigenome. (*a*) Global DNA methylation changes induced by miR-29s on A549 cells harvested 48 and 72 h after transfection. The results are compared with nontransfected (mock) cells and cells transfected with a scrambled oligonucleotide. (*b*) Determination of *FHIT* and *WWOX* mRNA levels in A549 and H1299 cells 48 h after transfection with miR-29s or a negative control by qRT PCR; miR-29s induced reexpression of *FHIT* and *WWOX* mRNAs. (*c*) Immunoblot of Fhit and Wwox proteins in A549 and H1299 cells 72 h after transfection with miR-29s or negative control; by 72 h, miR-29s induce increased expression of Fhit and Wwox proteins. The numbers above the immunoblot images represent the intensity of the bands relative to the *GAPDH* gene (upper row, Fhit; lower row, Wwox). (*d*) Graphical representation of the quantitative DNA methylation data for *FHIT* and *WWOX* promoter region by using the MassARRAY system. Each square represents a single CpG or a group of CpGs analyzed, and each arrow represents a sample. Methylation frequencies are displayed for each experiment in a color code that extends from light green (lower methylation frequencies) to bright red (higher methylation frequencies).

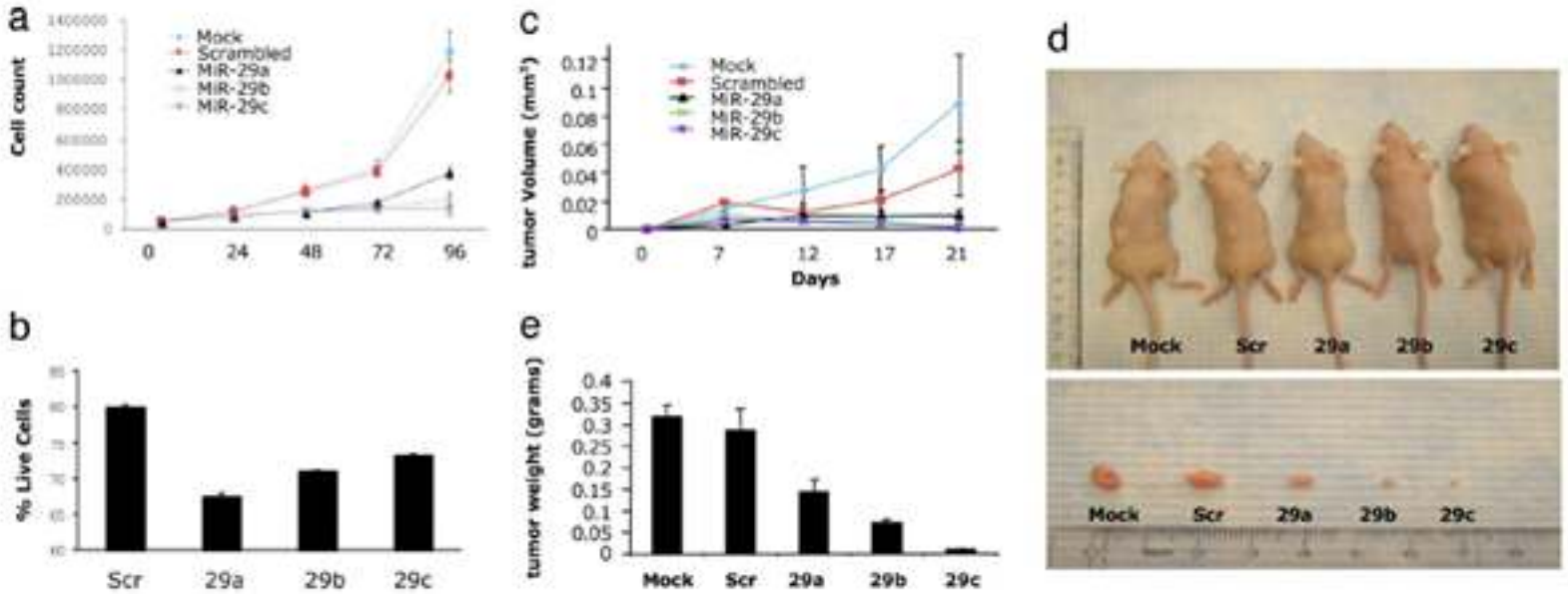

Fig. 6. Effects of miR-29s on tumorigenicity of A549 cells. (*a*) Growth curve of A549 cells transfected *in vitro* with miR-29s or scrambled oligonucleotide or mock-transfected. (*b*) Percentages of live cells were measured in A549 cells transfected with scrambled oligonucleotide or with miR-29s oligonucleotides (100 nM final concentration). (*c*) Growth curve of engrafted tumors in nude mice injected with A549 cells pretransfected (48 h before injection) with miR-29s, scrambled oligonucleotides, or mock transfected. (*d*) Comparison of tumor engraftment sizes of mock-, scrambled-, and miR-29s-transfected A549 cells 21 days after injection in nude mice. The images show average-sized tumors from among five of each category. (*e*) Tumor weights ± SD in nude mice.

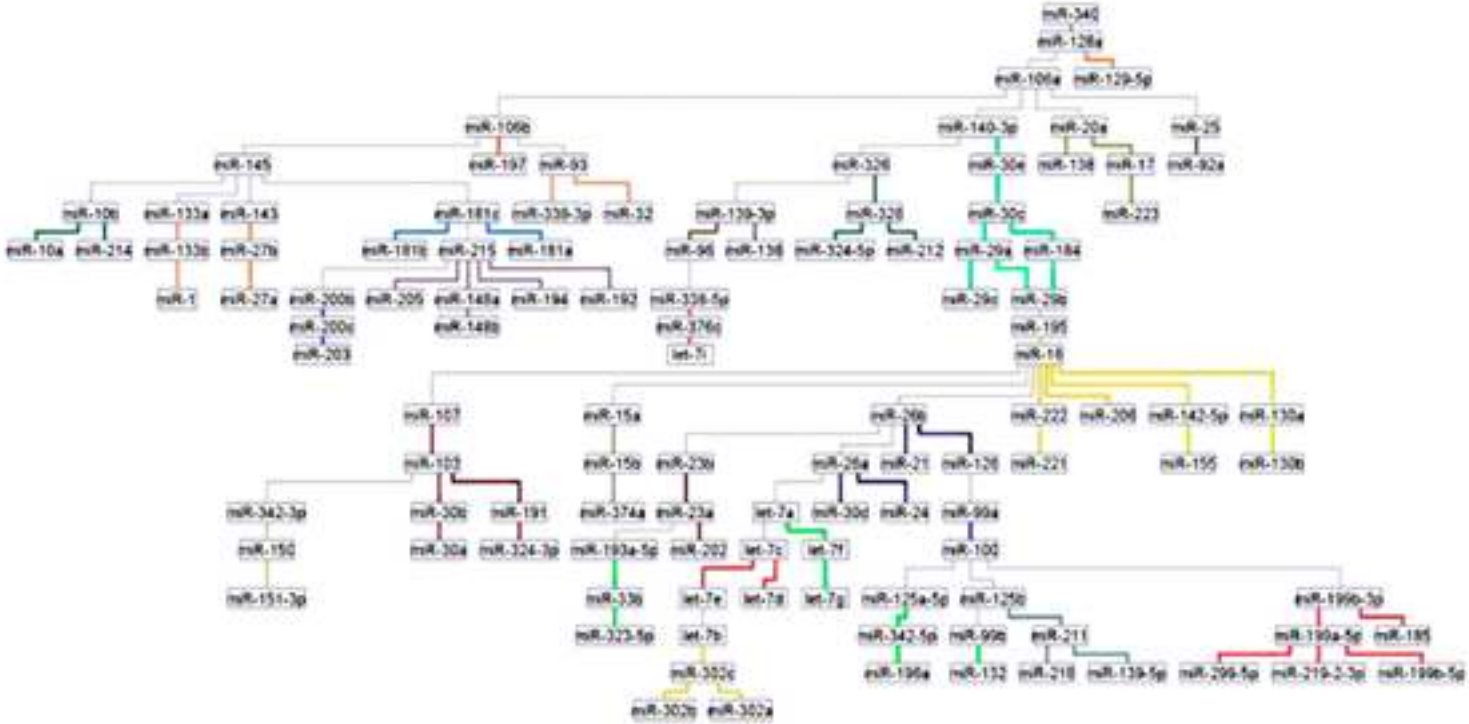

Figure 1. The miRNA network in normal tissues (1107 samples, 50 tissues, 115 miRNAs). The network was inferred for all expressed and varying miRNAs, without preselecting for differential expression. Standard Banjo parameters were adopted with a q6 discretization policy. The consensus graph depicted here was obtained from the best 100 nets (after searching through 8.3×10^9 networks). MCL graph-based clustering algorithm was applied to clusters extraction (miRNAs with highly related expression pattern have edges of the same color); thus, different clusters in the network are linked by different color edges. yEd graph editor (yFiles software) was employed for graphs visualization. See text for further discussion.

Table 1. Differentially regulated miRNA in solid cancers

Parametric *P*-value	FDR	Intensities in solid cancers	Intensities in normal tissues	Fold-change	miRNA	Chromosomal location
$<1 \times 10^{-7}$	$<1 \times 10^{-7}$	967	617.9	1.57	hsa-miR-21	17q23.1
$<1 \times 10^{-7}$	$<1 \times 10^{-7}$	1378.2	917.7	1.5	hsa-miR-25	7q22.1
$<1 \times 10^{-7}$	$<1 \times 10^{-7}$	902.7	626.3	1.44	hsa-miR-20a	13q31.3
$<1 \times 10^{-7}$	$<1 \times 10^{-7}$	925.7	646.9	1.43	hsa-miR-17	13q31.3
$<1 \times 10^{-7}$	$<1 \times 10^{-7}$	652.3	469	1.39	hsa-miR-106a	Xq26.2
$<1 \times 10^{-7}$	$<1 \times 10^{-7}$	410	297.8	1.38	hsa-miR-106b	7q22.1
1.30×10^{-6}	1.1×10^{-05}	918.8	697.9	1.32	hsa-miR-146a	5q34
$<1 \times 10^{-7}$	$<1 \times 10^{-7}$	11893.3	9370.9	1.27	hsa-miR-92a	13q31.3,Xq26.2
1.60×10^{-6}	1.2×10^{-5}	2354.9	1919.4	1.23	hsa-miR-103	5q35.1,20p13
$<1 \times 10^{-7}$	$<1 \times 10^{-7}$	289.4	237.8	1.22	hsa-miR-130b	22q11.21
$<1 \times 10^{-7}$	$<1 \times 10^{-7}$	452.7	372	1.22	hsa-miR-93	7q22.1
3.90×10^{-6}	2.7×10^{-5}	2116.4	1743.6	1.21	hsa-miR-107	10q23.31
$<1 \times 10^{-7}$	$<1 \times 10^{-7}$	297.7	248	1.2	hsa-miR-30e	1p34.2
7.4×10^{-6}	4.8×10^{-5}	225.6	259.4	0.87	hsa-miR-138	16q13,3p21.33
1×10^{-7}	1×10^{-6}	220.5	260.2	0.85	hsa-miR-326	11q13.4
3.7×10^{-6}	2.6×10^{-5}	419.9	507.8	0.83	hsa-miR-193a	17q11.2
2×10^{-7}	1.8×10^{-6}	382.5	471.2	0.81	hsa-miR-206	6p12.2
3×10^{-6}	2.2×10^{-05}	273.7	349.6	0.78	hsa-miR-205	1q32.2
$<1 \times 10^{-7}$	$<1 \times 10^{-7}$	714.9	1015.1	0.70	hsa-miR-145	5q32
$<1 \times 10^{-7}$	$<1 \times 10^{-7}$	275.7	403.0	0.68	hsa-miR-203	14q32.33

Solid cancer samples numbering 2532 vs. 806 corresponding normal samples, at least one class with intensity >250, *P*-value $< 1 \times 10^{-5}$.

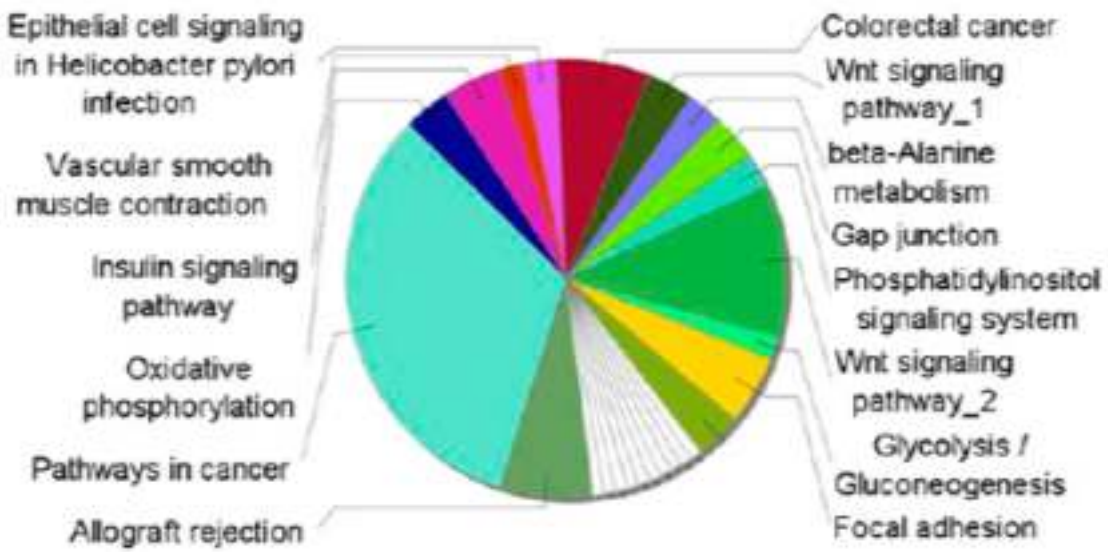

Figure 2. Cellular pathways regulated by differentially expressed miRNAs in cancer. KEGG analysis by ClueGO (Bindea et al. 2009) of pathways (score = 3, *P*-value $< 1 \times 10^{-3}$) simultaneously targeted by both up-regulated and down-regulated miRNAs (listed in Table 1; Supplemental Tables IV, V). The KEGG pie-chart shows the functional effect of differentially expressed miRNAs on cellular pathways in cancer. The large majority of the affected pathways is related to cancer or signal transduction (i.e., Wnt, VEGF, TGF-beta, insulin, and phosphatidylinositol signaling, focal adhesion, and colorectal cancer). Target genes selection was performed with DIANA-miRpath, microT-V4.0 (Papadopoulos et al. 2009). The union of the target mRNAs with a score above 3 was used as an input to ClueGO. Right-sided hypergeometric test yielded the enrichment for GO terms. Benjamini-Hochberg correction for multiple testing controlled the *P*-values. GO term fusion was applied for redundancy reduction.

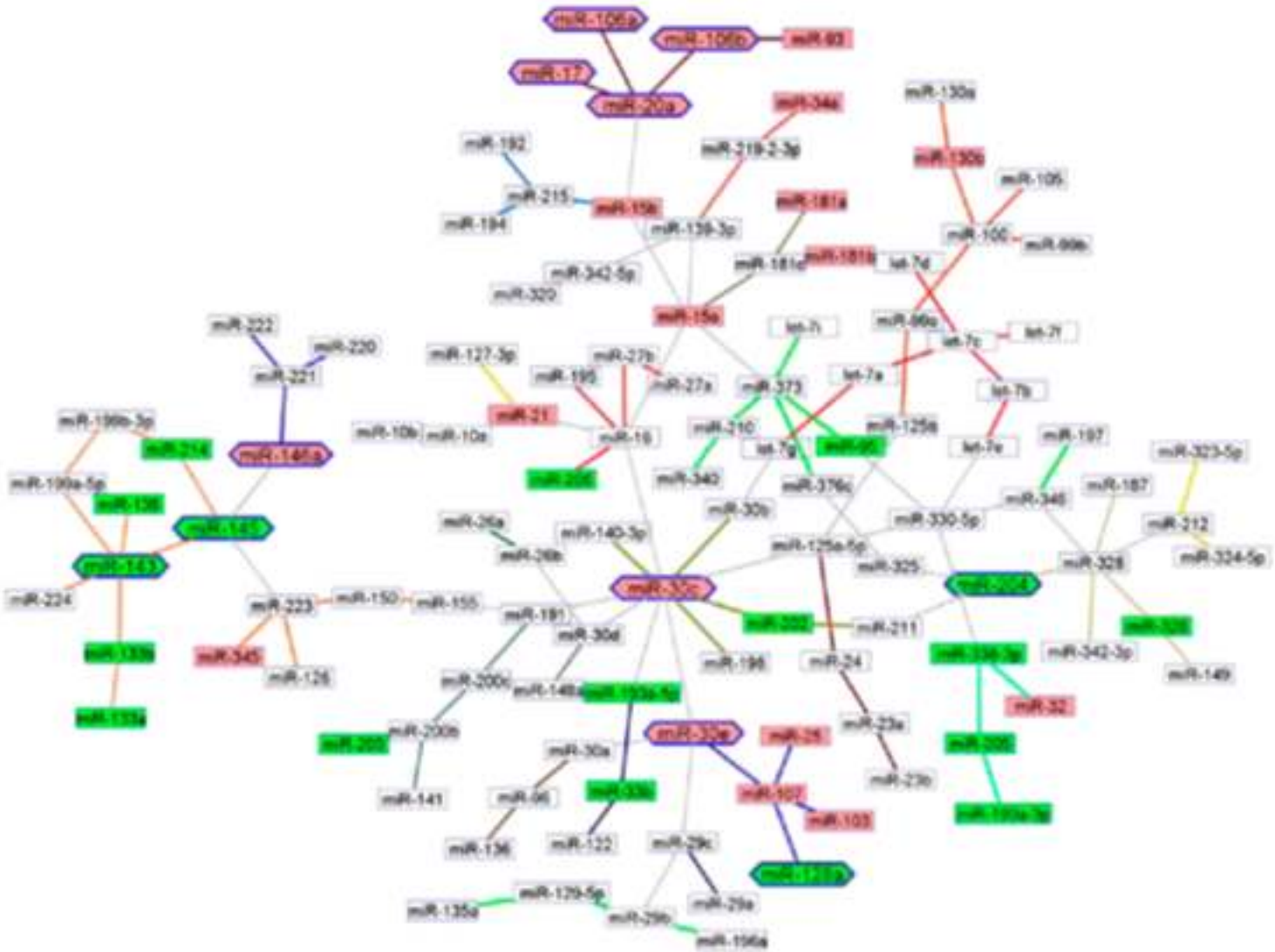

Figure 3. The miRNA network in solid cancers (2532 samples, 31 cancer types, 120 miRNAs). The network was inferred for all expressed and varying miRNAs, without preselecting for differential expression. Standard Banjo parameters were adopted with a q6 discretization policy. The consensus graph depicted here was obtained from the best 100 nets (after searching through 8.4×10^6 networks). MCL expression clusters are linked by different color edges. yEd graph editor (yFiles software) was employed for graph visualization. The miRNAs expressed differentially in the tumors are color-coded and in the graph miRNA neighbors are of the same color code: Closely clustered miRNAs are either pink (overexpressed) or green (down-regulated). The node labels, for which expression and physical alteration (CGH, see "miRNA copy number variations in cancer and leukemia" section) were concordant (i.e., overexpression and amplification), were emboldened and visually reinforced with a hexagonally shaped border.

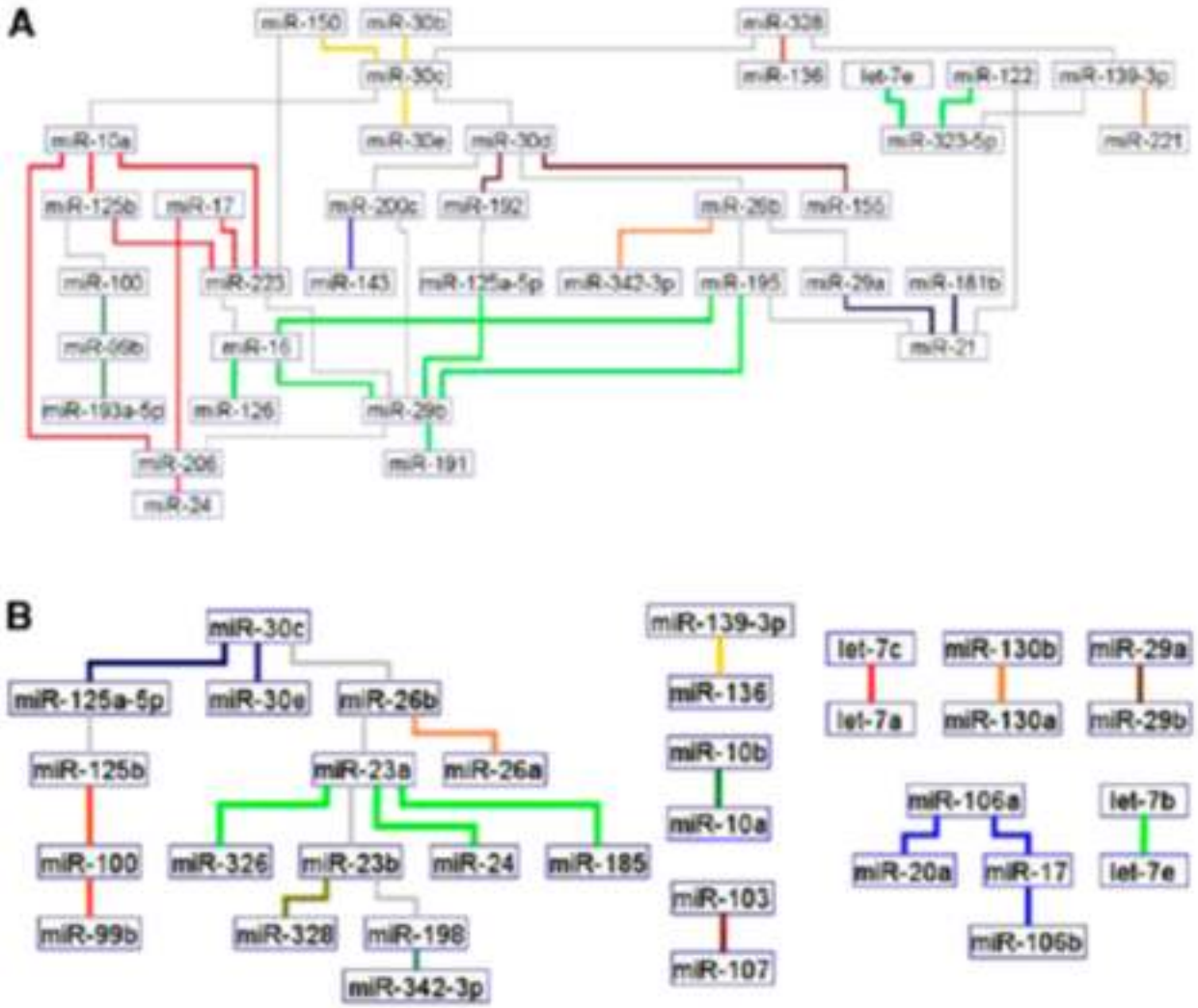

Figure 4. Comparison of miRNA networks in normal lung and adenocarcinoma. (*A*) Normal lung (71 samples). A single complete miRNA network is shown. (*B*) Lung adenocarcinoma (125 samples). In this graph, one major and eight minor subnetworks were detected. For example, hsa-miR-10a/b, hsa-miR-29a/b, hsa-miR-107, and hsa-miR-103 are in minor independent subnetworks disjoint from the main one.

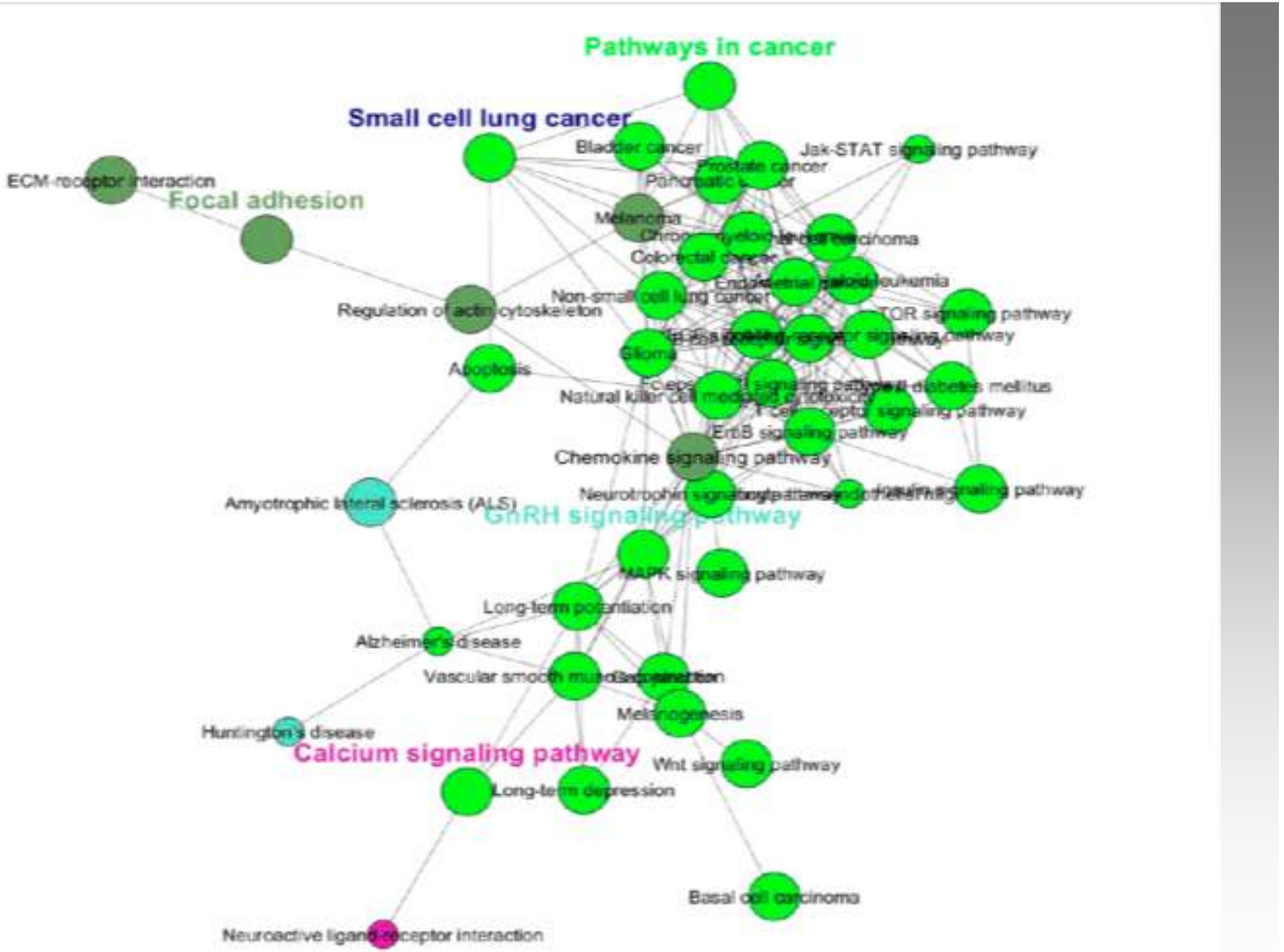

Figure 5. The KEGG functional analysis of eight disjointed minor miRNA networks in lung adenocarcinoma. The miRNA present in the unconnected cliques target genes are involved in many cancer-related terms, such as focal adhesion, small cell lung cancer, and calcium signaling. The detailed list of significant GO terms is shown in Supplemental Figure 7.

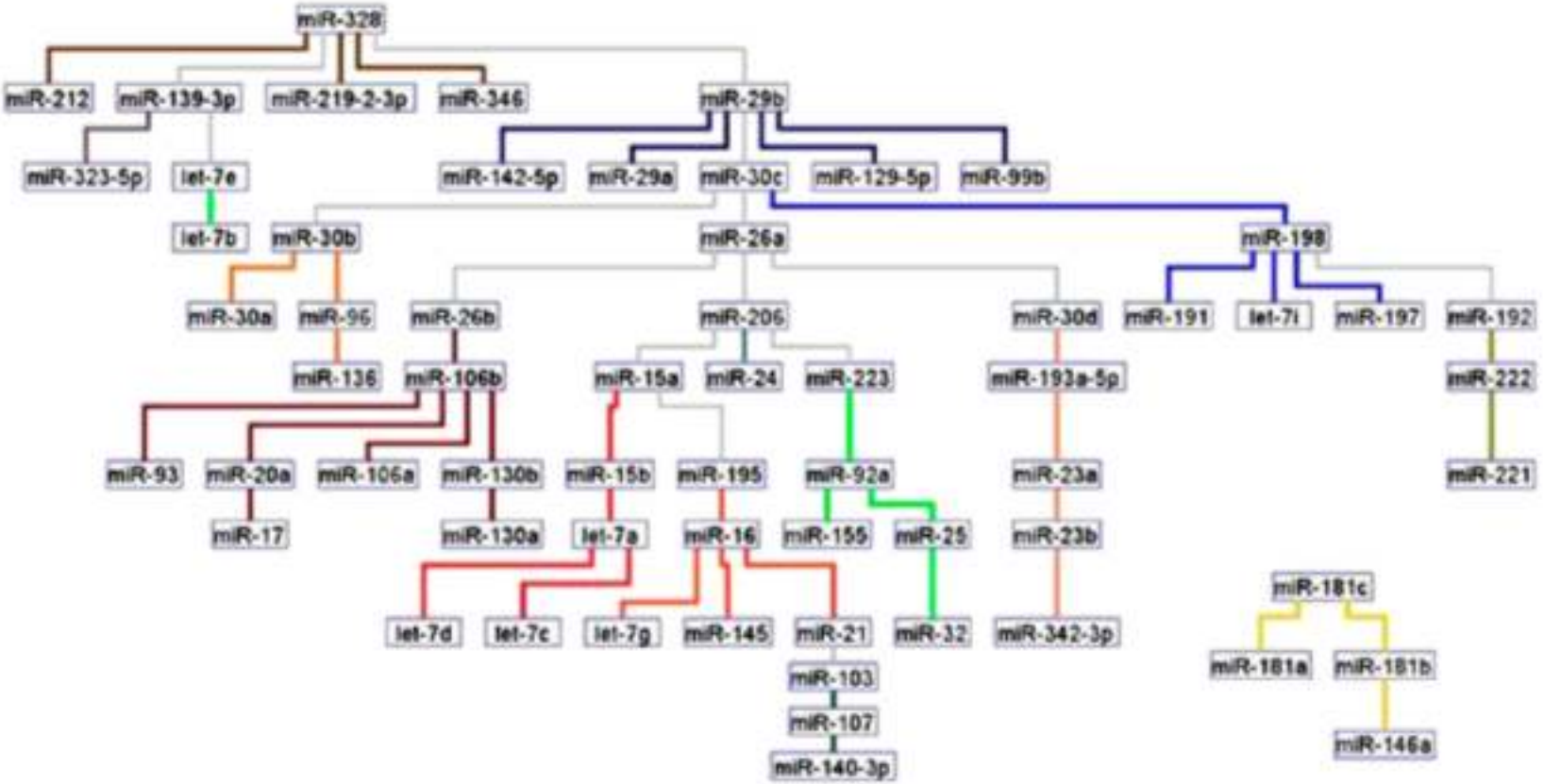

Figure 6. The miRNA network in acute myeloid leukemia (589 samples, two subnetworks). Standard Banjo parameters were adopted with a q6 discretization policy. The consensus graph depicted here was obtained from the best 100 nets (after searching through 8.5×10^9 networks). The miRNA network in AML has disjointed cliques. hsa-miR-155 and hsa-miR-181, two miRNAs with clinical relevance are in two separated subnetworks, as expected from their prognostic independence. hsa-miR-181 is associated with hsa-miR-146a in a detached yellow miniclique. mir-155 belongs to the main subnetwork, in the same red MCL clique of hsa-miR-223, hsa-miR-92a, hsa-miR-25, and hsa-miR-32. Finally, hsa-miR-29b has a key role in AML and acts as a hub in the AML net.

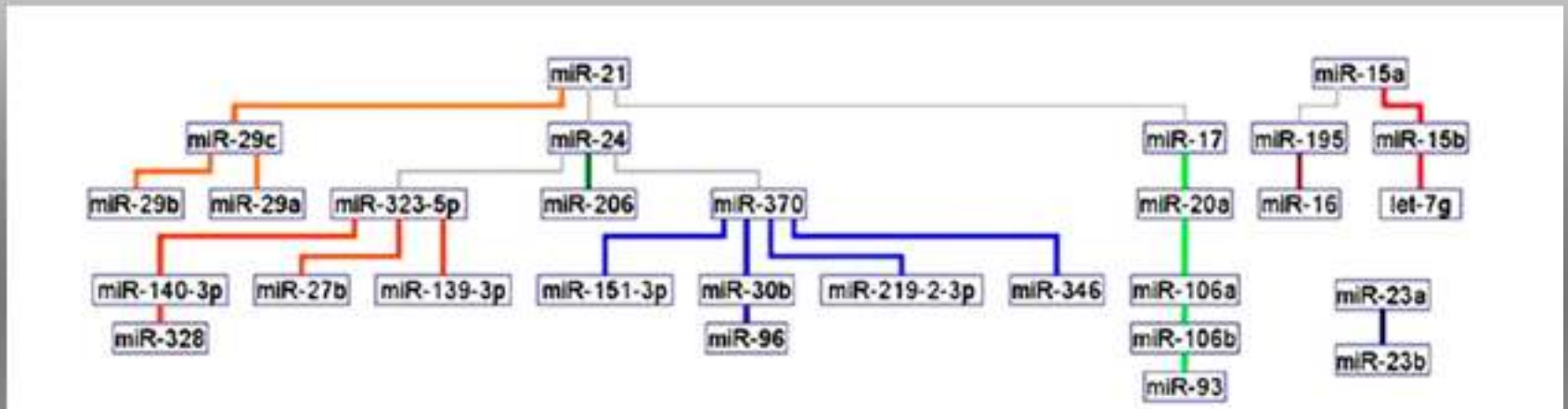

Figure 7. The miRNA network in chronic lymphocytic leukemia (254 samples, three subnetworks). Standard Banjo parameters were adopted with a q6 discretization policy. The consensus graph depicted here was obtained from the best 100 nets (after searching through $>1 \times 10^{10}$ networks). The network graph shows a major net and two separated minicliques: hsa-miR-23a/b and the hsa-miR-15/16 cluster. hsa-miR-15 and hsa-miR-16, two miRNAs frequently deleted in CLL, have been shown to regulate apoptosis via BCL2. The key hsa-miR-29b, acting as a hub in AML, is only a branch in CLL. AML prognostic hsa-miR-181 is disjointed in AML but not in CLL, while the reverse happens in CLL for prognostic hsa-miR-15/16 genes.

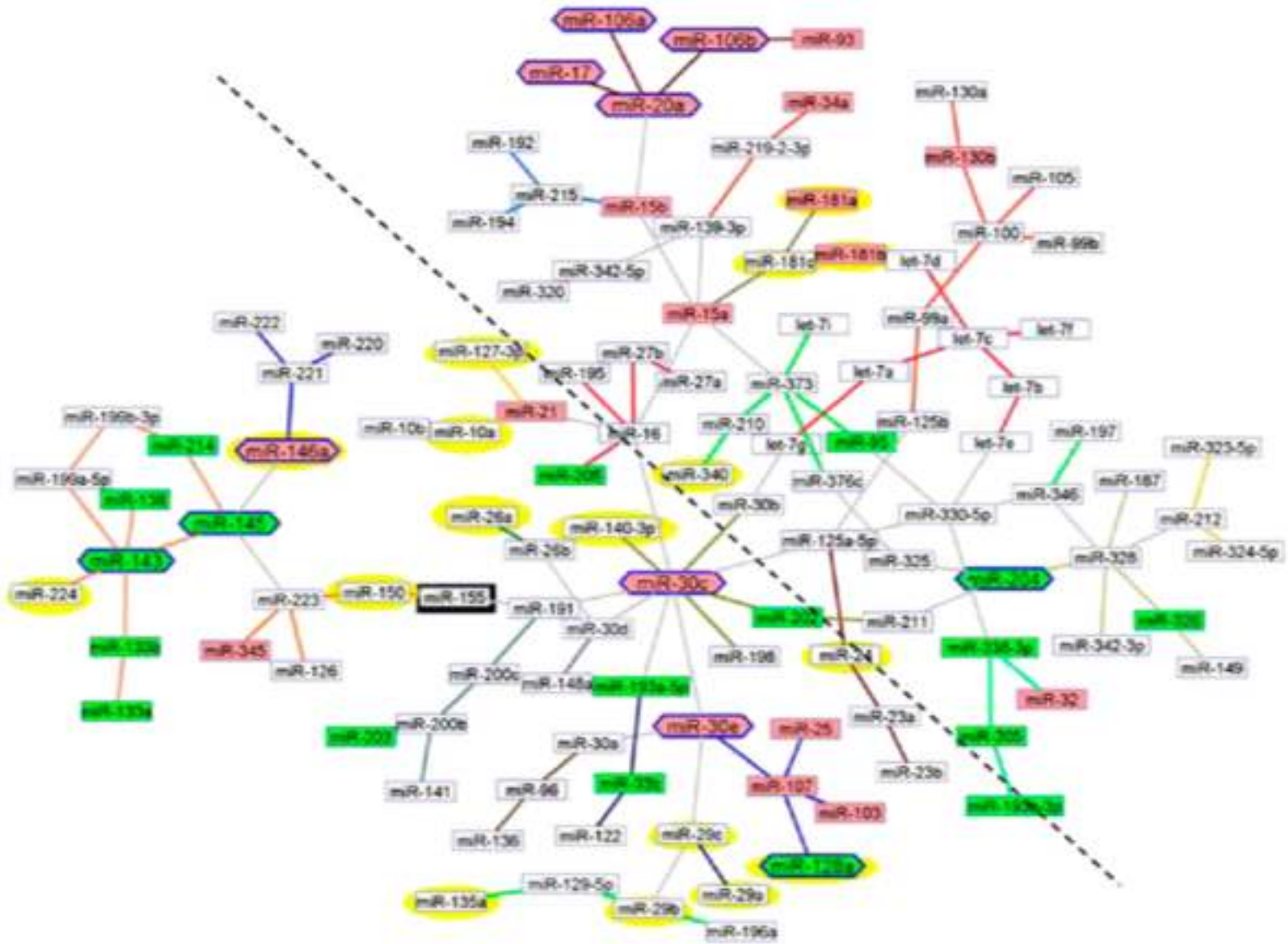

Figure 8. Deregulated miRNAs in leukemia from *Mir155* transgenic mice are preferentially located close to hsa-miR-155 in the cancer network. We compared miRNA profiles of three leukemia samples from *Mir155* transgenes to controls from wild-type mice. The deregulated miRNAs (Supplemental Table X) were mapped onto the cancer network and highlighted in yellow. Most of the other miRNAs are concentrated around hsa-miR-155 node (black). When a diagonal is drawn and the two sides compared the difference between yellow nodes is significant (Fisher's exact test, two-tail *P*-value < 0.009).